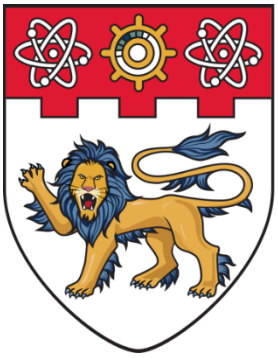

NANYANG TECHNOLOGICAL UNIVERSITY

SINGAPORE

LASER CLADDING RESEARCH FOR RAIL STEEL

REPAIR AND RELIABILITY ASSESSMENT

N ALAGU SUBRAMANIAM

SCHOOL OF MECHANICAL AND AEROSPACE ENGINEERING

2022

LASER CLADDING RESEARCH FOR RAIL STEEL REPAIR AND RELIABILITY ASSESSMENT

N ALAGU SUBRAMANIAM

Supervisor: Prof. John Pang Hock Lye

SCHOOL OF MECHANICAL AND AEROSPACE ENGINEERING

A thesis submitted to the Nanyang Technological University in partial fulfilment of the requirement for the degree of Doctor of Philosophy

2022

Statement of Originality

I hereby certify that the work embodied in this thesis is the result of original research, is free of plagiarised materials, and has not been submitted for a higher degree to any other University or Institution.

21 March 2022

. . . . . .

Date

. . . . . .

N Alagu Subramaniam

Supervisor Declaration Statement

I have reviewed the content and presentation style of this thesis and declare it is free of plagiarism and of sufficient grammatical clarity to be examined. To the best of my knowledge, the research and writing are those of the candidate except as acknowledged in the Author Attribution Statement. I confirm that the investigations were conducted in accord with the ethics policies and integrity standards of Nanyang Technological University and that the research data are presented honestly and without prejudice.

21 March 2022

. . . . . .

Date

. . . . . .

Pang Hock Lye John

Authorship Attribution Statement

This thesis contains material from 2 paper(s) published in the following from papers accepted at conferences in which I am listed as an author.

Chapter 3 and 4 is published as Nellian Alagu Subramaniam, Kok Ee Tan, Hoh Hsin Jen, John Hock Lye Pang, Ivan Christian, and Si Yun Chua, "Microstructure and Wear Performance Assessment of Laser Cladded Rail Steel for Service Life Extension at Sharp-Radius Curves." 2018 International Conference on Intelligent Rail Transportation (ICIRT). IEEE, 2018.

Chapter 4 is published as Hoh Hsin Jen, Wang Jinlong, Nellian Alagu Subramaniam, and John Hock Lye Pang, "Reliability Centered Maintenance (RCM) Assessment of Rail Wear Degradation", World Congress on Condition Monitoring (WCCM) 2019, Singapore.

The contributions of the co-authors are as follows:

- Prof John Pang Hock Lye initiated preliminary research direction and assisted in editing the manuscript drafts.
- I prepared the manuscript drafts with Jinlong. The manuscripts were revised by Dr. Tan, and Dr. Hoh.
- I co-designed the experiments with Prof John Pang Hock Lye and conducted all laboratory testing and trials at the School of Mechanical and Aerospace Engineering.
- All microscopy analysis and testing, which include sample preparation, was conducted by me in the Materials Laboratory 1.
- Ivan and Si Yun assisted in collecting the maintenance data records for analysis.
- Dr Hoh assisted in the data analysis by providing direction and guidance in the methodology development.

21 March 2022

. . . . . .

Date

. . . . . .

N Alagu Subramaniam

Acknowledgement

First and most deserved acknowledgements are reserved for my research supervisor Prof John Pang who throughout my PhD study has been an exemplary guide and facilitator. His sincere and insightful advice always motivated me to continue persevering with my research in times of difficulty. His technical know-how and passion for research was a beacon that rubbed on to me and always guided me in fulfilling my research requirements while maintaining a high standard of scholarship.

I also extend my sincere appreciation to the thesis advisory committee: Prof Yang Yaowen and Assoc. Prof Zhou Kun for their insightful feedback to improve and widen my research. The research staff and students also deserve special mention for their guidance and valuable feedback particularly in the initial phases of my research when I was striving to steer my research out of the zones of ambiguity.

As my research work involves collaboration with SMRT, I am grateful for all the support from the public transport operator for providing the platform to understand the challenges in the railway network and how my research has the potential to immediately benefit the rail network. I am also appreciative of the support received from the respective project in-charge (PI), engineers and technicians for providing the required rail specimens, relevant data and arranging the track visit sessions which helped enhance my learning.

The cladding work on rail specimens which were used in my study was done in collaboration with Wilhelm Cladding Services, a third-party vendor I am thankful to for their assistance.

Special mention to all the NTU staff from Mechanics of Materials (MoM) Lab, Materials Lab 1, and SMRT-NTU Smart Urban Corporate Lab without the help of whom I could not adequately prepare my specimens for a long series of experimental works.

Table of Contents

List of Figures

List of Tables

Abstract

Rail failures due to excessive wear and other rail head defects is still predominant owing to the advanced railway systems with greater train traffic, higher train speed and axle load requirements. The sharp-radius curve tracks and crossing nose sections are especially susceptible to failures from extensive wear damage leading to significantly reduced service life. Regular maintenance and replacement of rails to address these failures will lead to lengthy queue for rail total replacement maintenance and high costs are incurred. Although premium rail steels and hardened rail heads can be considered as an alternative solution, it is not economically viable to replace the entire rail network using them. Hence laser cladding repair research was supported by the SMRT-NTU corporate lab project work.

The objective of this research is to investigate laser cladding technique for rail steel repair and reliability assessment. The research objective is categorised and focused to address four main concerns with regards to adopting laser cladding for rail steel repair which include: 1) Laser cladding material process characterisation study, 2) Wear testing & analysis for durability study, 3) Shear testing & analysis for delamination study, and 4) On-track reliability studies by installing laser cladded test specimens on depot test track and mainline test trials.

The present research direction involves a two-pronged approach. The first approach is to develop a strategy to research laser cladding experimental characterisation of rail steel and develop methodology for laser cladding repair and testing of localized rail head defects on critical rail components such as rails and crossing nose. The second involves pioneering research work to validate the durability and wear performance study as part of the SMRT-NTU research project on-track testing programme.

This is achieved by installing the laser cladded rail specimens on both test track and mainline track environment to evaluate full-scale reliability and performance of laser cladded rail steel when subjected to actual train loading conditions. Following the comprehensive reliability study, a portable and modular laser cladding machine design was developed for on-track rail steel clad repair operations.

Wear life prediction study for the different track and traffic conditions is of paramount importance in developing effective maintenance procedures. As part of the wear life prediction research, historical wear data is used to analyse rail wear degradation. In this statistical wear-life data analysis, the 2-parameter Weibull distribution model is used for wear-out degradation analysis and prediction which characterise wear out failure response for the rail sections at R300 radius and R500 radius curves. Additionally, Zarembski's rail service wear life model which correlates wear life and fatigue life is modified and extrapolated to conform with Singapore's railway system loading requirements where nominal wheel load is between 8 to 16 tons.

The experimental method for laser cladding of Stellite 6 premium alloy on R350HT pearlitic grade rail steel is developed. The cladding alloy is pre-selected based on literature study due to its promising wear resistant properties whereas the substrate material is a high carbon steel already employed in the railway tracks at sharp-radius curves of (Radius $\leq$ 500 m). As part of the detailed material characterisation research, microstructural analysis and hardness properties of the clad, the fusion zone, the heat-affected zone (HAZ), and the rail steel substrate has been studied.

To study accelerated testing of rail wear, the laboratory scale ball-on-disc tribometer test setup is used to study the wear behaviour of the clad material in comparison to the rail steel substrate. The wear coefficients for the clad material and rail steel are derived from the wear volume analysis using Archard's wear model. The experimental characterisation research also involves shear testing and analysis to study the clad/substrate material interface bond which is important for the assessment of delamination. The interface bond strength evaluated, and failure mode analysis demonstrate the presence of strong metallurgical bond between cladding material and rail steel.

Chapter 1 Introduction

1.1 Background

The railway industry has been constantly evolving with continued advancements in technology contributing to an accelerated growth of the railway transport system [1, 2]. The emergence of higher train speeds and larger axle loads along with increased traffic densities result in larger stresses & strains to be induced on the rails [3-5]. With these aggressive operating conditions, rail failures and replacement can escalate rapidly which is a major concern. Rails at curves and crossings are more susceptible to wear and failures as shown in Fig.1-1. In addition to increased maintenance and replacement of rails due to wear related failures, the constant train service disruptions will have a detrimental impact on the railway system performance and reliability. Laser cladding research for railway applications has been investigated and considered as a feasible solution to improve rail steel performance [6-12].

Figure 1-1: Worn Curve Rail Section (left) Worn Crossing Nose Section (right)

Wear and fatigue are two of the most important failure mechanisms affecting rail steel failures over the service life. In addition to significant reduction in service life, excessive rail wear also increases the likelihood of train derailment due to rail steel fractures.

As such, the ability to predict rail wear life is of importance in examining and developing suitable maintenance procedures. Besides wear, several other rail head defects also contribute significantly to rail degradation.

Some common defect types occurring on the rail head surface are presented in Fig.1-2 [13]. While the use of premium rail materials to install entire rail sections is not economically viable, laser cladding repair of these localized rail head defects will allow service life extension with enhanced wear properties. Hence, the need to mitigate total replacement and reduce financial burden resulting from replacing high-value rail components such as the crossing nose or rails at sharp curve sections essentially serve as a driving force to develop strategic laser cladding research objectives for repair & restoration.

Figure 1-2: Common rail defect types with potential for repair [13]

Laser cladding process, which is also termed as laser metal deposition (LMD) or direct energy deposition (DED) has emerged as a possible solution for repair and remanufacturing of worn or damaged surfaces of high value industrial components – turbine blades in the aerospace, drill shafts in the oil and gas, and engine valves in the automotive industry [14]. The deposition of premium clad material alloy is in the form of either wire or powder.

Laser cladding in the form of powder deposition offers diverse material selection range, relatively low dilution rates and precise deposition that is ideal for most industrial applications.

Unlike conventional surface coating techniques such as plasma arc welding (PAW) and gas tungsten arc welding (GTAW), laser cladding allows strong metallurgical bond formation between clad layer and substrate while ensuring minimal dilution [15].

Although past research carried out demonstrate feasibility of implementing laser cladding for railway applications, there is constrained scope of research on the reliability study of rail steel repair and application on actual test track environment.

The motivation for the research study arises from an opportunity to test and evaluate laser cladding durability, delamination and reliability performance of laser cladded rail steel in service.

Experimental characterisation of laser cladding on rail steel is studied to evaluate feasibility for laser cladding repair of localized rail head defects on critical rail components such as the rails at curves and crossing nose. Research methodology is developed to investigate rail wear, using a laboratory scale ball-on-disc tribometer test setup to investigate the wear behaviour of the clad material in comparison to the rail steel substrate. The purpose of the rail wear testing and analysis study is to evaluate durability of the clad material with respect to the rail steel substrate for service life extension. The study of clad/rail substrate material interface bond shear strength by shear testing and analysis is also important for the assessment of delamination.

On-track studies are conducted by installing the laser cladded rail specimens on both test track and mainline track environment to evaluate full-scale reliability and performance of laser cladded rail steel when subjected to actual running train load conditions. The reliability assessment is then followed up to investigate and study on-track rail steel repair and testing capability by designing and developing a portable and modular laser cladding system.

1.2 Research Objectives & Novelty

The purpose of the present research is to investigate durability and delamination of laser cladding on rail steel with the aid of experimental characterisation and reliability test studies. On-track reliability test methodology is then developed for laser cladding repair of rail head defects. The laser cladding research involves the design and development of a portable laser cladding system for rail steel defect repair study of critical rail components such as rails on curves and crossing nose on railway track.

The research objectives are as follows:

1. Study and analysis of rail wear degradation by using maintenance service data. Rail sections are subjected to different track, train traffic, maintenance and operating conditions which may lead to failure at different time intervals. The time to failure obeys a probability distribution which indicates whether a particular rail section fails within a specified time. While different probability distribution models are used for failure analysis and prediction, the 2-parameter Weibull distribution model is used in the current analysis as it is most widely used in research due to its ability to provide reasonably accurate failure analysis and prediction [16, 17]. A research methodology is developed for failure analysis and prediction using the historical rail wear data.

2. Material characterisation research of laser cladding Stellite 6 clad material with R350HT rail steel substrate. A cobalt-based alloy, and Stellite 6 grade in particular is selected in this research due to its superior mechanical properties and proven capability in high wear applications such as the marine, and oil & gas industries [18-25]. The metallurgical study involves: (a) Cross-section micrographic analysis of the cladded rail steel, (b) Cross-section microstructural analysis of the cladded rail steel, (c) Compositional analysis, (d) Hardness analysis across the clad-rail section.

3. Experimental characterisation study involving wear testing and analysis of laser clad material and rail steel. A laboratory ball-on-disc setup is used to investigate rail wear and evaluate durability of cladding layer.

4. Shear testing and analysis is used to investigate and evaluate the clad/substrate material interface bond shear strength for assessment of delamination.

5. On-track studies to evaluate full-scale reliability and performance of laser cladded rail steel on track environment when subjected to actual train loading conditions was conducted. The full-scale reliability test is a strategic approach to assess feasibility of laser cladding repair of localized rail head defects on critical rail components such as rails at curves and crossing nose.

6. Design and development study for a portable and modular laser cladding system for on-site rail repair is investigated. The approach of conducting laser cladding repair of rail head defects which involves extracting specimens from the railway track and carrying out repair trials off-site in a laboratory environment prior to reinstalling the specimens on the track for service from an operational perspective was first investigated. The current study aims to develop a portable, modular laser cladding system design for on-track repair of localised rail head defects and crossing nose defects.

Novelty and research contribution

Research on implementing laser cladding technique in various industrial applications for enhancement of surface properties or component repair has been discussed and reported in literature as an alternative solution to total replacement [26-30]. The study of railway component repair for service life extension have demonstrated the potential for using laser cladding for rail and crossing nose defect repairs.

A comprehensive reliability test methodology was developed to deposit 1-mm cladding layer on rail steel specimens which are then installed on running rail tracks to investigate reliability performance when subjected to actual running train loads to determine if the cladded material develop interface cracks or service wear behaviour.

The current study contains novel aspects of laser cladding research for rail steel repair and reliability assessment that requires deeper research investigations. A portable, modular laser cladding system was developed for repair of localised rail head surface defects and crossing nose repair applications. The design and characterisation of the robotised laser cladding system enables rail and crossing nose repair operations on the railway track.

Laser Cladding Research for Rail Steel Repair and Reliability Assessment

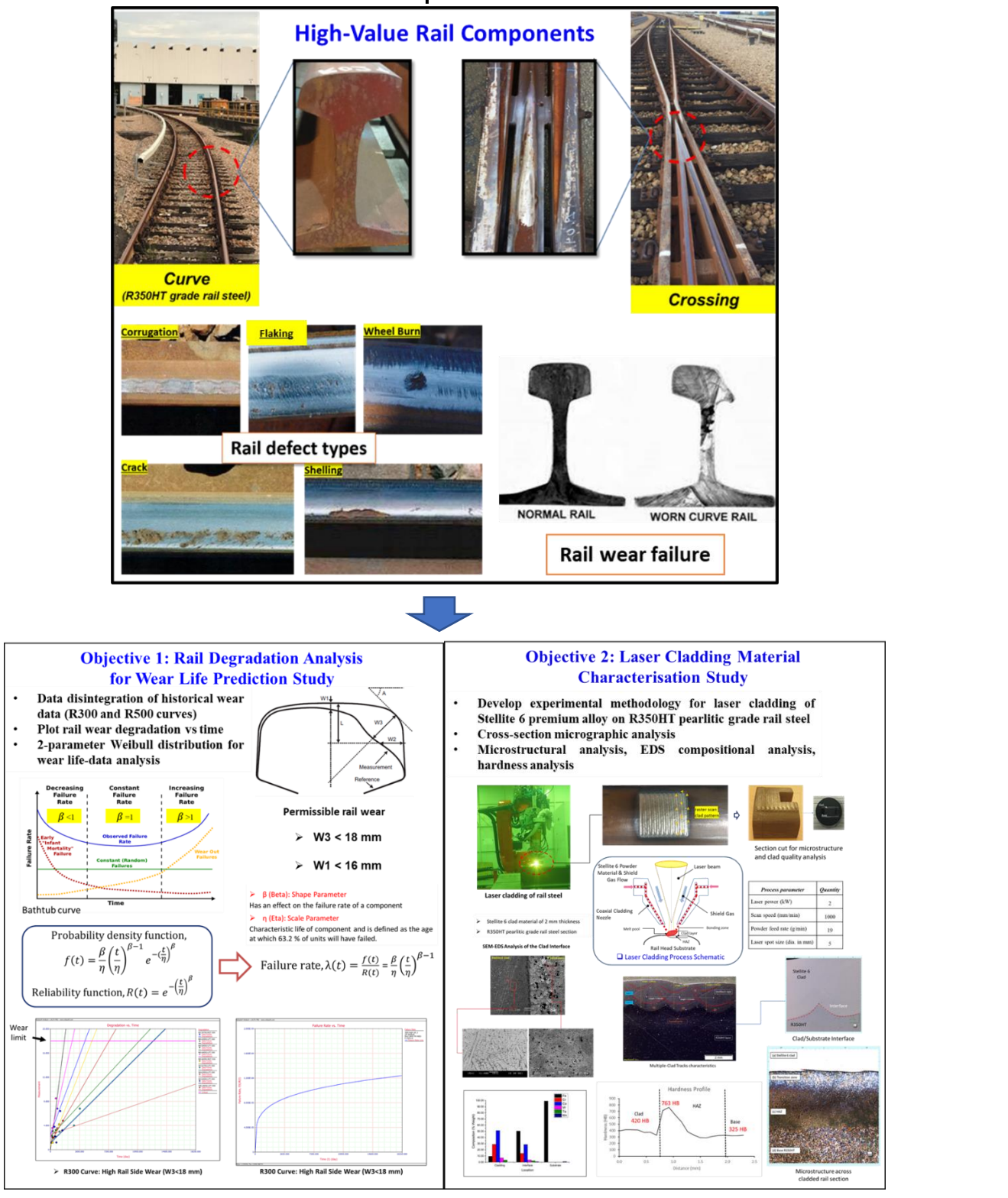

Figure 1-3: a) Framework highlighting the main objectives of PhD research (continued…)

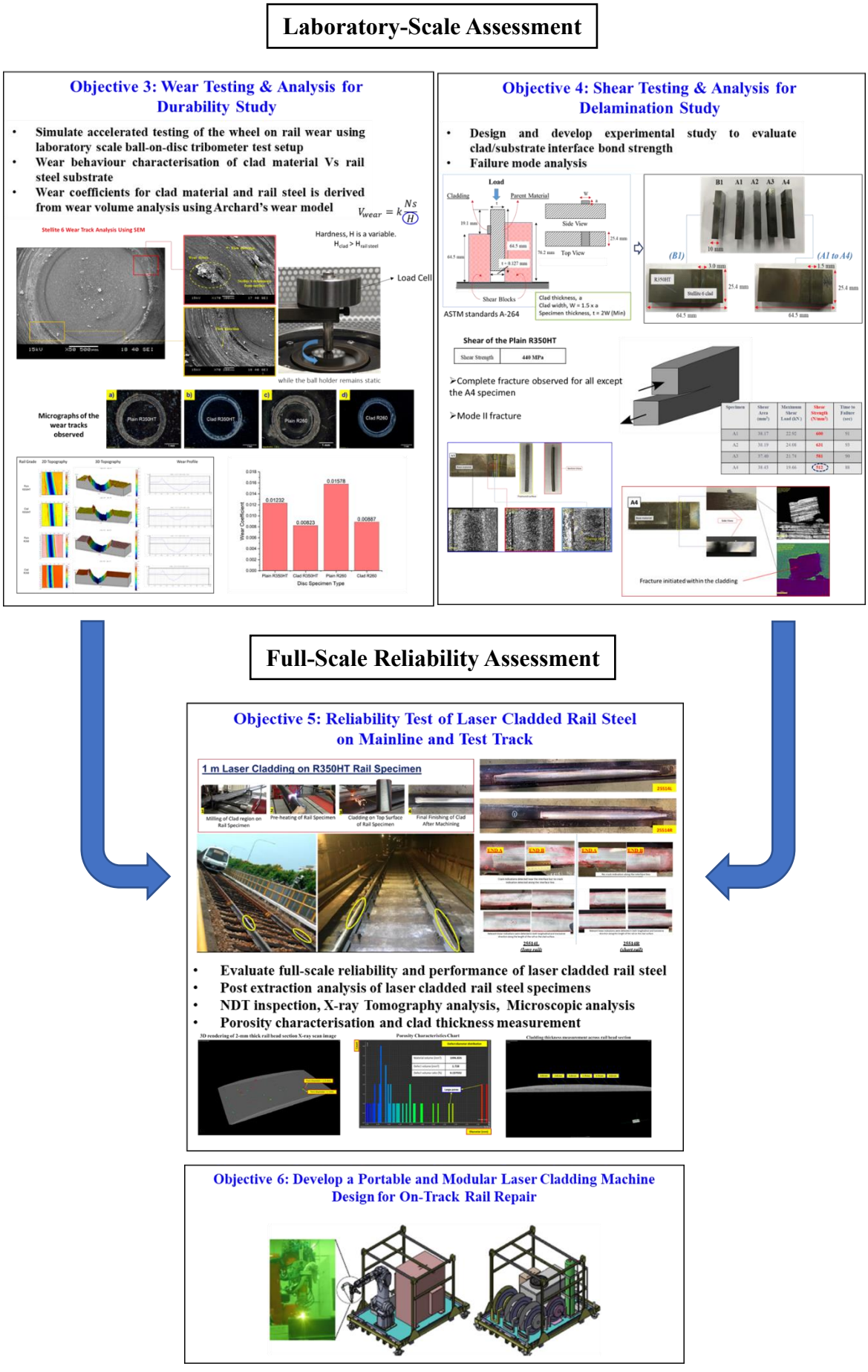

Figure 1-4: b) Framework highlighting the main objectives of PhD research

A framework of the current research progress is presented in Fig.1-3. It comprises of the wear degradation analysis, laser cladding experimental method, wear and shear testing study, reliability assessment of the cladded rails installed on actual track environment, and the design and development of a portable, modular laser cladding system.

1.3 Scope and Outline of Thesis

The thesis has been categorized into eight chapters and is as follows:

Chapter One introduces the key challenges faced in maintaining a reliable rail network and how strategic implementation of laser cladding has the potential to address these challenges. The PhD research framework underlining the main objectives and novelty are also clearly identified in this chapter.

Chapter Two discuss the literature review carried out and research gap identified. In this section, a detailed study of the laser cladding process is conducted, and the suitable premium alloy cladding materials and its properties are evaluated. A comprehensive review on pearlitic grade rail steel and rail wear assessment has also been conducted with the different methods for evaluating rail wear discussed. Finally, the existing research on laser cladding for railway applications and the potential for further research has been summarized.

Chapter Three presents research on rail wear degradation by conducting analysis of real time maintenance wear data. Statistical wear-life data analysis using the 2-parameter Weibull distribution model for failure analysis and prediction is valuable in developing effective maintenance strategies for reliable operation of the railway track system. Additionally, rail service wear life from Zarembski's model is modified by extrapolating to conform with Singapore's railway system loading requirements.

Chapter Four describes the experimental methodology for laser cladding of Stellite 6 material on R350HT pearlitic grade rail steel. Material characterisation involving cross-section microstructural and hardness measurement analysis of the clad, fusion zone, HAZ, and the rail steel substrate demonstrates clad material compatibility with rail steel.

Chapter Five presents study on wear testing and analysis using the ball-on-disc tribometer setup to investigate rail wear. The study comprises of characterizing wear performance of clad material in comparison to the rail steel. The wear coefficients for the clad material and rail steel are derived from the wear volume analysis using Archard's wear model.

Chapter Six describes further characterisation research work that focus on shear testing and analysis to investigate the clad/substrate material interface bond shear strength for the assessment of delamination.

Chapter Seven covers pioneering research work to perform full-scale reliability test of laser cladded rail steel on railway track environment and evaluate structural integrity of the cladding layer when subjected to actual train loading conditions. Post extraction analysis of the laser cladded rail steel specimens is also discussed which include Non-Destructive Testing (NDT) inspection, X-ray tomography analysis and micrographic analysis.

Chapter Eight examines the industrial implementation of laser cladding technology for on-track rail repair operations with the design development of a portable and modular laser cladding system.

Chapter Nine focus on the overall conclusion of the research and recommendation for future work.

Chapter 2 Literature Review

An extensive review investigating existing laser cladding research on rail steel materials and rail wear life prediction models has been carried out. In this chapter, key research gaps are identified with objectives aligned towards developing a strategy for laser cladding rail steel repair and testing methodology for reliability assessment.

The scope of review focus on the various classification of premium materials that are available for selection in the current laser cladding research which is presented in Section 2.1. The limitations in scope of research are identified by reviewing previous studies on laser cladding for rail steel applications, discussed in Section 2.2. The experimental characterisation work to evaluate delamination and durability of cladding layer in comparison to rail steel substrate material is studied and discussed in Sections 2.3 and 2.4 respectively.

The chapter is concluded with the research gaps and potential for new research identified in Section 2.5.

2.1 Review on Material Selection for Laser Cladding

2.1.1 Laser Cladding Process Definition and Applications

Laser cladding, also referred to as laser metal deposition (LMD) technique is a powder blown metal additive manufacturing technique widely used for surface treatment. A laser is used as the energy source to direct heat input across the metal substrate surface to be clad. The heat input then creates a thin melt pool on the substrate surface while cladding powder material from a coaxial powder nozzle head is deposited concurrently onto the melt pool and fused with the substrate forming a single-track cladding layer. Subsequent deposition of overlapping clad track layers allows cladding whole metal surfaces [14]. A schematic representation of the cladding process is shown in Fig.2-1.

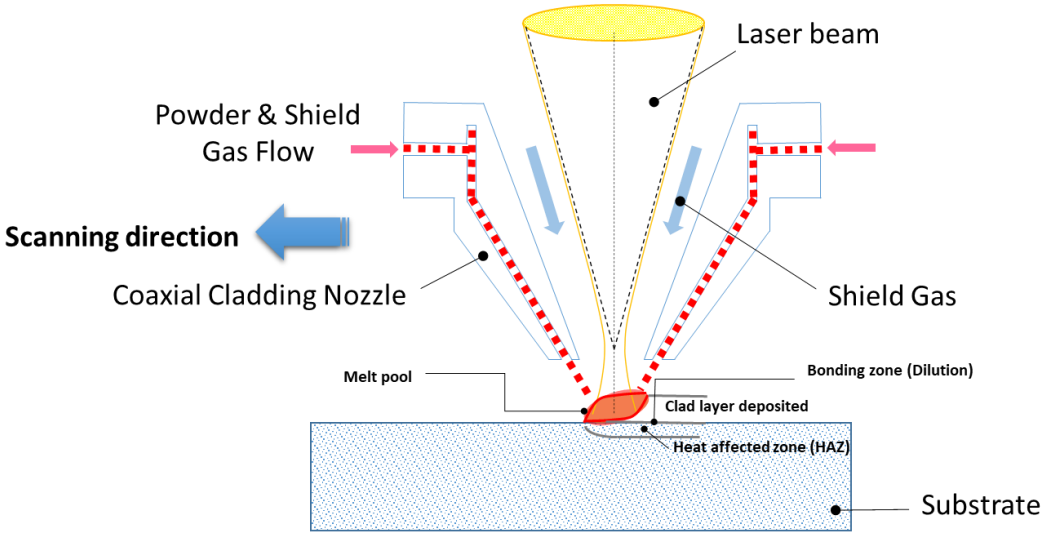

Figure 2-1: Laser cladding process illustration [31]

Laser cladding is an emerging technology in the field of surface engineering. The high energy density, versatility and selectivity of the laser beam allow production of high quality thick metallic coatings with fusion bonding to the substrate and required amount of dilution. The characteristic of this process permits applicability for rapid prototyping and component repairing [30, 32-35].

As compared to conventional coating techniques, laser cladding offers an extensive range of advantages which include the formation of excellent metallurgical bonding between coating and the substrate while maintaining acceptable dilution (mixing) percentage.

The process overcomes some of the obvious drawbacks evident in plasma, thermal spray coating and arc welding techniques. In the case of plasma and thermal spray coating, the coating layer maybe susceptible to delamination or detachment due to lack of fusion between coating materials and substrate, whereas the likelihood of distortion is very high as a result of excessive heat input when arc welding techniques are used [14, 36, 37].

A few commercial applications of laser cladding that demonstrate capability to repair surface high-value damaged components such as the steam turbine blades, and wheel hub of mining truck to improve surface wear and corrosion resistant properties for service life extension are presented below in Fig.2-2.

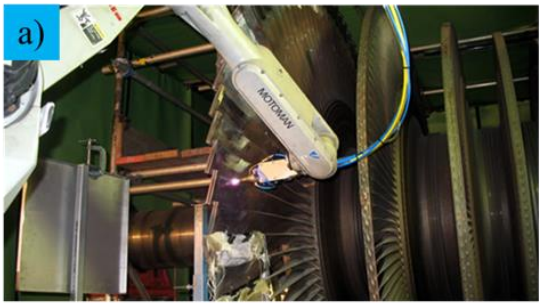

Source: Hardwear Pte Ltd

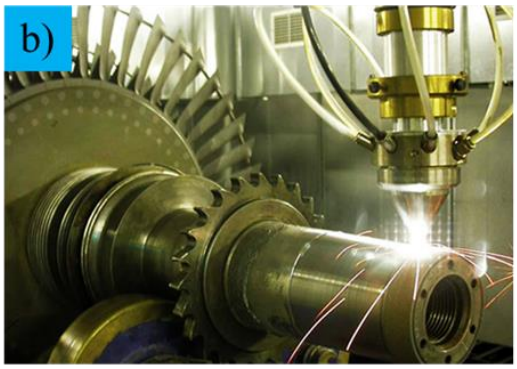

Source: GE Oil & Gas

Source: F.W. Gartner Thermal Spraying

Figure 2-2: a) In-situ laser cladding repair of turbine blades, b) Laser cladding of worn steam turbine blades, c) Wheel hub from a mining truck undergoing robotized laser cladding

2.1.2 Clad Geometry Characteristics and Process Parameters

A cross section illustration of a clad track metallurgically bonded on a substrate indicating the clad geometry characteristics is presented in Fig.2-3 below.

The parameters marked in the figure are as follows: clad height h_c, clad width W_c, clad area A_c above the substrate surface, fusion area A_f below the substrate surface, melt depth h_f, and heat affected zone (HAZ). Dilution is one among the various aspects that is used to quantify clad quality.

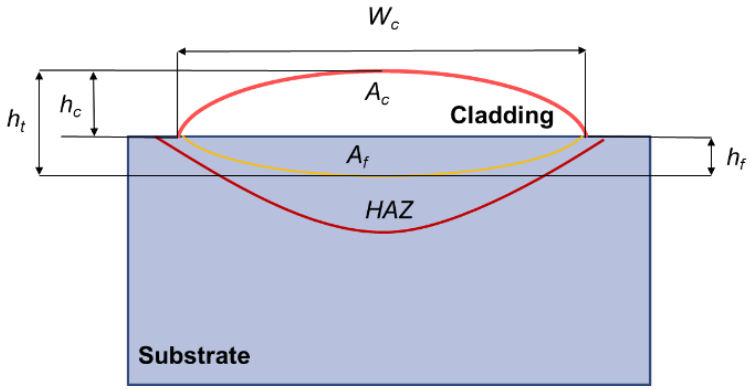

Figure 2-3: Illustration of a clad track cross section [38]

Dilution is referred to as the fusion ratio between the cladding and substrate material. This ratio can be correlated with clad geometry which is then defined by *Equation (1)* below [39, 40].

$$d = \frac{A_f}{A_f + A_c} \times 100\% \approx \frac{h_f}{h_f + h_c} \times 100\% \quad (1)$$

For multiple clad track deposition where overlapping is present, the overlap ratio is determined as follows:

$$O_R = \frac{W_c - d_R}{W_c} \quad (2)$$

Where d_R is the lateral displacement of successive tracks. A schematic representing the overlapped clad tracks is shown in Fig.2-4. The dashed circles in the figure indicate regions where the clad toes are formed between overlapping clad tracks.

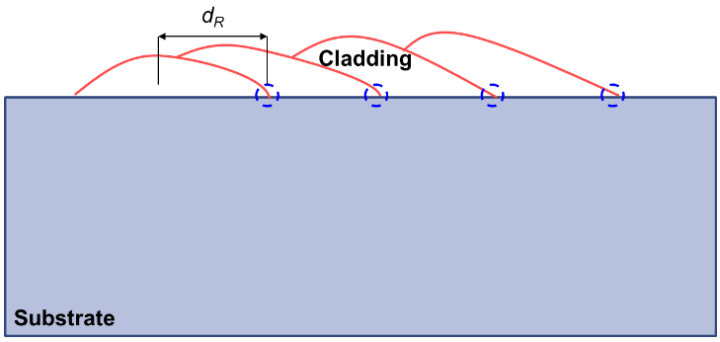

Figure 2-4: Schematic representation of overlapping clad tracks [38]

The properties and quality of laser cladding coatings are extremely sensitive to the type of laser system, materials and process parameters. The selection of each factor is mostly dependent on the application. With the laser system and materials decided, an optimal laser cladding process is attained by adjusting the process parameters accordingly. Process optimizations include deposition of uniform and continuous clad tracks (clad width ≈ laser spot size) with minimum melting of the substrate while ensuring good metallurgical bonding. The duration for post machining is also affected by clad geometry since the cladded surfaces are produced by overlapping adjacent tracks.

While there is a whole complex network of variables that are involved in the laser cladding process, the most significant process parameters which influence cladding quality are **laser power**, **cladding speed**, and **powder feed rate** [41, 42].

The current research objectives however do not involve investigating the influence of process parameters on clad quality.

2.1.3 Premium Laser Cladding Powder Metal Alloys

Cobalt, nickel and iron based alloy powders are three types of the fundamental cladding materials used for surface enhancement [38]. The powder is typically generated through gas atomization which permit the melted powder particles to cool rapidly during the cladding process resulting in formation of extremely small grain sizes [43]. Addition of various carbide and ceramic powder such as WC, SiC, TiC, Al2O3, Cr2O3, etc. in the alloys enhance mechanical properties such as wear resistance and strength [38].

Among the three alloy types mentioned, the cobalt-based alloys also known as Stellite are widely accepted class of alloys for applications that involve wear resistance improvement of mechanical components.

Besides the carbon element, Stellite comprise of other elements such as chromium, nickel, tungsten, and molybdenum. The property of each element is defined below [44]:

- Chromium form carbides providing additional strength in the cobalt matrix for improved oxidation and corrosion resistance
- Nickel enhances ductility and minimizes susceptibility towards cracking
- Tungsten and Molybdenum, due to their relatively large atomic sizes have capability to deform the crystal lattice of cobalt matrix and contribute to increased strength

The dominant type of carbides present in the Stellite clad layers are usually of the chromium rich type (M_7C_3, M-metal) with an approximate hardness ≈ 2200 HV, hence providing the required hardness in cladding (550 HV) resulting in superior wear properties [44]. Depending on the type of application, carbides, borides, and nitrides of high melting point can be further combined with the existing cobalt alloy directly to increase wear resistance [45, 46].

Altering the chemical composition of the powder alloy material can result in the cladding deposited to have superior mechanical properties and withstand aggressive operating conditions. However, the present scope of study does not cover this aspect of analysis. On the contrary, the objective of this section is to understand and identify the premium cladding alloy materials prior to selection of a suitable cladding material for laser cladding on rail steel.

A cobalt-based alloy, and Stellite 6 grade in particular is selected in this research due to its superior mechanical properties and proven capability in high wear applications such as the marine, and oil & gas industries [18-25].

Early research on Stellite class alloys have successfully investigated and correlated the microstructural behaviour with its superior wear resistant properties [47, 48].

Stellite 6 then emerged as a popular choice of study in thermal and plasma spray coating techniques where its mechanical and metallurgical properties were characterized [20, 49, 50]. Besides wear assessment at room temperature, the wear properties and were evaluated at high temperature along with the thermal fatigue performance [51-53].

With the emergence of laser cladding, several research studies aim to characterize the clad microstructure of Stellite alloy and assess material compatibility with the substrate material [19, 54, 55]. Impact wear analysis of laser cladded valve seats, comparison of microstructure and wear behaviour between laser cladded and arc weld produced Stellite 6, nano-indentation study to evaluate mechanical properties of laser clad Stellite 6, and, solid particle erosion and cavitation resistance investigation of laser cladded Stellite 6 are some of the other laser cladding research works that has been carried out with Stellite 6 clad material [18, 56-58].

While existing research aims to characterize the metallurgical aspects and wear characteristics of Stellite alloys from cladding process but usually do not discuss its implications on the mechanical performance of rail steel and its reliability for railway track applications.

2.2 Review on Laser Cladding of Rail Steel

2.2.1 Rail Steel Metallurgy (R260 Grade Vs R350HT Grade)

Rail can be considered as the most critical element in a railway track system and is commonly made from pearlitic steel due to their favourable metallurgical structure and superior wear resistance [59, 60]. The standard R260 grade (at straights and gentle curves of radius $R \geq 500$ m) and premium R350HT grade (at sharp curves of radius $R \leq 500$ m) are used in service on the Singapore railway tracks.

In a pearlite structure, the arrangement of iron and iron carbide lamellae, grain size, and the inter-lamellar spacing have a significant role in determining the hardness of the rail steel which directly relates to its wear resistance. The standard R260 grade rail steel has pearlitic microstructure whereas the head hardened premium R350HT grade rail steel has a fine pearlitic structure [61]. A comparison of the microstructure and lamellar spacing for R350HT and R260 are presented in Fig.2-5.

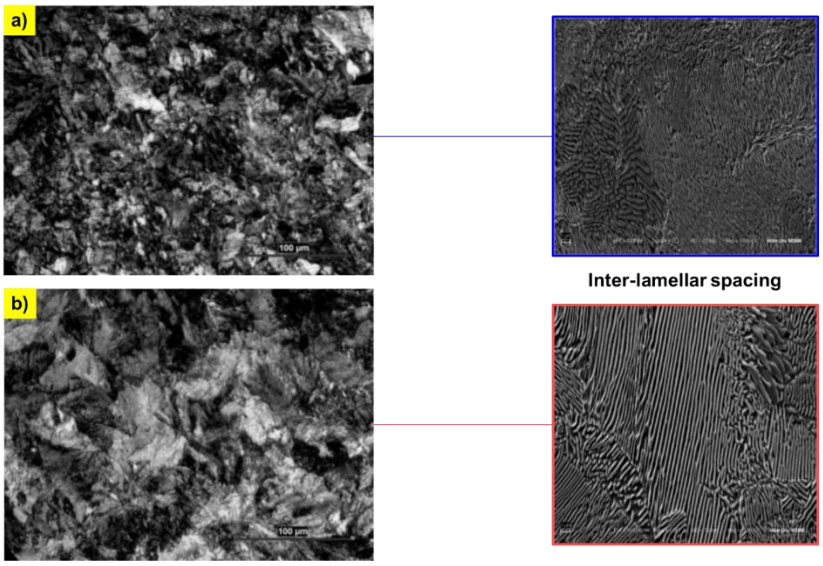

Figure 2-5: Micrographs of a) R350HT b) R260 rail steel [61]

Reducing the inter-lamellar spacing and grain size of pearlitic structure via appropriate heat treatment and controlled cooling leads to higher hardness of the rail steel.

In accordance to the European rail standard EN13674, both the rail steel grades are observed to have an identical chemical composition whose carbon content lies between 0.6 and 0.8 %.

The primary difference between the two steel grades are as follows [62]:

- Heat-treatment condition
    - "Naturally cooled" for R260, and "controlled cooling" for R350HT
- Minimum Hardness
    - 260 HB for R260 grade and 350 HB for R350HT grade
- Tensile Strength
    - 880 MPa for R260 and 1,175 MPa for R350HT

Due to its superior mechanical properties, the R350HT grade exhibits excellent wear resistant properties in comparison to the standard R260 rail steel - 3 times more wear resistant than standard rail grade [63]. For this reason, railway track systems make use of the R350HT grade rail steel, particularly in tight curves to withstand severe wear and other rail head failures.

2.2.2 Laser Cladding Research on Rail Steel

There is a need to mitigate total replacement and reduce financial burden resulting from failures of high-value rail components such as rail sections at sharp curves and crossing nose by developing a strategic approach for laser cladding repair.

Laser cladding research in the railway industry has shown considerable promise. Some of the substantial research conducted to assess feasibility of laser cladding for rail steel is summarized in Table 1.

Table 1: Review of Laser Cladding Research on Rail Steel

Type of study	Key Objectives	Research Gap	Author/citation
[A] Laser cladding for railway repair and preventative maintenance	- Assess suitability of premium clad materials for R260 grade rail repair - Clad-rail interface study with emphasis on microstructure and hardness property	1) Nd: YAG laser source is a dated laser technology with relatively poor energy efficiency. 2) Only investigated standard R260 grade rail steel 3) Proper wear analysis was not done from ball-on-disc tribometer tests as focus was on comparing the work-hardening behaviour of rail and cladding	*Adam Clare et al [8]* ***2012***
[B] Laser cladding of rail steel with Co–Cr	- Assess suitability of clad material on R260 grade steel - Clad-rail properties such as microstructure, hardness and wear performance studied		*Adam Clare et al [7]* ***2013***

[C] Assessment of laser cladding as an option for repairing/enhancing rails	- Assess rolling contact fatigue (RCF) performance of premium clad materials on R260 grade rail steel	1) Laser source used for cladding Nd: YAG/CO_2 laser 2) Type of cladding methodology differs as disc specimens were extracted from rail and wheel sections whereas for the other research cladding was done on flat plate specimens extracted from rail. 3) Type of wear test methodology differs where a twin disc setup is used to assess wear and RCF performance.	*Lewis et al [6]* ***2015***
[D] Improving rail wear and RCF performance using laser cladding	This 2nd phase of research is an extension of previous work that involves testing of new clad materials with increased number of test cycles for a more comprehensive assessment of RCF performance		*Lewis et al [9]* ***2016***

[E] Laser cladding of rail; the effects of depositing material on lower rail grades	- Evaluate wear performance of laser clad material, martensitic stainless steel (MSS) on two specific lower rail steel grades (R260 & R200)	1)Focus was on the study of laser cladding effect on lower rail steel grades. (Mainly R260 and R200) 2)Wear study on a different laser clad material proposed which is the martensitic stainless steel (MSS).	*Lu Ping, Lewis, et al [64]* ***2019***

Clare demonstrated via on rail deposition the potential of laser cladding to enhance rail service life [7, 8]. Likewise, Lewis, et al evaluated capability for rail repair by conducting twin disc tests to study wear and rolling contact fatigue (RCF) performance of laser cladded rail steel [6, 9]. Among the several clad materials examined, a cobalt-chromium alloy known as Stellite 6 exhibited favourable characteristics with the standard R260 grade rail steel. The cladding research on rail steel from Sheffield and Nottingham is illustrated in Fig.2-6 below.

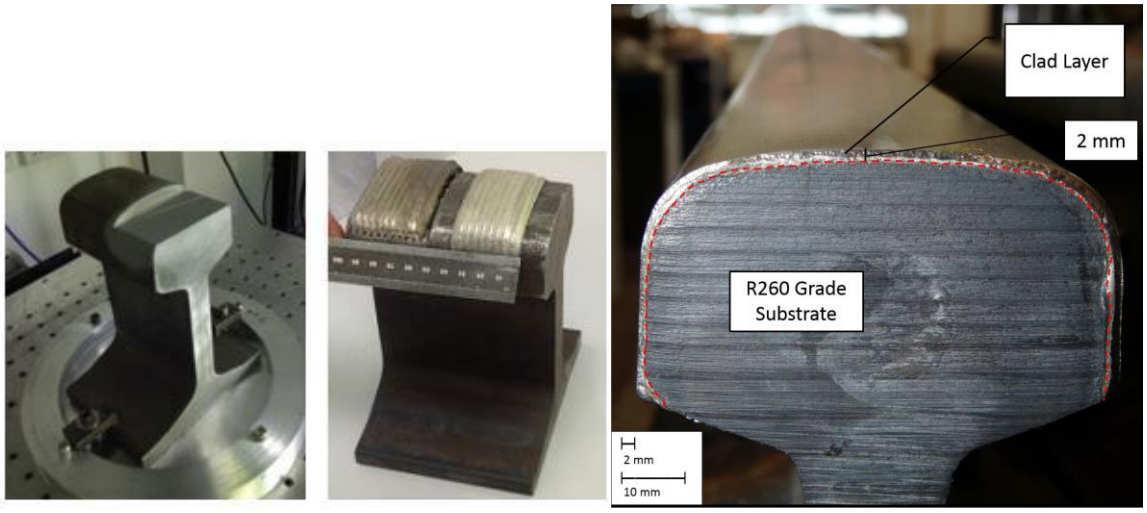

Figure 2-6: Laser cladding on rail steel research by Nottingham University *(left)* and Sheffield University *(right)* [8, 65]

The objectives of existing research primarily focused on substrate material study involving the standard R260 grade rail steel. Twin disc wear setup has been used primarily to demonstrate improved rolling contact fatigue (RCF) performance of the cladding. Whereas ball-on-disc wear setup is used to characterize work hardening behaviour of the clad-substrate.

Lai, Quan and Roy, Taposh, et al have also achieved promising results from studies demonstrating laser cladding feasibility on hypereutectoid rail steels and investigating the effects of heat treatment on mechanical properties, wear and RCF performance of the cladded hypereutectoid rail steels [10-12, 66].

Research on experimental characterisation of laser cladded rail steel addressing concerns on the durability and delamination study of Stellite 6 cladding on R350HT premium grade rail steel substrate has not been investigated.

2.3 Review on Shear Testing and Analysis

Shear testing and analysis is an important assessment criterion to evaluate bond strength at the clad/substrate interface. The present characterisation study requires identifying the suitable testing method to validate the cladding layer forms a strong metallurgical bond with the rail steel substrate in order to avoid delamination.

A customized shear test setup as shown in Fig.2-7 was used by Mingsan to investigate the influence of different powder materials and process conditions on bonding shear strength and hardness in laser cladding for remanufacturing applications [67]. In addition to a round carbon steel bar as the substrate, cladding materials such as iron-based and nickel-based metallic powders were selected in the study to evaluate the bond strength. The iron-based clad material possessed greater bond strength with the carbon steel substrate when compared to the nickel-based alloy as results showed powder type to have the greatest influence on bonding strength while laser power was observed to have the least impact.

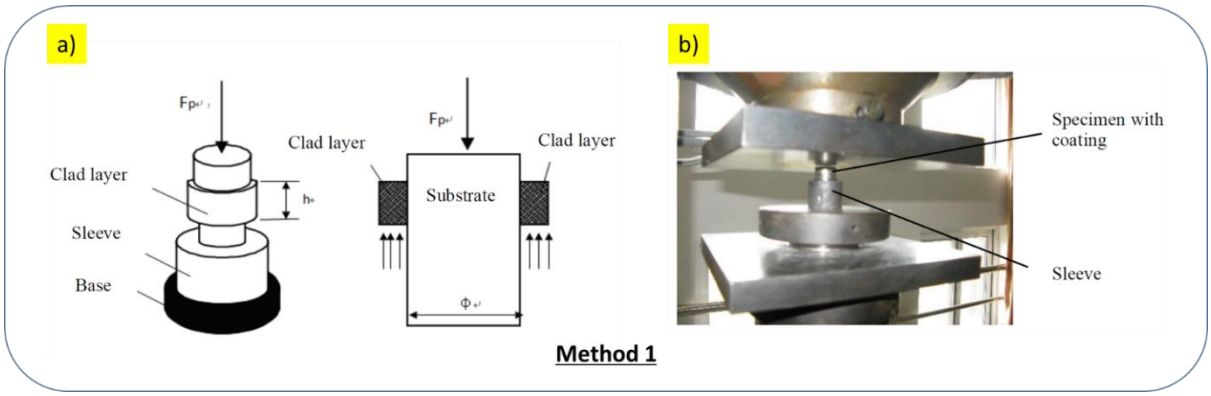

Figure 2-7: a) Schematic representation and b) Actual shear test setup [67]

According to another study by Zina, shear testing was conducted in accordance to American Standards ASTM A-264-12 (Fig.2-8) to evaluate the interfacial morphology and characteristics of low-carbon steel/austenitic stainless steel clad composite fabricated by hot-roll bonding [68, 69]. Shear strength was one of the parameters used to assess the bonding quality of the clad material and then correlate mechanical properties with the interfacial morphologies.

The tests revealed the cladded steel plates to exhibit 22% higher bond strength than that of the parent metal and fracture was observed to occur in the parent metal hence corresponding to strong metallurgical bond between the cladding and parent metal.

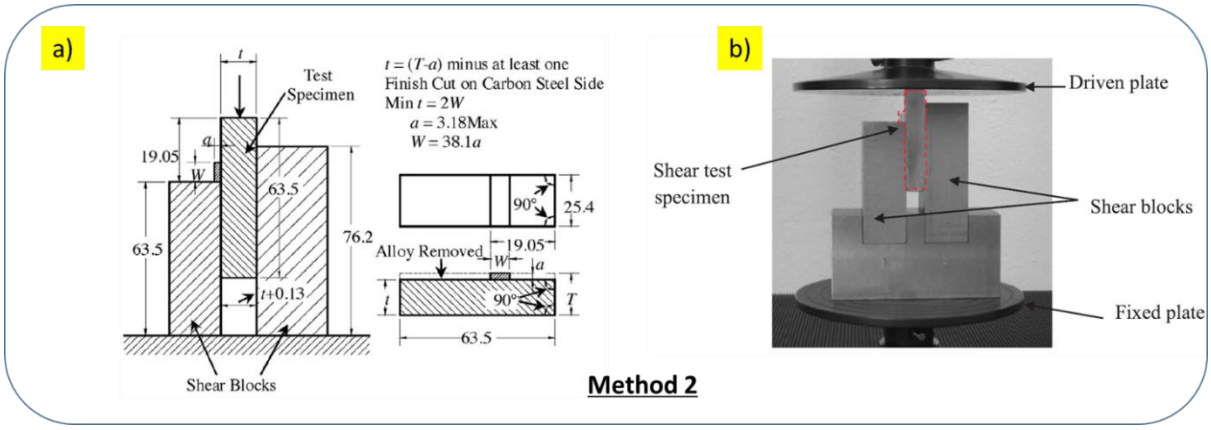

Figure 2-8: a) Schematic representation and b) Actual shear test setup based on ASTM A-264 [69]

Among the two methods reviewed, *Method 1* is ideal for laser cladding analysis of pipe structures for offshore remanufacturing applications such as the oil and gas, and mining industries.

In the case of laser cladding study of railway components, where the track is subjected to multiple loading elements as shown below in Fig.2-9, *Method 2* is more appropriate and hence selected for evaluating the structural integrity of the clad layer. Results from the study will be important in determining whether delamination is likely to occur when the cladded layer on the rail head surface is subjected to train loads.

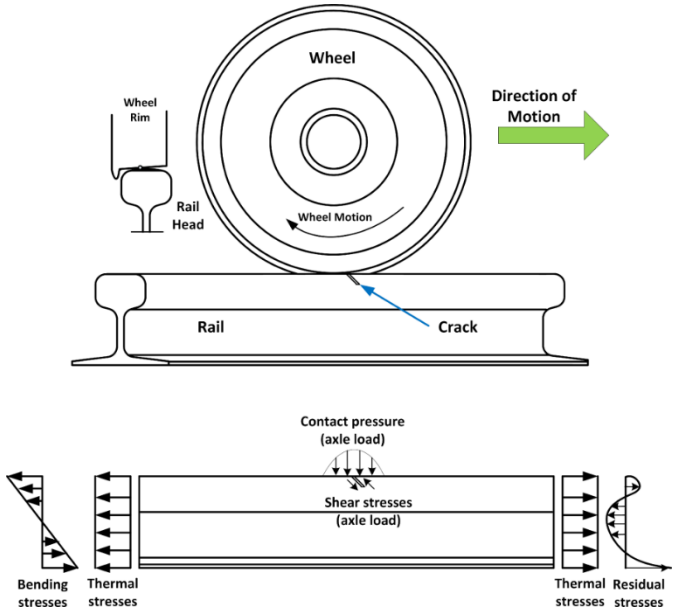

Figure 2-9: Rail-wheel contact zone in correlation with stress distribution [70]

The literature reviewed show very limited research has been carried out with regards to the shear testing and analysis of laser clad/substrate material interface and no study is conducted to investigate the interface bond strength between cladding and rail steel.

2.4 Review on Wear Life Prediction & Models

In order to develop a strategy for rail wear life prediction based on laboratory scale assessment and actual service wear life, the review of the rail wear assessment and relevant wear models is important.

2.4.1 Wheel-Rail Contact System

Rail wear is a phenomenon that occurs primarily due to the wheel-rail interaction (contact). This interaction can be either vertical, lateral or longitudinal (Fig.2-10). While vertical interaction arises from vertical forces between the wheel and the rail, lateral/longitudinal interaction includes forces that act in either lateral or longitudinal direction due to wheel-rail creep or flange forces [71].

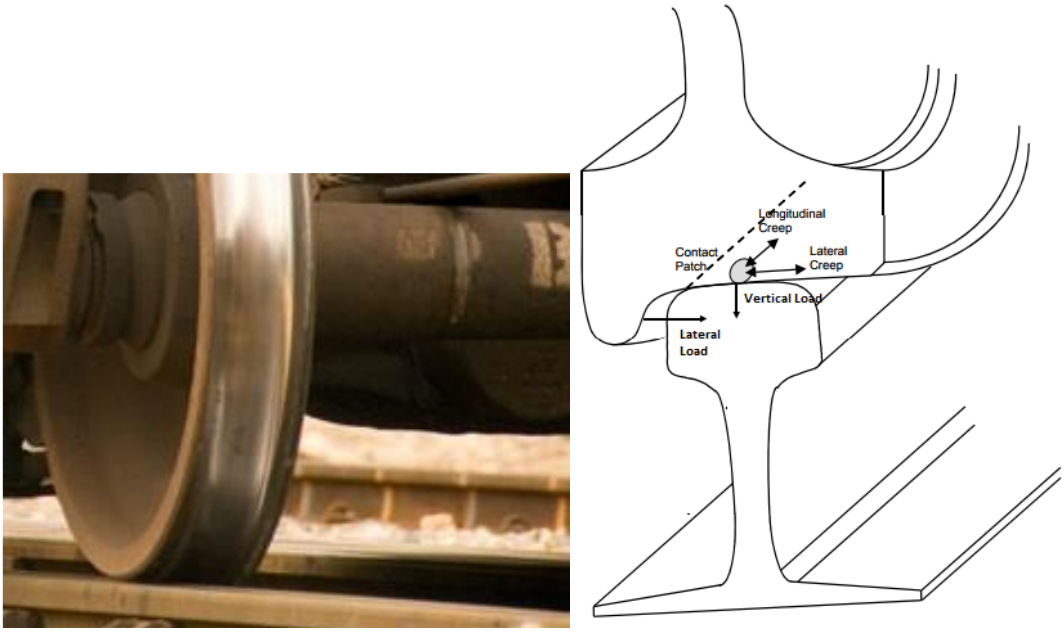

Figure 2-10: Wheel-rail contact pair and loading illustration [13, 72]

The contact geometry between wheel and rail has a major impact on the railway vehicle dynamics and is influenced by several factors including the wheel and rail profile [73]. The usual contact patch size based on research was identified to be about 1 cm^2. The precise location of contact between the wheel and the rail is dependent on the wheel/rail profiles and the degree of curvature of the track. For a straight track, the contact is between rail head and wheel tread whereas in the curved track, the contact occurs on wheel flange and rail gauge corner. The wheel-rail contact zones are illustrated in a schematic in Fig.2-11.

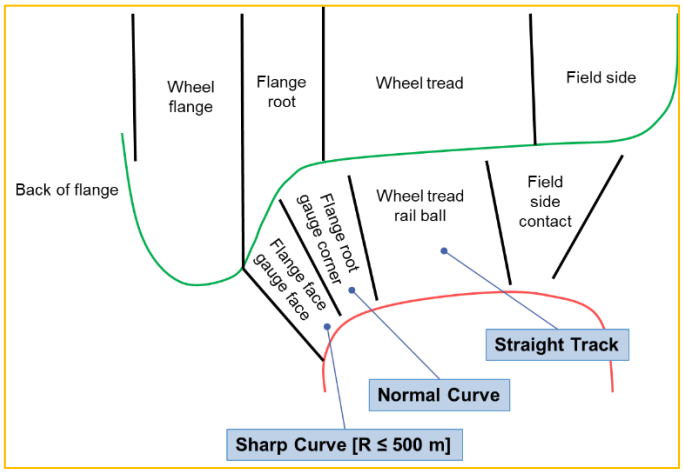

Figure 2-11: Wheel-rail contact zone [74]

Generally, the dominant form of contact in straight tracks is rolling as there is little slip and the type of wear mechanism is vertical abrasion wear. Characterisation of contact area in straights is as follows [74]:

- Wheel-rail contact stresses much lower in comparison to other regions
- Longitudinal creep forces are larger than lateral creep forces
- Likelihood of wheel depression due to wear

2.4.2 Rail Wear Testing

Measurement and monitoring of rail wear performance on track is performed via two methods.

- Use of a laser-based rail profile scanner (Fig.2-12)

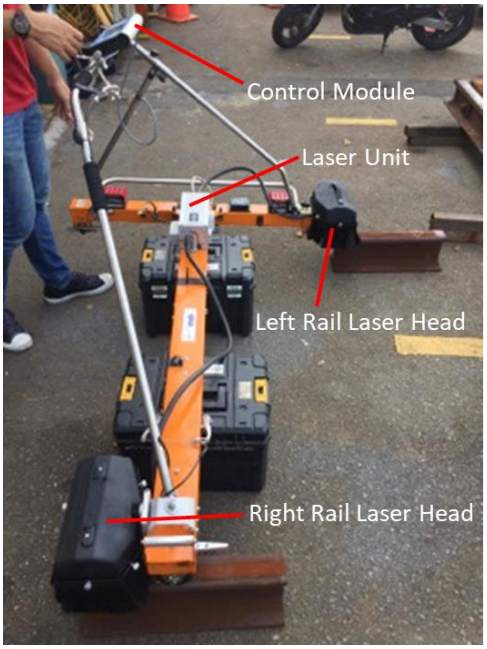

Figure 2-12: Rail profile scanner*

*Picture Courtesy – SMRT Corporation

- Using a taper gauge to manually measure the wear (Fig.2-13)

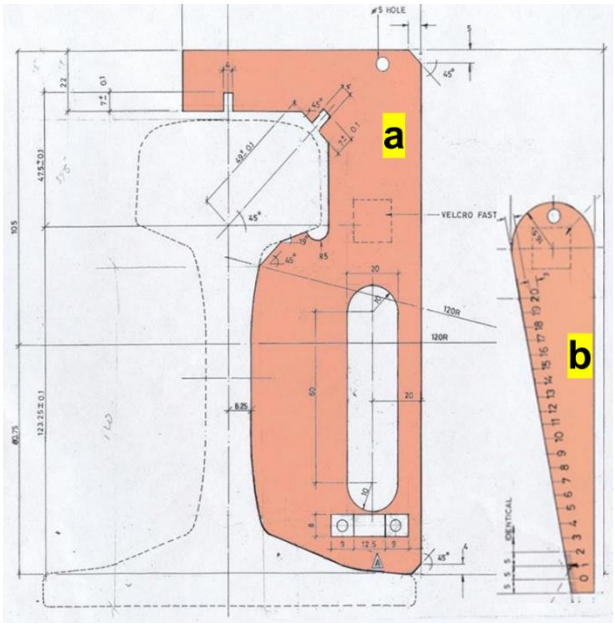

Figure 2-13: Rail wear measurement tool*- a) Rail measurement template b) Taper gauge

*Picture Courtesy – SMRT Corporation

However, some drawbacks of field wear measurement and monitoring include track accessibility, lack of control over the environmental conditions, and limited capability for accelerated wear testing. Hence there is a need for laboratory-scale wear testing setups to characterize and predict wear in a simplified manner. Several wear testing methods are reviewed and described in detail below.

- **Ball/Pin-On-Disc Tribometer Wear Test Setup**

In a ball-on-disc wear tester, shown in Fig.2-14, a ball is loaded and in contact against a flat rotating disc specimen such that a circular wear track is produced. The instrument can be used to evaluate wear and friction properties of materials under pure sliding conditions. Either the disc or the ball can serve as a test specimen, while the other acts as counter-face. For wear assessment of the disc specimen, it is preferable to use ball made from commercially available materials which are of extremely high hardness such as silicon nitride, tungsten carbide or alumina (Al2O3) as counter-face, to ensure minimal wear of the ball material [75-78].

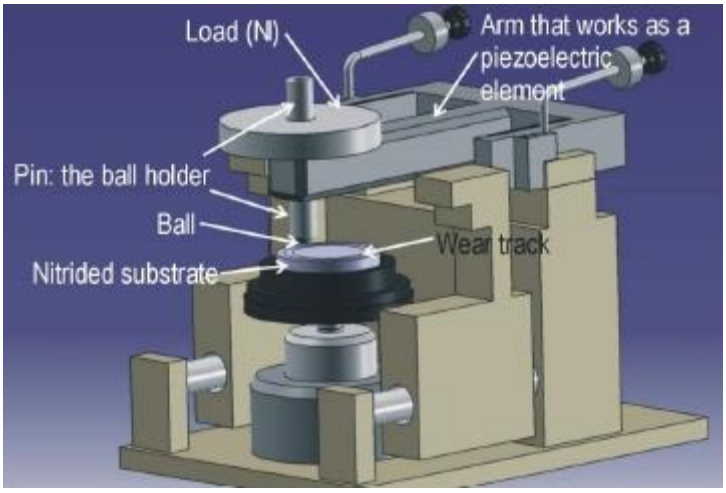

Figure 2-14: Schematic representation of a ball/pin-on-disc wear test setup [79]

As an alternative, the test can be performed using a pin configuration. The test procedure can be carried out with reference to ASTM standards G99 guidelines [80]. As discussed earlier, this wear setup is favourable for evaluating wear performance of rail steel at sharp curves where contact is purely of sliding mode at the wheel flange face and gauge corner face and is commonly used for preliminary assessment of accelerated wheel and rail wear [59, 72, 74, 81-84]. An actual wear test configuration of ball/pin-on-disc test system is shown in Fig.2-15 below.

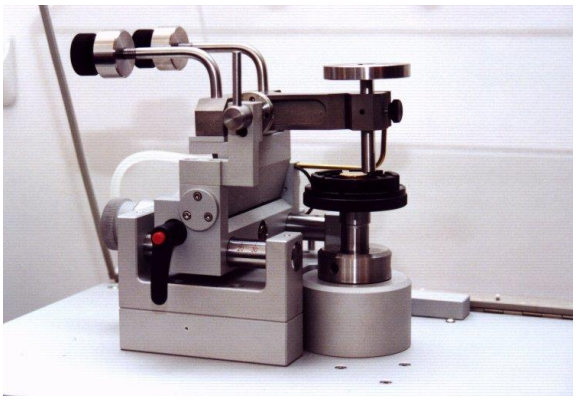

Figure 2-15: An actual ball/pin-on-disc wear test setup [85]

- **Twin-Disc Wear Test Setup**

This testing technique has the capability to simulate both rolling and sliding motion that closely resembles actual rail-wheel contact scenario as compared to the ball-on-disc wear testing where only pure sliding is possible.

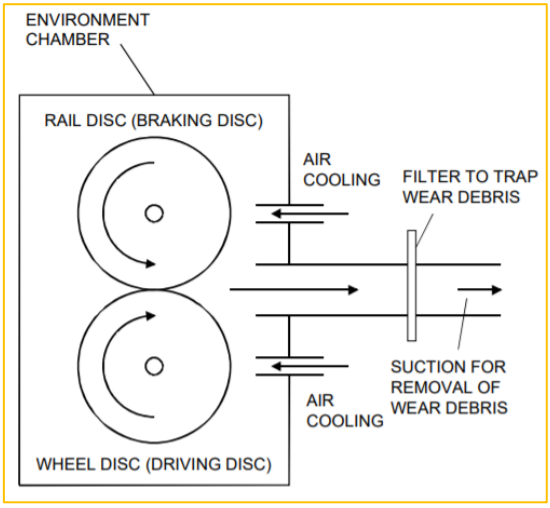

Figure 2-16: Schematic of a twin-disc wear test setup [86]

Also known as rolling-sliding wear testing, this is a popular tribometer setup for investigating wear as well as frictional behaviour of a material under conditions of rolling, sliding, or a combination of both. Two discs, as show in Fig.2-16, are fixed to two parallel shafts and pressed against each other under a constant contact load. Driven by a motor through a train of gear, the specimens are rotating along with the shafts. The rotating speed can be controlled, so that when the linear speeds of two wheels are equal at the contact point (V1=V2), a pure rolling contact is achieved. When V1 and V2 are different ($V1 \neq V2$) and both discs are rotating, then a combined rolling-sliding motion can be achieved. Besides the study of wear, this technique is widely used by researchers for rolling contact fatigue (RCF) analysis at the wheel-rail interface [86-91].

Figure 2-17: Sheffield rolling sliding twin-disc facility [92]

- **Full Scale Wheel-Rail Wear Test Setup**

The ball-on-disc tribometer and twin disc wear test setup described previously are scaled down versions of laboratory testing methods wherein specimens have to be cut and extracted from the actual wheel and rail sections and hence are ideally suited for a simplified assessment of rail and wheel wear. Design and development of a full-scale wheel-rail test setup (as shown below in Fig.2-18) allows wear and fatigue tests to be conducted at laboratory while simulating real loading and contact conditions. University of Sheffield, UK, is one among the few research institutes that has successfully demonstrated capability to conduct wear analysis with the aid of a well-designed and developed wheel-rail test rig while achieving positive results from the study [65, 93, 94].

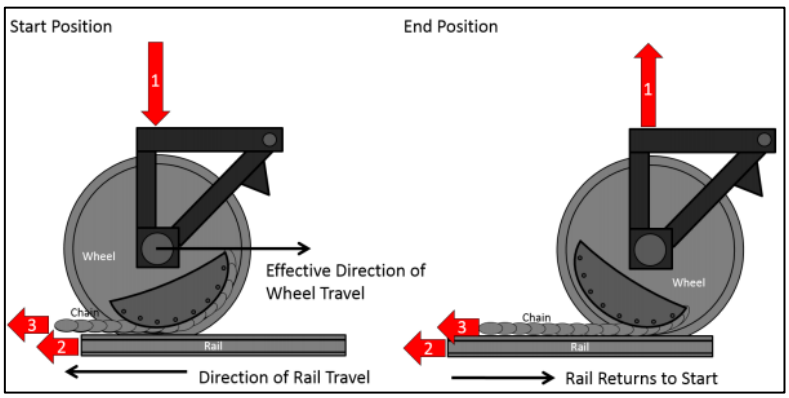

Figure 2-18: Schematic of the full-scale test facility at Sheffield University [65]

The procedure of how the test rig operates is listed below [65]:

- Apply required vertical load (half axle load) on wheel
- Tow rail along the direction of travel to allow free rotation of wheel
- Actuator connected to wheel rim via a chain to simulate creep as the wheel is pulled

Full scale laboratory testing with the aid of a wheel-rail test rig is ideally suitable for conducting accelerated wear or rolling contact fatigue assessment as it can provide real time, useful data generation that closely resembles the actual wheel-rail contact while allowing for flexibility over the test conditions.

On the downside however, there is very limited availability of such test rigs and owing to the design complications and high setup costs, this test approach is not extensively sought after [95].

Figure 2-19: Full-scale rail wheel test rig at voestalpine Schienen GmbH [96]

2.4.3 Rail Wear Measurement

Wear measurement approaches can be categorized into linear wear dimension, mass difference, wear area, and wear volume. Table 2 below is a summary of the list of measurement techniques and the corresponding units to quantify wear for each type [97].

Table 2: Common Wear Measurement Methods and Units to Quantify Wear

	Measurement Methods	**Units of Wear**	**Units of Wear Rate**
Loss (in terms of mass)	a) Direct measurement by a precision balance b) Calculated from volume loss for known material density	μg g	μg/m, g/m, μg/N, g/N, μg/ (N.m), g/ (N.m)
Loss (in terms of volume)	a) Calculated from depth, width, wear profile and/or other forms of wear track dimensional data. b) Measurements can be carried out via surface profilometry or microscopy techniques c) Calculated from mass loss for known material density	mm^3	mm^3/m, mm^3/N, mm^3/(N.m)
Wear track distance	Direct measurement by surface profilometry, microscopy and dimension measurement techniques	μm, mm	μm/year, mm/year

Besides quantifying wear, characterisation of wear and damage mechanism is important for understanding how failure is initiated due to wear and minimizing wear. The relevant wear mechanisms for rail-wheel contact system are described below.

Abrasive wear can be primarily categorized into two forms: two-body and three-body abrasion wear. In the case of two-body abrasion, a hard particle surface would plastically penetrate the softer counter-face upon slipping motion resulting in groove formation (scratch marks) and weight loss of the softer body. For three-body on the other hand, there is the presence of a third abrasive matter separating the two sliding surfaces at the interface leading to debris being trapped which contributes to wear. Two-body abrasion is a very severe form wear in comparison to three-body abrasion [98].

There are four stages to abrasive wear mechanism as shown in Fig.2-20. The micro-plowing phenomenon is primarily seen on very soft surfaces. In this case, scratches on the soft body would not scrape off the material, and the material only move on the surface and is often stored as a lump on both sides of the created track. The transfer of micro-plowing mechanism to micro-cutting takes place when the hardness of the material is increased. Upon further increase of the hardness of the sliding surface, the abrasive wear can eventually transform into micro-cracking. In this mechanism, the particles are rubbed off due to the formation and growth phenomenon of a crack embedded in the grooves. Particles accumulated in slots around the abrasive surface move constantly that would then lead to a micro-fatigue phenomenon [99].

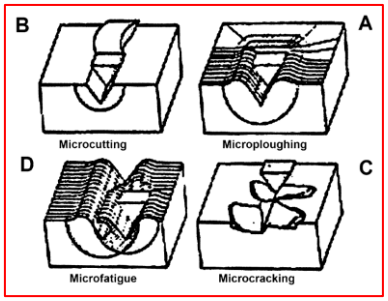

Figure 2-20: Four stages of abrasive wear mechanism [74]

Adhesive wear is another common type of wear which occurs when there is local slip between two surfaces in the joints, and in the course of time, results in failure by transfer of material from one surface to the other as depicted in Fig.2-21. The asperities formed can break in the softer material or in the harder material which leads to a mutual transfer of materials in sliding contact [72].

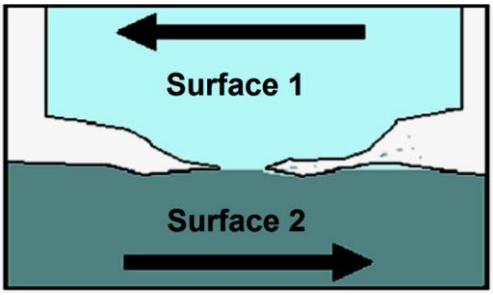

Figure 2-21: Adhesive wear mechanism [74]

Surface fatigue wear is a phenomenon which occurs when the surface yields to cyclic loading. At the point of contact where the shear stress is maximum, small cracks are initiated which then propagate to the material's surface [100, 101]. Fatigue wear can be observed under several wearing processes such as rolling, sliding, and impact. As shown in Fig.2-22, the cracks first initiate upon repetitive contact, then continue to grow and propagate through the surface. Beyond yield, the material on the contact surface breaks off causing wear debris to be generated.

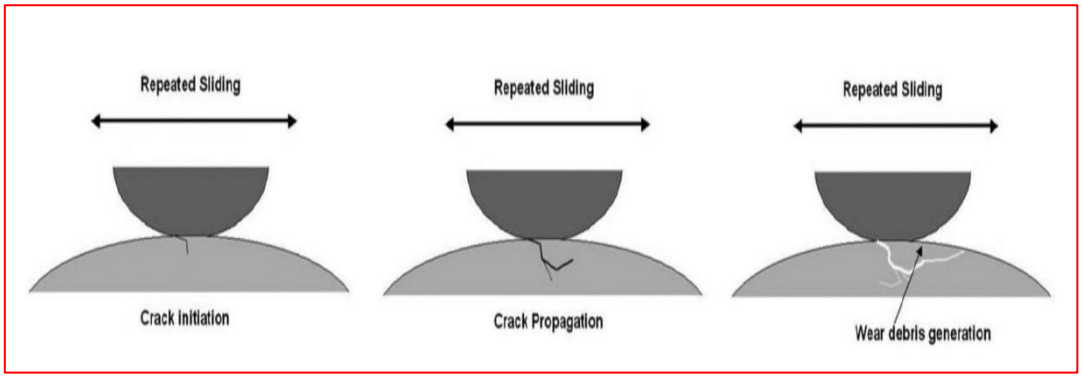

Figure 2-22: Fatigue wear [72]

Delamination wear is a process where material loss occurs from the surface due to forces of another surface in contact with it under sliding motion. The procedure describing delamination wear is as follows [74]:

- Plastic deformation of the surface
- Nucleation of cracks below the surface
- Crack propagation from these nucleated cracks and joining with neighbouring one
- Upon separation from surface, laminates form the wear debris

Impact wear arises from two or more bodies that are in continuous contact with each other, involving elements of elastic and plastic deformation. Depending on the ductility of materials, and when the impact energy is high, fatigue is accompanied with wear debris as a result of crack propagation. This mechanism is generally found in many mechanical devices [74].

The review and understanding of the five wear mechanisms is both essential and relevant for the study of rail wear performance assessment.

2.4.4 Rail Service Wear Life Prediction

Since wear and fatigue are two of the most significant failure mechanisms for rail, the predominant failure mode between the two is often determined by the train and track conditions.

Zarembski derived the relationship between fatigue life and wear life for differing set of wheel loads as shown in Fig.2-23 [1]. Fatigue failure was observed to occur first for larger wheel loads and higher stresses whereas for lower axle loads and sharp curvature, failure due to wear is dominant.

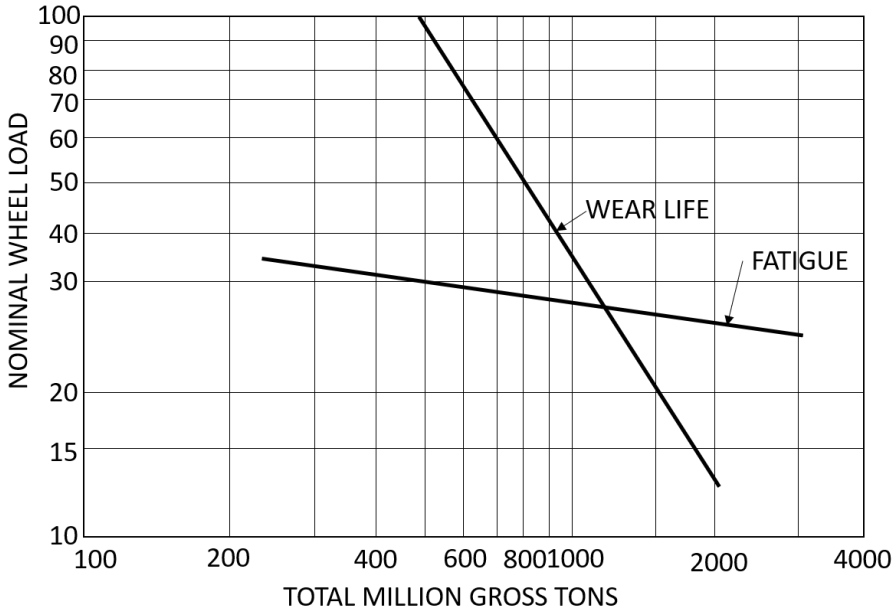

Figure 2-23: Wear life vs fatigue life [1]

Million Gross Ton (MGT) in railway:

- Weight experienced over a given track, in millions of tons for a specified period of time.
- Usually used cumulatively as a measure of rail life.

The current research aims to modify the rail wear service life model by extrapolating it to conform with Singapore's railway system loading requirements where wheel load is between 8 and 16 tons. This model will then be used for correlation study with rail wear life predicted from laboratory tests.

2.4.5 Wear Life Prediction from Laboratory Tests: Archard's Wear Model

Rail wear life prediction has been a popular research topic over the years with several empirical studies being carried out to predict and model wear based on laboratory assessment [2, 72, 82, 89, 102-106].

According to Reye in 1860, the volume loss of body during wear was correlated with the energy dissipated into the body by relative motion of the two contact surfaces as illustrated by *Equation (3)* [107, 108].

$$V = K_R W \tag{3}$$

Where V is the volume loss, K_R is Reye's wear constant and lastly W is the work dissipated into the material. It is also to be noted that Reye's approach is one of the fundamental techniques used to evaluate wear in terms of energy dissipated.

The classic wear theory involves considering the rate of material loss as a function of parameters such as load, sliding distance, sliding speed and material hardness [109].

Holm (1946) associated wear with the relative motion of surface asperities such that discrete atoms on opposite asperities collide upon contact with each other resulting in wear [108, 110-112]. *Equation (4)* shows the wear volume loss per unit sliding distance, V as a function of Z which is the probability of atom removal per atomic collision (influenced by the material properties of contacting body), load applied, p and, flow pressure p_m of the worn surface which can also be referred to as "material hardness".

$$V = Z\frac{p}{p_m} \tag{4}$$

Burwell and Strang then proposed a similar model for the wear volume per unit sliding distance [111]:

$$V = k\frac{W}{H} \tag{5}$$

Where k is the probability of removing wear particles, W represent the applied load and H is the hardness of material.

In 1953, Archard investigated wear by analysing the critical parameters to be included in a wear model. His work is regarded as a continuation of Holm's wear model with the assumption that contact between the two bodies is discrete and hence can be treated as individual spots [72].

As illustrated in Fig.2-24, the spot area initially increases from zero to a maximum of πa^2 and then drops to zero again.

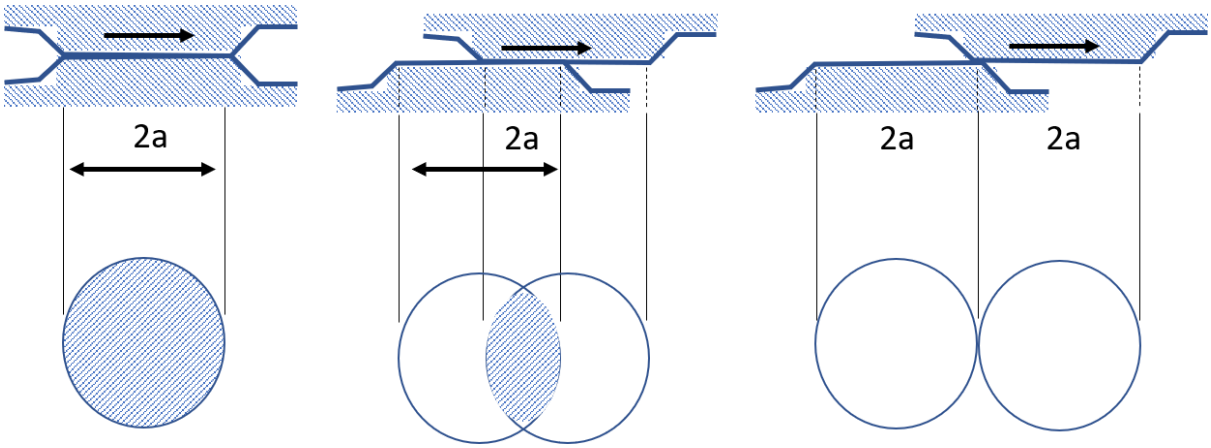

Figure 2-24: Contact surface between two bodies based on Archard's assumption [72]

The normal load is then defined by *Equation (6)* where P_m is the yield pressure of a plastically deformed asperity while a is the contact spot radius.

$$P_n = \pi a^2 P_m \tag{6}$$

With the assumption that the contact volume is a half sphere of radius a, then the volume is

$$V_n = \frac{2}{3}\pi a^3 \tag{7}$$

and wear rate per unit distance for a single spot is denoted as

$$i_n = \frac{V_n}{2a} \tag{8}$$

Combining *Equations 6, 7, and 8*, the total wear rate considering all the contact spots is then evaluated to be

$$\mathrm{I}^{*} = \sum i_n = \frac{P}{3P_m} \tag{9}$$

With Archard's assumption of

$$\mathrm{I} = \mathrm{kI}^{*} = \frac{kP}{3P_m} \tag{10}$$

Where k is a constant.

The equation for wear rate (wear volume per unit sliding distance) can then be further simplified to the following form

$$I = K\frac{P}{H}\ (mm^3/mm) \tag{11}$$

Replacing $\frac{k}{3} = K$ the wear coefficient, whereas $P_m = H$ is the hardness of the softer material.

The final wear equation represented by Archard's model is as follows [102]:

$$V_{wear} = K\frac{Ns}{H}\ (mm^3) \tag{12}$$

The model states that the wear volume V_{wear} (mm^3) is proportional to the dimensionless wear coefficient K (always < 1), the normal load N (N), and the sliding distance s (mm) while is inversely related to the hardness H (N/mm^2) of the softer material.

Archard's wear model, is a semi-empirical approach which is most widely used for modelling wear processes in the tribological society and presents a simplified approach which is typically adopted for rail-wheel wear modelling [72, 82, 102].

The wear coefficient in the Archard model is a complex parameter to be determined and varies significantly depending on factors including the sliding velocity, contact pressure, temperature, as well as the amount of lubrication present at the contact region [102].

A wear coefficient map has been ideally developed in terms of sliding velocity and contact pressure for wheel and rail steels based on pin-on-disc and twin-disc tests under dry conditions in Fig.2-25 [113].

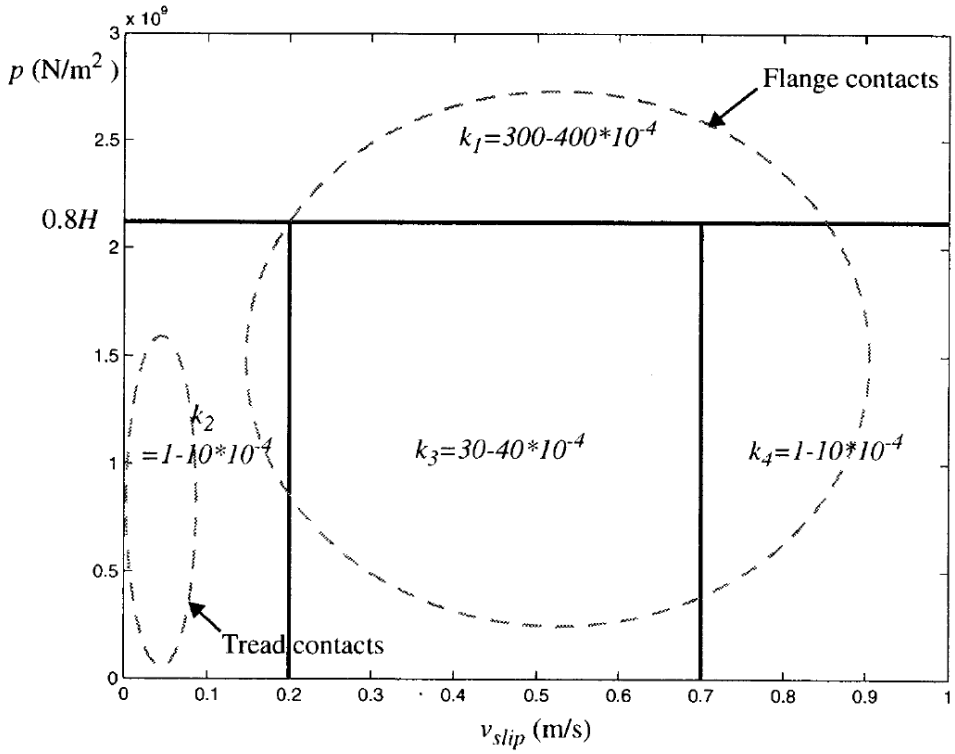

Figure 2-25: Wear coefficient map for wheel and rail steels under dry and room temperature conditions; *k* as a function of sliding velocity v_{slip} and contact pressure *p* [102]

The contact pressure is capped at 0.8H corresponding to 80 % of the hardness, below which the wear coefficient solely depends on the sliding velocity. In the first region, the wear coefficient is relatively small for low sliding velocities. Then it increases for the range between 0.2 and 0.7 m/s before dropping again to the initial low value for sliding velocities exceeding 0.7 m/s. Above the contact pressure limit of 0.8H, the wear coefficient is extremely high reflecting catastrophic wear conditions that could lead to derailment.

Wear coefficients obtained from laboratory scale wear testing methods can then be integrated with Multi-Body Dynamics (MBD) simulations for prediction of wheel or rail profile evolution [90, 114-117].

Archard's wear model is investigated to be sufficiently accurate for wear modelling in practical engineering applications including rail wear assessment and as such is used in this present research.

2.5 Research Gaps Identified

Laser cladding research in the railway industry has demonstrated substantial promise. With prior assessment through rail wear degradation study, more efficient laser cladding rail repair maintenance strategies can be developed. Chapter 3 presents research on wear life prediction and failure analysis of sharp radius curves (typically R300 and R500 rails) using a statistical modelling approach which is yet to be investigated in literature.

Upon identifying the high-value rail components such as curves and crossing nose that undergo failure due to wear-out and localized surface damages, there is an opportunity to develop a strategical approach to implement laser cladding repair of such localized rail head defects which has not been looked into.

The experimental methodology and material characterisation research in Chapter 4 evaluates clad material compatibility of Stellite 6 with the premium R350HT pearlitic grade rail steel substrate. Research in laser cladding of Stellite alloys is focused in many areas, however specific studies of the effect of a clad layer on the wear performance of the rail steel substrate material has not been investigated.

More research efforts are required to investigate on durability of cladding layer to characterise the wear performance of laser clad rail steel specimens. A laboratory-scale wear testing methodology to simulate accelerated testing of rail wear is as such proposed for research in Chapter 5. Wear characterisation is conducted by examining the experimental wear test performance of clad material and rail steel substrate using Archard's wear model.

The delamination study of laser cladded rail steel specimens is dependent on the interface characteristics of the clad-substrate pair. Chapter 6 presents an opportunity for research involving shear testing and analysis of the clad material and rail steel substrate interface. A methodology to investigate clad layer delamination is not developed yet, hence experimental shear testing is important to evaluate laser cladding interface bonding strength between the clad layer and rail steel which captures the failure and fracture effects.

A strategy to evaluate full-scale reliability of the cladded rail steel by installing the specimens on a test track and mainline track environment that conforms with Singapore's railway track system has not yet been studied. Research on reliability and performance assessment of laser cladded rail steel is proposed in Chapter 7 while presenting an opportunity to investigate rail repair feasibility on track. There is scope for further research in Chapter 8 with the design of a portable, modular laser cladding system for repair and testing of localised rail head defects on track not been developed.

Chapter 3 Rail Wear Life Prediction & Model Study

This Chapter presents research on rail wear degradation by conducting analysis of real time maintenance wear data. In rail wear degradation analysis, the Weibull distribution model is used for failure analysis and prediction based on historical maintenance data records. Additionally, Zarembski's rail wear life model is modified to predict wear life of rail steel based on the Singapore railway system.

The scope of research iterates the significance of rail wear degradation study in Section 3.1 and Section 3.2 discusses the methodology developed for degradation analysis. The selection of Weibull model for failure analysis and prediction, as well as the approach to derive Degradation Vs Time plot is presented in Sections 3.3 and 3.4. The failure analysis results are further discussed in Section 3.5. Zarembski's rail wear life model is modified to predict wear life of rail steel that conforms with the Singapore railway system and is presented in Section 3.6. The chapter is then summarised in Section 3.7.

3.1 Rail Wear Degradation Analysis

Rail wear degradation durability performance is an important aspect that needs to be addressed due to its significant impact on railway track maintenance and planning to mitigate and prevent lengthy downtime and exorbitant costs resulting from rail steel failures. The study and prediction of rail wear degradation will allow for planning of effective rail maintenance strategies [118].

The current research adopts a statistical modelling approach to predict rail wear degradation trends from the maintenance service data.

Rail sections are subjected to different track, train traffic, maintenance and operating conditions which may lead to failure at different time intervals. The time to failure obeys a probability distribution which indicates whether a particular rail section fails within a specified time [119].

While different probability distribution models are used for failure analysis and prediction, the 2-parameter Weibull distribution model is used in the current analysis as it is most widely used in research due to its ability to provide reasonably accurate failure analysis and prediction [16, 17]. The challenge involved in modelling and predicting rail degradation using probability distribution models is in acquiring a complete historical data set required for performing the degradation analysis.

Chattopadhyay utilised the rail wear failure data from the Swedish National Rail Administration to analyse and predict rail breaks for R500-600 curve sections [120]. Time-to-failure information was recorded in terms of MGT (Millions of Gross Tonnes) and the Weibull distribution was used to estimate parameters for modelling and prediction of rail wear life. Freitas et al. applied linear degradation path and Weibull distribution model to rail wheel wear analysis in the Brazilian railway network and showed that degradation provided better estimates than time-to-failure analysis [121].

While considerable literature study has been conducted with regards to degradation data analysis, there is limited progress on predicting rail wear degradation trends at sharp-radius curve track sections.

The next section describes the methodology developed to perform failure analysis and prediction using the historical rail wear data.

3.2 Development of Methodology for Rail Wear Degradation Analysis

In this analysis, the Reliasoft software is applied to process the failure data where similar analysis to predict failure of pipe degradation due to corrosion has been studied [122].

As discussed previously, severe rail wear is observed at sharp radius curves instead of the straight tracks, hence the rail wear data obtained from 1999 to 2017 was filtered to include only the R300 and R500 radius curves. Post-processing of the wear data to extract the necessary information required such as the Chainage, NSEW bound, rail foundation type, rail geometric type (straight, curve or transition), etc.

The rail-wheel contact pair at the curves is such that head wear is observed to be more significant on the low rail while side wear is the dominating component on the high rail [123]. A typical contact condition of the leading wheelset and the rails when a train negotiates a tight curved track is presented in Fig.3-1 below.

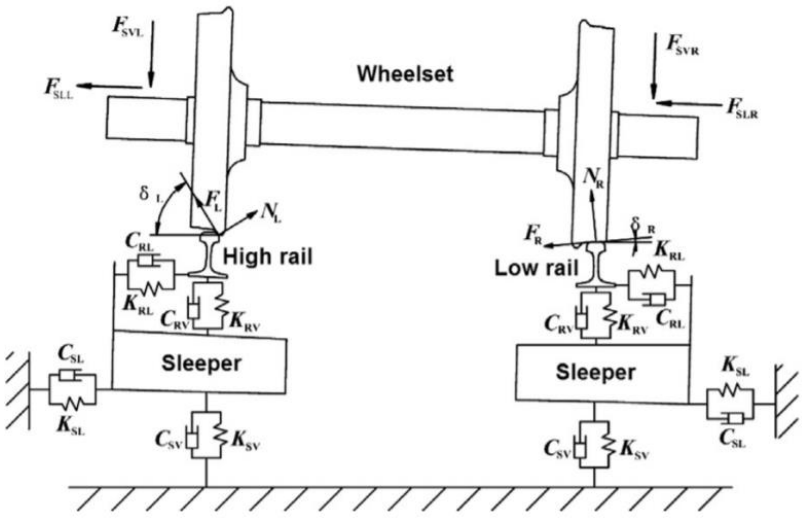

Figure 3-1: Wheel-rail contact condition on a tight curve radius track [124]

Hence depending on the contact type, the quantity of wear varies. The permissible rail wear based on the requirements of Land Transport Authority (LTA) Singapore is presented in Fig.3-2.

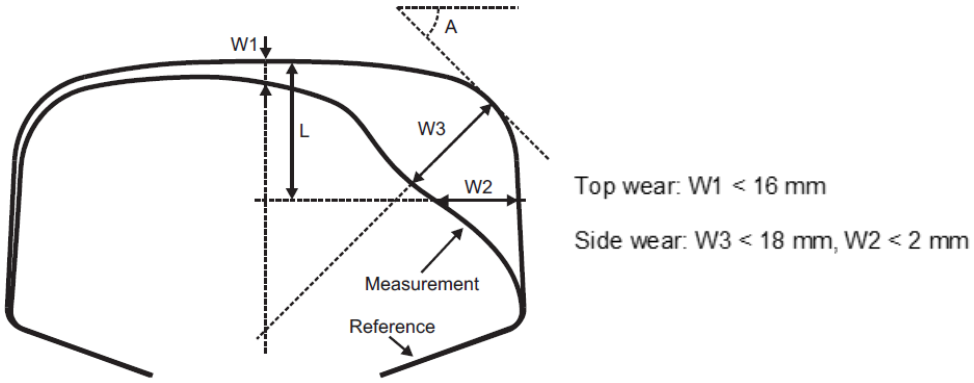

Figure 3-2: Permissible rail wear according to LTA's requirements

- High rail in a curve: Gauge side wear (W3) is the dominant wear region [**W3 < 18 mm]**
- Low rail in a curve: Head top wear (W1) is the dominant wear region [**W1 < 16 mm]**

With the critical wear parameters known, the wear data is plot with respect to time and regression analysis is performed using to determine the time to failure. Statistical wear life data analysis is then performed using the 2-parameter Weibull distribution model. The framework of the method is shown in Fig.3-3 below.

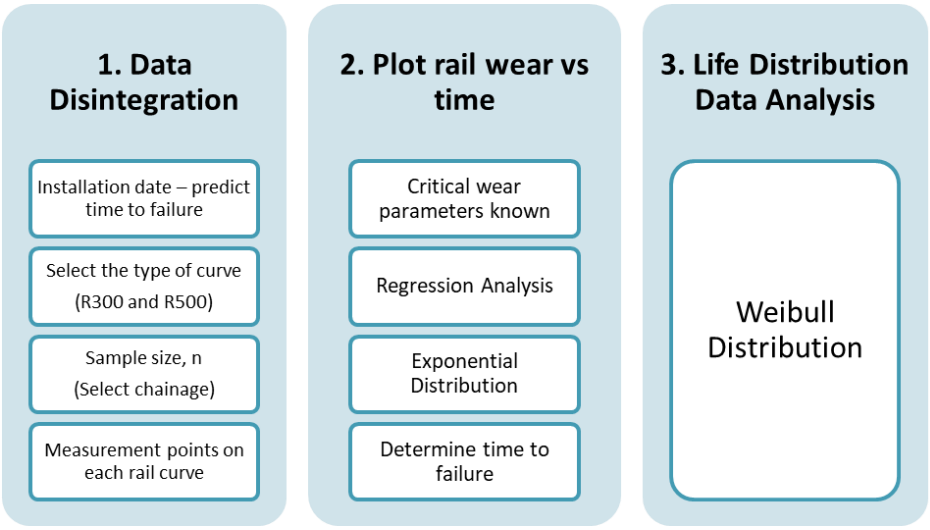

Figure 3-3: Rail Wear Degradation Analysis Method Framework

3.3 Weibull Distribution Model for Failure Analysis and Prediction

Among the various types of probability distribution models used in reliability analysis, Weibull distribution is diversified one which is a good approximation of normal distribution and an exact representation of exponential distribution. Due to its adaptability, Weibull distribution is the most commonly used life distribution for reliability analysis which can classify all kinds of components that have a decreasing, constant or increasing failure rate by the use of a graphical plot.

The plot is then used to analyse the trend of these data in order to determine the root cause of the failures cause by unanticipated or premature failures [125].

There are two main parameters in the Weibull distribution model:

- β (Beta): Shape Parameter (Slope)
- η (Eta): Scale Parameter (Characteristic Life)

The Weibull probability density function can be referred to as a 2-parameter distribution.

2-parameter Weibull PDF distribution:

$$f(t) = \frac{\beta}{\eta}(\frac{t}{\eta})^{\beta-1}e^{-(\frac{t}{\eta})^{\beta}} \quad (13)$$

$$R(t) = e^{-(\frac{t}{\eta})^{\beta}} \quad (14)$$

Where $R(t)$ is reliability and t is the operating time.

Parameter β value is an indication of the failure rate reference to the bathtub curve [126]. The first condition is β <1.

Component in this region experienced infant mortality and fails in their early life. It can be eliminated by having a burn in period where the equipment is operated at its actual operating stress level to eliminate any infant mortalities. This can be due to many factors such as manufacturing defect, poor design and low-quality products, etc.

The second type of failure rate is the constant failure rate and it occurs when β =1. Constant failure rate is generally associated with various random failures occurring and is usually at the middle of the bathtub curve, in-between infant mortality and wear out life. This type of failure rate may not be ideal in a maintenance perspective as it meant that the component's failure rate stays constant with age regardless of different maintenance procedures. The last type of failure rate is when β >1 where the failure rate is increasing with time giving a wear out life and indicating a fatigue failure. This is very common in aging components especially mechanical parts and automobiles as the failure rate increases with age.

An illustration of the bathtub curve is presented in Fig.3-4 below.

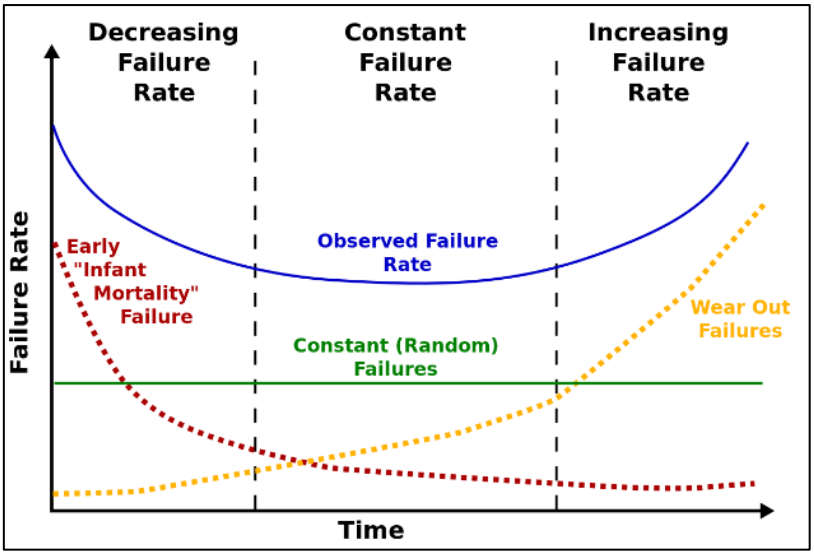

Figure 3-4: Rail Wear Degradation Analysis Bathtub curve illustration [127]

Parameter η defines the spread of the distribution. For the same β condition, larger η will result in the stretching of the Weibull distribution as shown below in Fig.3-5.

The parameter unit of measurement for eta can be in work load history (e.g., cycles) or work time scale. Eta value is defined as the time taken for 63.2% of the component to fail.

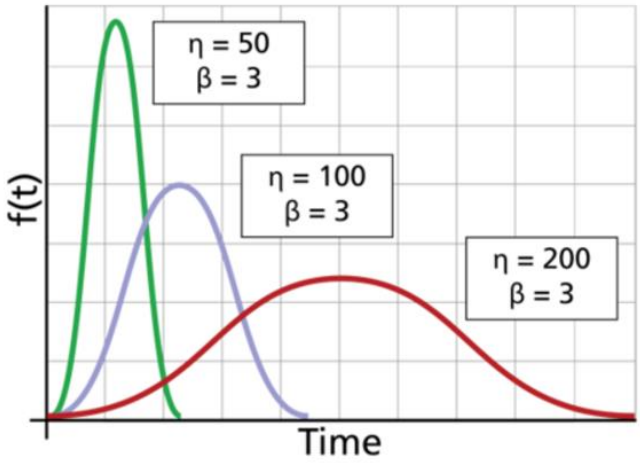

Figure 3-5: Effect of parameter η on the distribution [128]

The degradation vs time plots for the wear degradation analysis performed for R300 and R500 curves are presented in the next section.

3.4 Degradation Vs Time Plot

The time to failure data for R300 curve is obtained from the degradation vs time plots for failure analysis and prediction (Fig.3-6 and Fig.3-7). The graphs show the 'fitting' of the wear data based on the regression analysis performed. Similarly, the time to failure data for R500 curve is obtained from the degradation vs time plots for failure analysis and prediction (Fig.3-8 and Fig.3-9).

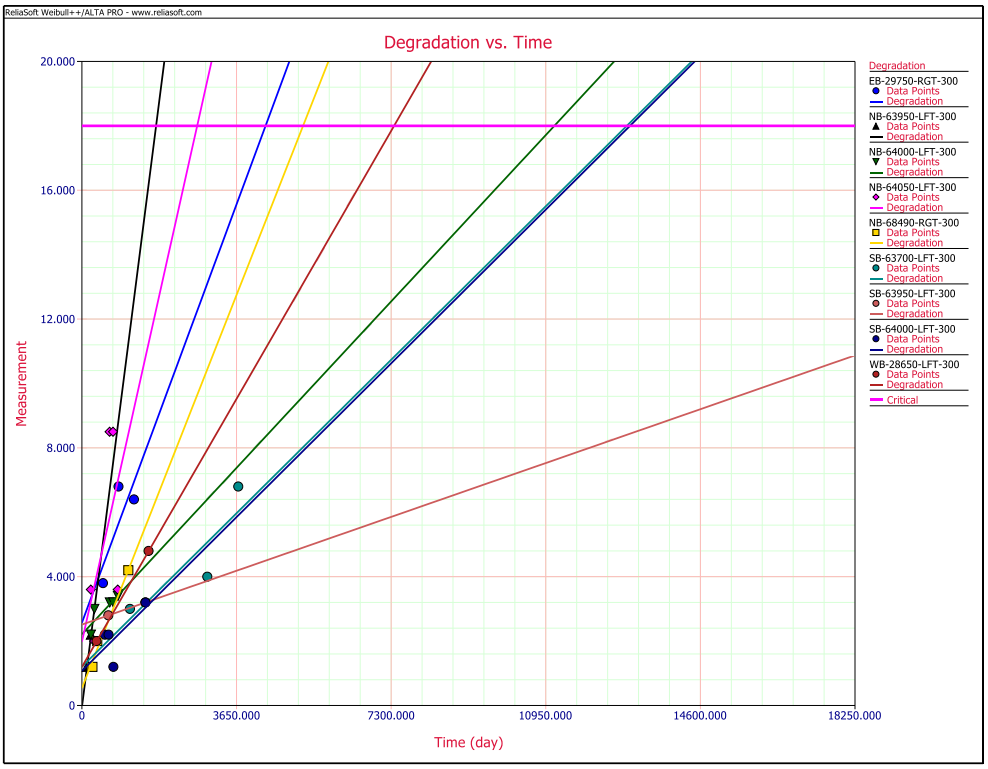

Figure 3-6: R300 Curve: High Rail Side Wear (W3<18 mm)

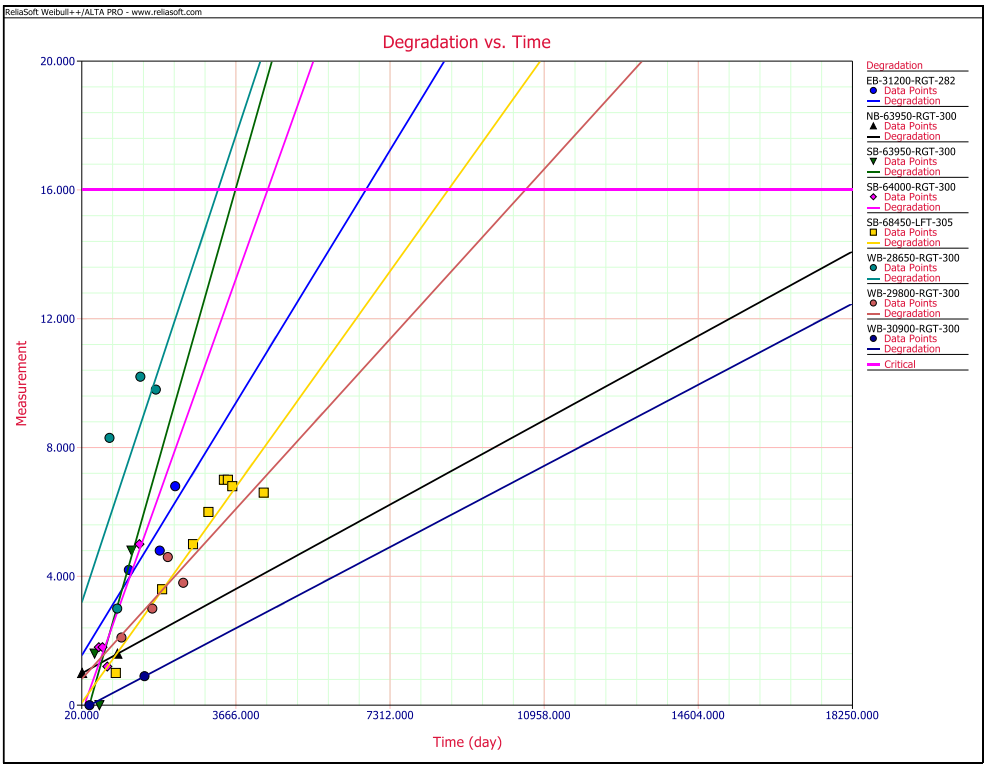

Figure 3-7: R300 Curve: Low Rail Head Wear (W1<16 mm)

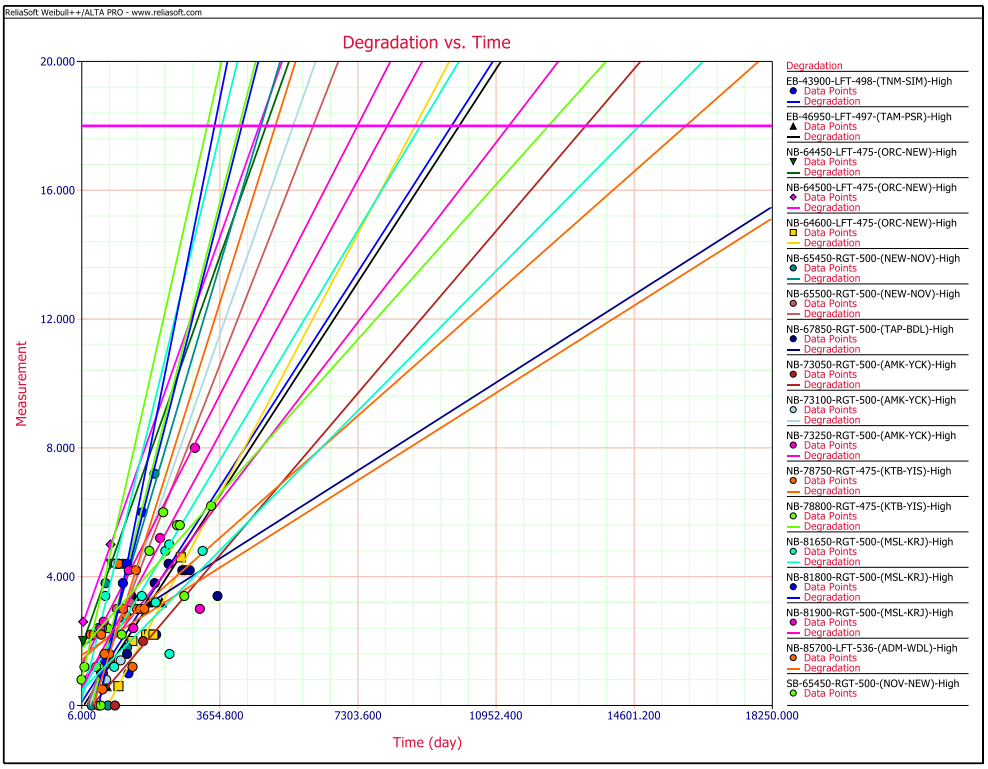

Figure 3-8: R500 Curve: High Rail Side Wear (W3<18 mm)

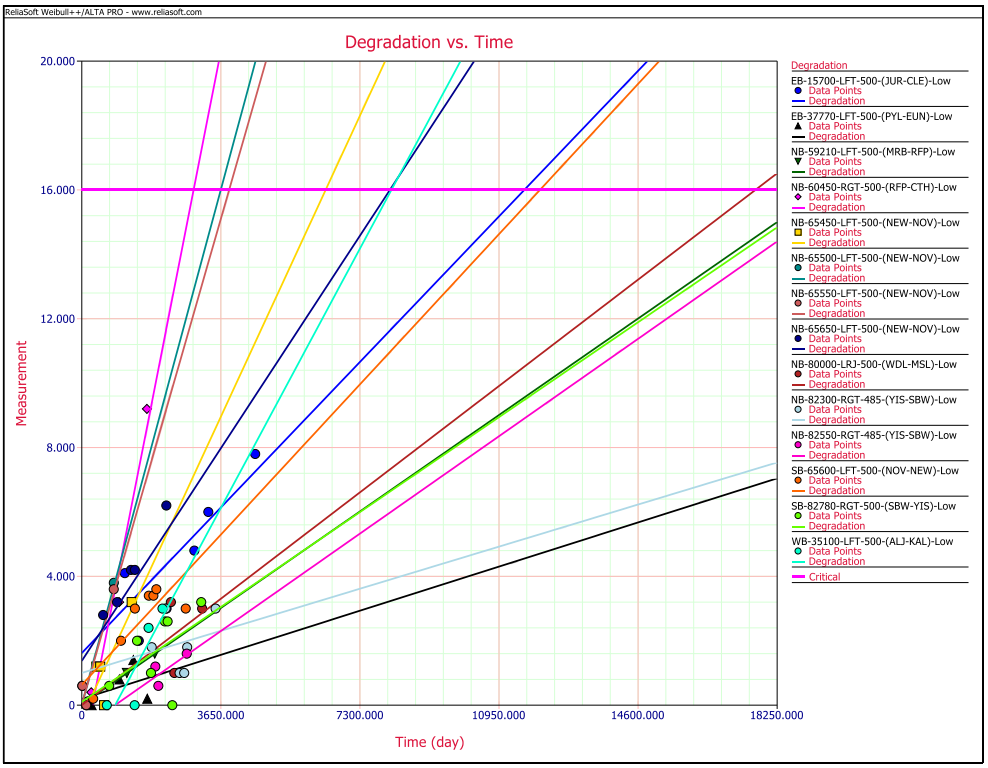

Figure 3-9: R500 Curve: Low Rail Head Wear (W1<16 mm)

3.5 Weibull Failure Analysis of Rail Wear

The time to failure data obtained for the R300 and R500 curve rail sections (high and low rail) is then fit using the Weibull distribution model for failure analysis and prediction. Besides the comparison of the Weibull parameters, the mode and median were also evaluated.

- **The Mode**
  - To predict the time to failure at which most rail sections are expected to fail
- **The Median**
  - To predict the time to failure at which 50 % of the rail sections are expected to fail

Based on the wear depth limits for low rail and high rail sections at R300 and R500 radius curves, the time to failure data points were derived. The failure rate plots were then determined using the 2-parameter Weibull distribution model. The β (shape parameter) and η (scale parameter) also termed as the slope and characteristic life respectively were evaluated for comparison between R300 and R500 radius curves. Although the mode and median are evaluated, they are of insignificant value in the 2-parameter Weibull analysis and not considered in the failure decision analysis.

The Weibull parameters for R300 radius curves were estimated to be $\beta = 1.220$, $\eta \approx 30$ years for the high rail section and $\beta = 1.490$, $\eta \approx 31$ years. In both cases, β is larger than 1 which indicates wear out failure.

The failure rate plots for the R300 curve high rail and low rail are shown in Fig.3-10.

a)

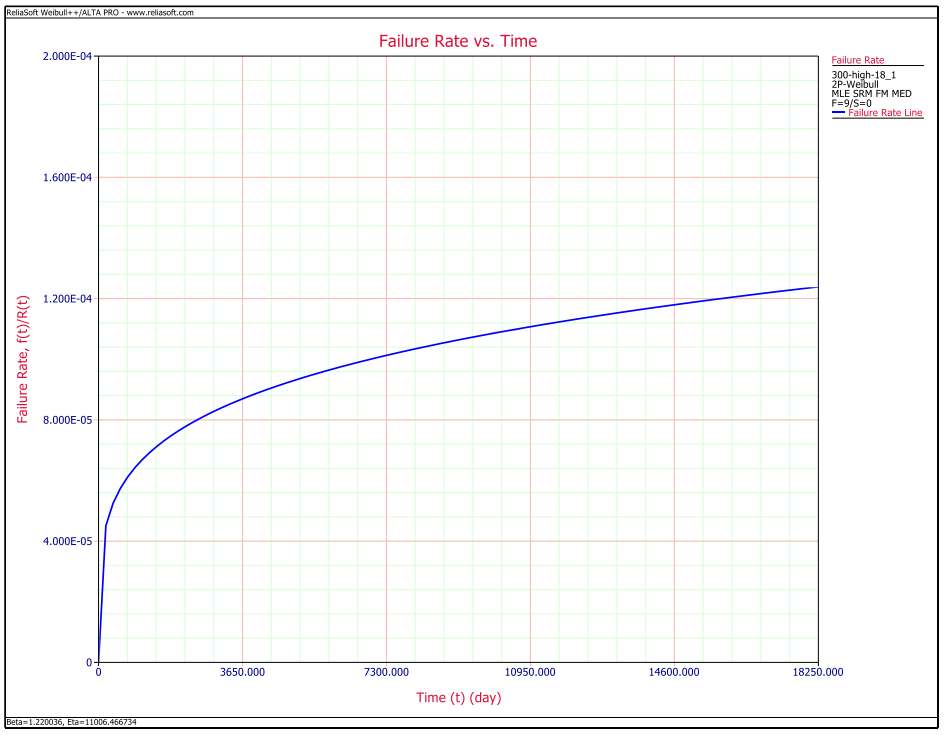

b)

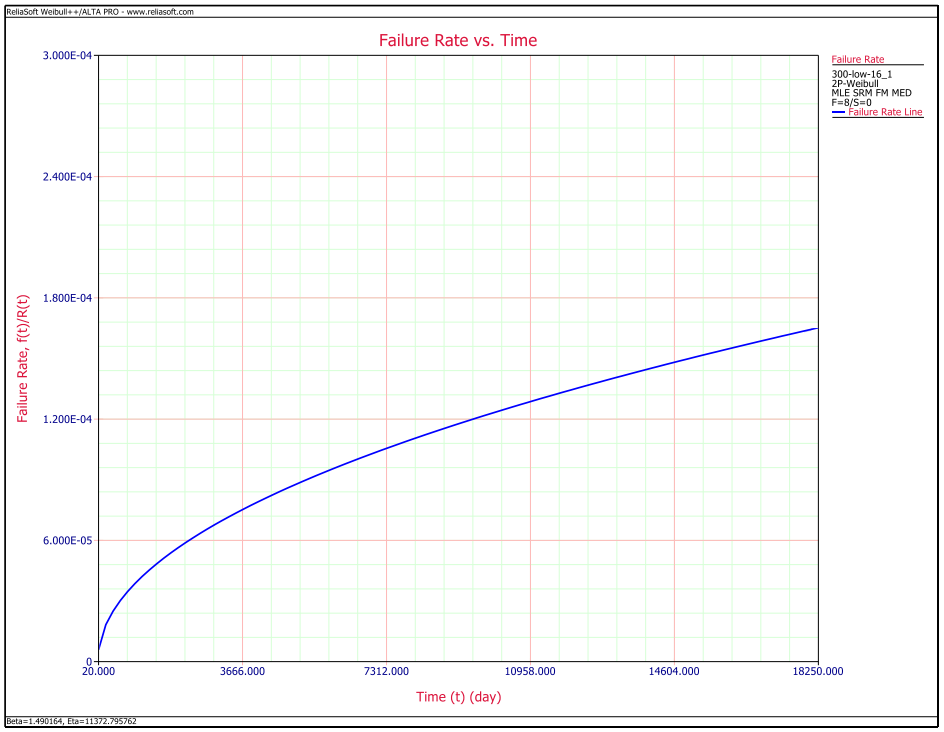

Figure 3-10: Failure Rate of a) High Rail Side Wear (W3<18 mm) b) Low Rail Head Wear (W1<16 mm)

The failure rate plots for the R500 curve high rail and low rail are shown in Fig.3-11.

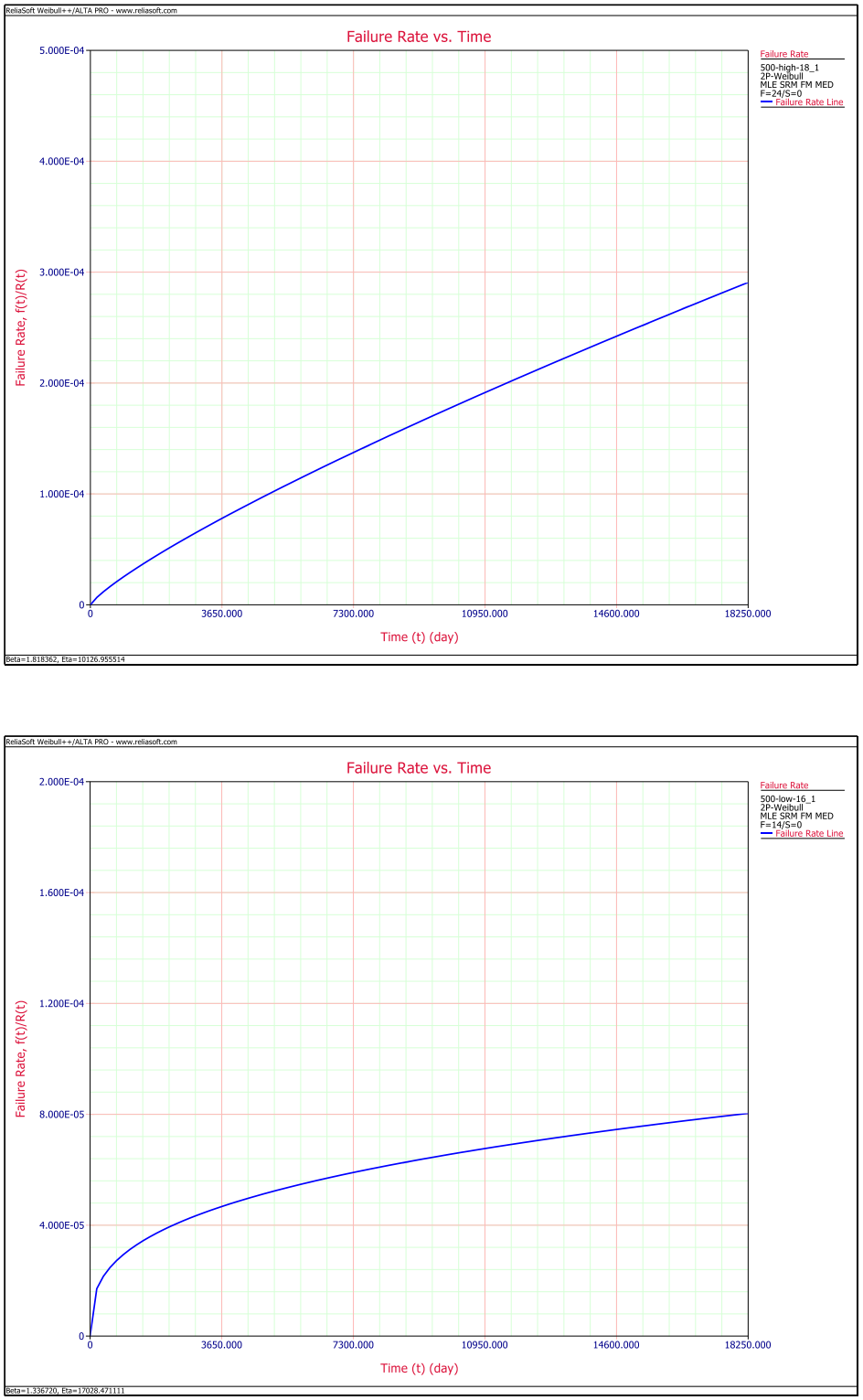

Figure 3-11: Failure Rate of a) High Rail Side Wear (W3<18 mm) b) Low Rail Head Wear (W1<16 mm)

The Weibull parameters for R500 radius curves were estimated to be β = 1.818, η ≈ 28 years for the high rail section and β = 1.337, η ≈ 47 years. In both cases, β is larger than 1 which indicates wear out failure.

A summary of the Weibull parameters obtained from the failure analysis are compared for both the R300 and R500 curve rail sections and presented in Table 3.

Table 3: β and η Value Comparison

Sharp-Radius Curves (Rail Wear Degradation)	***β***	***η* /years**
R300 (High Rail)	1.220	30
R300 (Low Rail)	1.490	31
R500 (High Rail)	1.818	28
R500 (Low Rail)	1.337	47

Wear out failure is observed for all the rail sections at sharp-radius curves as indicated by the β larger than 1 value. While the time for 63.2 % of the rail sections at R300 and R500 curves to fail is relatively long as indicated by the eta (η) value, the mode and median presents a different view.

- R300 rail wear to limit (Linear degradation, 2p-Weibull distribution)
  - High rail side wear – Mode 7.45y, Median 22.68y
  - Low rail head wear – Mode 14.46y, Median 24.42y
- R500 rail wear to limit (Linear degradation, 2p-Weibull distribution)
  - High rail side wear – Mode 15.10y, Median 22.63y
  - Low rail head wear – Mode 16.99y, Median 35.32y

Life Data Analysis is critical and, in this regard, allow prediction of rail wear service life which occur on the track. Effective maintenance strategies can be developed by performing reliability assessment.

3.6 Modified Rail Service Wear Life Model

Zarembski's service wear life model obtained from literature was extrapolated to conform with the railway system loading requirements in Singapore where nominal wheel load is between 8 and 16 tons.

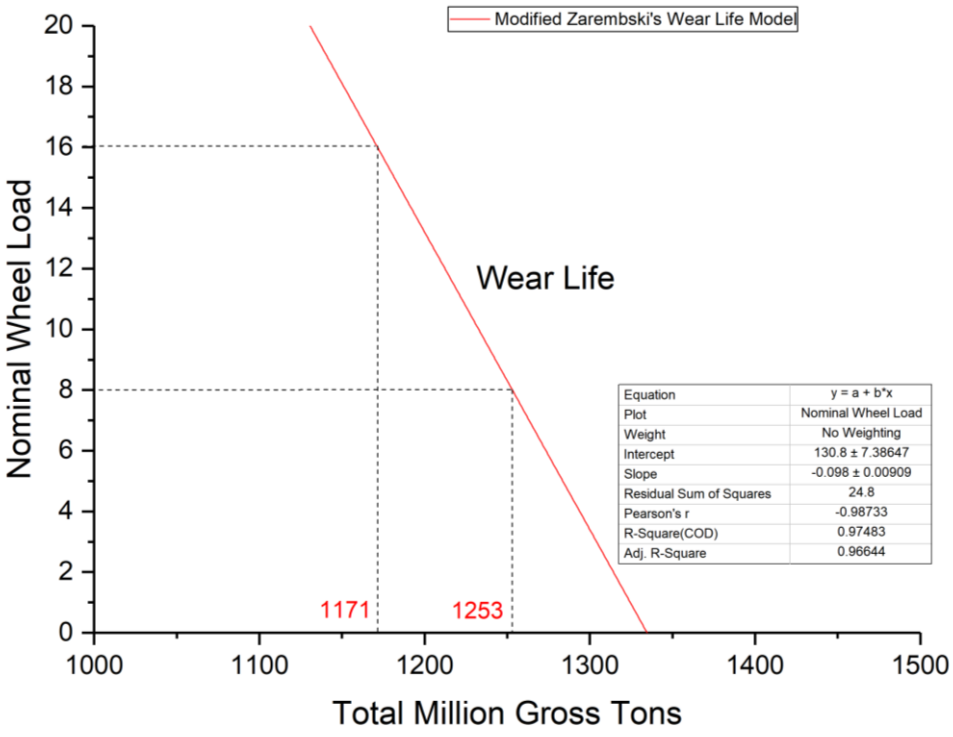

Figure 3-12: Rail Service Wear Life Model

The wear equation obtained from the Wheel Load Vs MGT relation of the wear life model in Fig.3-12 is as follows:

$$y_{wheel\ load} = 130.8 - 0.098x_{MGT} \quad (15)$$

Based on SMRT provided ridership information, the Wheel Load Vs MGT can be further transformed into Load Vs Time (In Years):

$$y_{wheel\ load} = 130.8 - 2.94x_{Time} \quad (16)$$

and Load Vs Train Cycles:

$$y_{wheel\ load} = 130.8 - 23.814x_{Cycles} \quad (17)$$

Note: x_{Cycles} value is in terms of x 10^6

The extrapolated service wear life model presents an alternative method to correlate wear in terms of Load Vs MGT, Load Vs Time, and Load Vs Train Cycles as compared to the Wear Vs Depth plots in the Weibull model analysis.

3.7 Chapter Summary

The wear life prediction and model study provide the following concluding remarks as:

Rail wear degradation methodology using the 2-parameter Weibull probability distribution model is developed to perform failure analysis and prediction of R300 and R500 radius curves based on historical rail wear maintenance data. Degradation vs time plots for the wear degradation analysis performed for R300 and R500 curves are derived and then fit using the Weibull distribution model for failure analysis and prediction. Wear out failure is observed for all the rail sections at sharp-radius curves as indicated by the β larger than 1 value. Zarembski's service wear life model obtained from literature was extrapolated to conform with the railway system loading requirements in Singapore where nominal wheel load is between 8 to 16 tons.

Chapter 4 Laser Cladding Material Characterisation Study

With sharp radius curves and crossing nose identified as critical components for failure, Chapter Four comprises of the material characterisation study to develop strategy for laser cladding repair of localized rail head defects. The experimental method for laser cladding of Stellite 6 material on R350HT pearlitic grade rail steel is presented [129]. Results obtained from the metallurgical study are discussed.

The laser cladding experimental setup and cross-sectioning methodology for material characterisation study is presented in Section 4.1. Results from the micrographic analysis, microstructural analysis and the hardness data of the cladded rail steel cross-section are discussed in Sections 4.2, 4.3, and 4.4 respectively. Concluding remarks from the chapter are summarised in Section 4.5.

4.1 Laser Cladding Experiment

The laser cladding setup comprised of a 4-kW fiber coupled diode laser system with 5 mm diameter laser spot size integrated to a four-axis CNC system for precise control of the laser beam's motion relative to the substrate during the deposition process. The other associated components include a cladding head, a powder feeding system with coaxial feeder nozzle and a chiller system for cooling the laser head and cladding nozzles during the process.

A section of head hardened R350HT rail was used as the base material for the laser cladding experiment. Stellite 6 powder was used as the cladding material due to its excellent tribological properties and proven capability in laser cladding of rail steel (R260 grade) based on literature [6-8, 130, 131].

Table 4: Material Composition of R260, R350HT and Stellite 6

Material Composition			
Elements (wt-%)	***R260***	***R350HT***	***Stellite 6***
Co	-	-	56.7
Cr	0.15	0.15	31.0
W	-	-	5.0
Mo	-	-	0.5
C	0.60 to 0.82	0.70 to 0.82	1.0
Fe	97.08 to 98.37	97.23 to 98.27	1.7
Ni	-	-	2.3
Si	0.13 to 0.60	0.13 to 0.60	1.3
Mn	0.65 to 1.25	0.65 to 1.25	0.4
P	0.025	0.030	0.002
S	0.030	0.030	0.005
Al	0.004	0.004	-
V	0.030	0.030	-
N	0.010	0.010	0.09

The chemical composition of Stellite 6 alloy, R350HT grade rail along with the standard R260 grade (for comparison) are given in Table 4. The clad powder material was gas atomized and have a spherical morphology with particle size ranging from 53 – 150 μm.

The rail section was first pre-machined as 1 mm depth of material was removed to ensure there was no presence of impurities on rail head surface. The surface was pre-heated to ensure a crack-free, high quality clad is obtained.

Laser cladding was performed by directly depositing the clad material onto the rail while the laser beam is scanned across the surface. A schematic of the coaxial laser cladding process on a rail head surface is shown along with the actual cladding process in Fig.4-1.

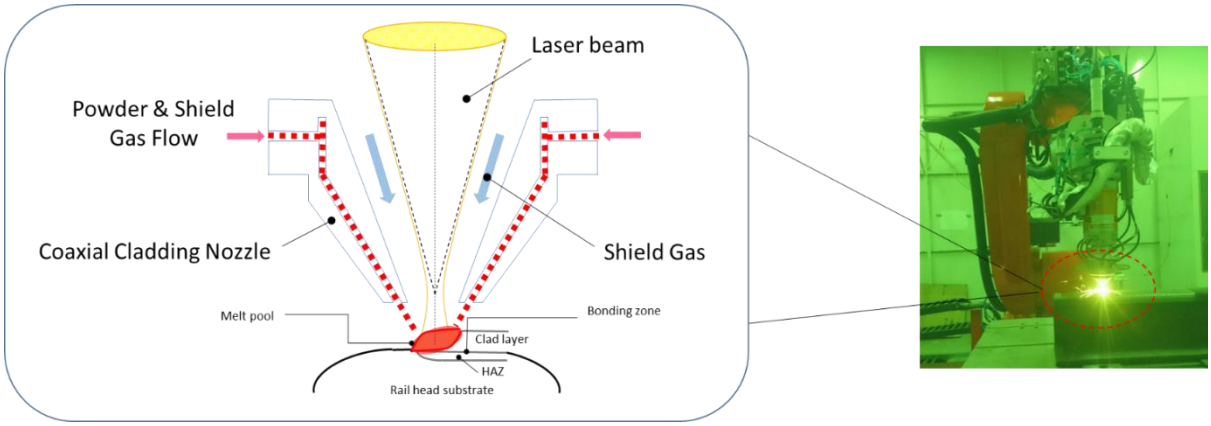

Figure 4-1: Laser cladding process schematic on rail head surface

The heat input from the laser source creates a thin melt pool on the rail surface and the Stellite 6 powder discharged via the coaxial feeder nozzle is melted and bonded with the melt pool. Two layers of 1 mm thick multitrack clads with 50% overlap were deposited in a raster scan pattern.

The processing parameters for deposition are presented in Table 5.

Table 5: Laser Cladding Process Parameters

Process parameter	***Quantity***
Laser power (kW)	2
Scan speed (mm/min)	1000
Powder feed rate (g/min)	19
Laser spot size (dia. in mm)	5

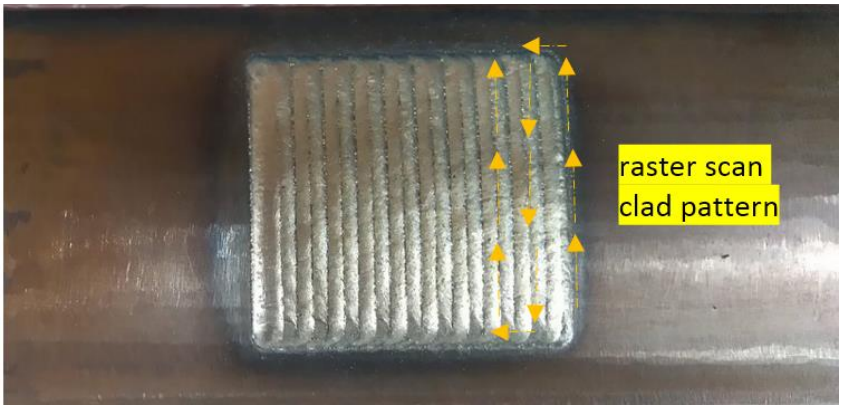

Figure 4-2: Laser cladded R350HT rail head section

The final as-cladded rail head surface is shown above in Fig.4-2 with the shiny cladding layer deposited representing the Stellite hard facing.

Prior to microstructural analysis of the clad, small samples were sectioned from the laser cladded surface in a direction perpendicular to the clad track using wire electrical discharge machining (EDM). Thereafter, the specimens were prepared following a standard metallographic procedure by hot mounting in a resin, ground using SiC abrasive papers (P400, P800, P1200) and polished with diamond paste to a 1 µm surface finish (see Fig.4-3). 2 % nital solution was then used to etch the specimens.

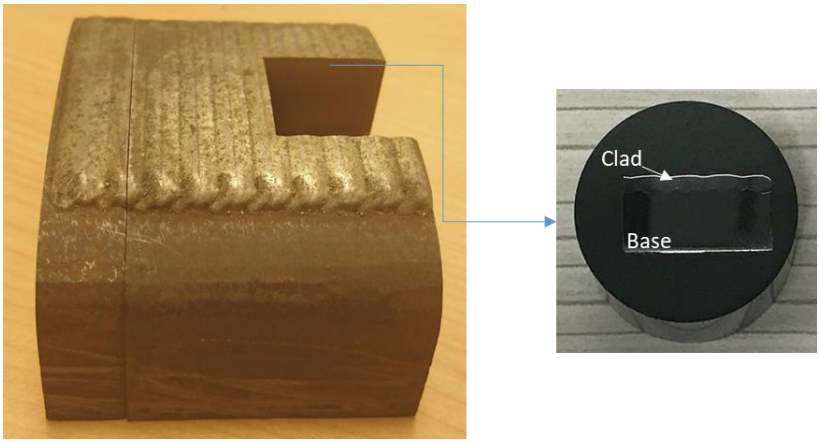

Figure 4-3: Cladded section extracted from rail and polished to 1 µm surface finish

Besides a Light Optical Microscope (LOM) - Carl Zeiss International, Axioskop 2 MAT, Laser Scanning Microscope (LSM) - OLYMPUS LEXT OLS4100 and Scanning Electron Microscope (SEM) – JEOL JSM-5600LV were used to examine the clad sections for characterization of clad-rail microstructure and HAZ within the substrate.

Microhardness measurements were performed using a Struers, DuraScan Vickers hardness tester and the hardness distribution was recorded along the clad depth with measurements taken at equidistant positions of 115 μm, extending into the parent rail material. The applied load was 0.3 N over 15 seconds of indent. The hardness data was then converted from Vickers to Brinell using ASTM standards A370 for compliance with EN 13674 European rail standards [132].

4.2 Cross-Section Micrographic Analysis of Cladded Rail Steel

The clad-substrate interface obtained from the LSM is shown in Fig.4-4 which displays clear metallurgical bonding with minimal dilution as Stellite 6 clad layers were deposited onto the rail head surface without any presence of defects. No cracking or delamination was observed which can be attributed to the initial pre-heating of the rail substrate to relieve thermal stresses.

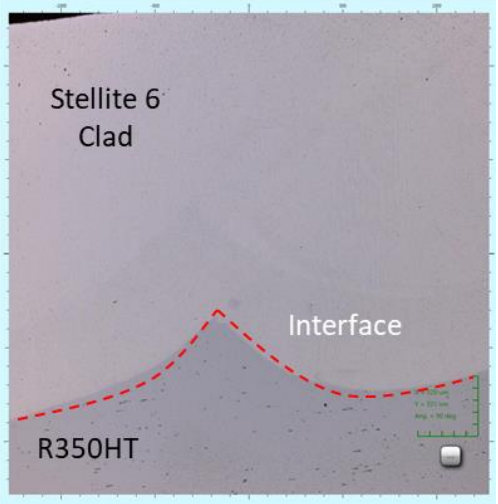

Figure 4-4: LSM image of clad-rail interface

Fig.4-5 presents the optical micrographs of the deposited clad layers and fusion zone between Stellite 6 clad and R350HT rail substrate. Based on the lateral displacement measured between the successive tracks deposited and the 5 mm clad bead width, the overlap ratio is approximately 0.5.

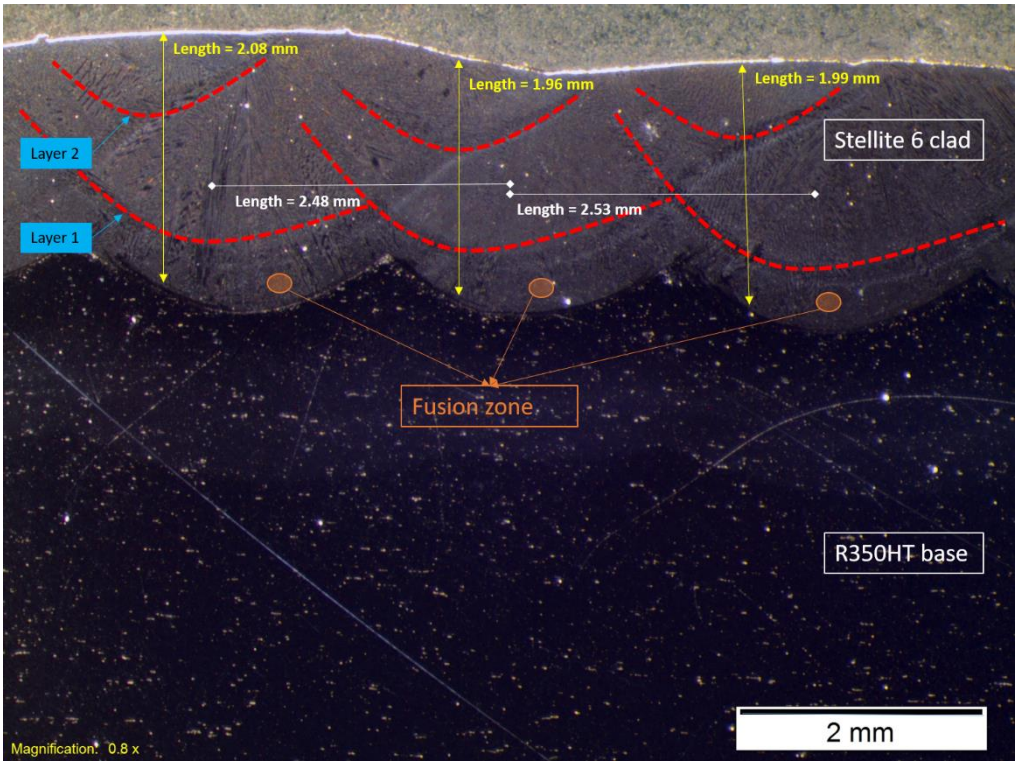

Figure 4-5: Clad-rail cross section

The clad rail cross section can be ideally characterized with the presence of four main features which are the deposited clad layer, fusion (transition) zone, heat affected zone (HAZ) and the bulk material (substrate). Table 6 below shows the size of HAZ and fusion zone which were measured and compared with the cladding layer thickness in order to evaluate the amount of dilution of the cladding with the rail steel substrate.

Table 6: Cladding – Substrate Dilution

Clad thickness, h_t (µm)	*Fusion zone, h_f (µm)*	*HAZ (µm)*	*Dilution (%)*
2010	290	944	14.4

4.3 Cross-Section Microstructural Analysis of Cladded Rail Steel

Microstructural evolution across the rail steel substrate, interface and cladding layer are studied and characterized accordingly in this section and the initial observations from LSM images are presented in Fig.4-6. The influence on hardness and wear resistant characteristics of Stellite 6 can be deduced from the microstructure observed at the clad region. The microstructure of Stellite 6 is separated into clad zone, transition zone, HAZ, and the base metal zone.

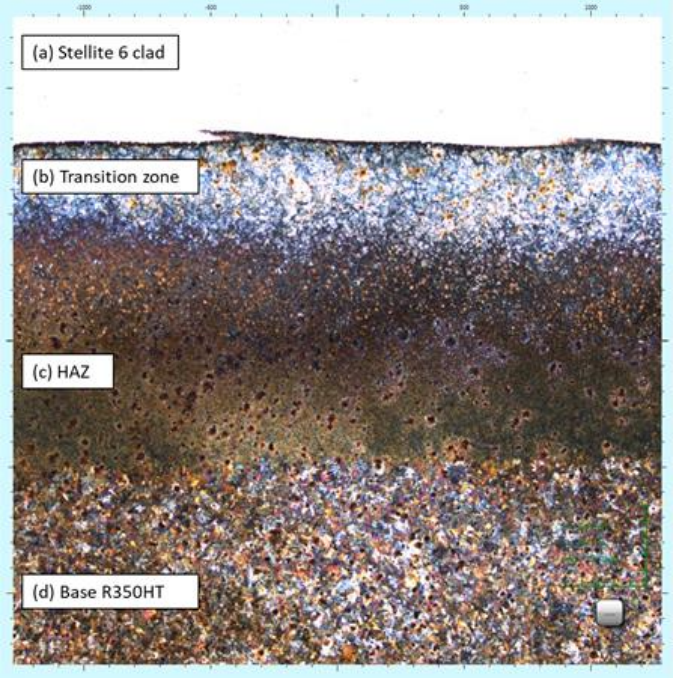

Figure 4-6: Microstructural evolution across the clad rail cross-section

It consists of dendrite phase rich in cobalt phase solid solution (f.c.c. structure) and inter-dendritic mixture formed from the eutectic Co and Cr with carbides (h.c.p structure) which is in agreement with the earlier research observations of Stellite 6 microstructure [7, 8]. The intermetallics (Co, Cr and W elements) react with carbon to form the necessary carbides that contributes to the hardness, abrasion, corrosion and wear-resistant properties. Dendritic morphology is exhibited at the interface of the cladding layer towards the top surface. The dendrites which are initially formed as cellular and columnar are transformed into dendritic structure during the solidification process.

During the cladding process, the typical cooling rates are in the range of 10^2°C/s to 10^3°C/s [133]. Referring to Fig.4-7, martensitic phase is primarily observed at the transition zone due to the rapid cooling and solidification. The HAZ comprises of diluted elements of the R350HT rail steel substrate and Stellite 6. Heat transfer changes that take place during melt pool formation and pre-heat treatment prior to cladding resulted in finer pearlite structure at the HAZ compared to the base R350HT.

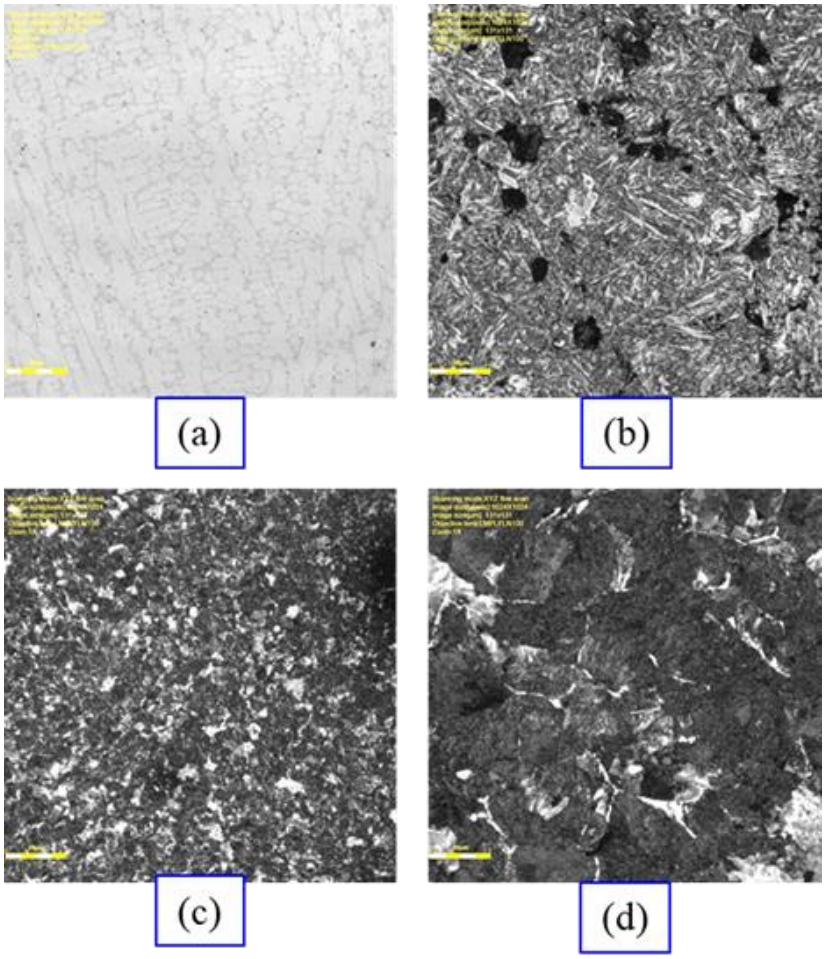

Figure 4-7: Microstructure at the respective regions from (a) Stellite 6 clad, (b) Transition zone where the clad fuses with the base rail, (c) Heat affected zone (HAZ), (d) Base R350HT

The SEM image at the interface between the Stellite 6 cladding and the fusion zone is presented and analysed in Fig.4-8. Needle-like martensitic phases are observed at the clad-fusion zone interface whereas columnar and dendritic growth within the clad structure is observed.

Rapid cooling in the clad layer leads to the predominant phase being fine martensitic phase within the columnar dendritic morphology of the clad during fusion. The dendrite morphology formed is dependent on the thermal transient while growth direction is the direction of solidification. Since cooling rates are expected to be highest near the surface, this results in temperature gradient in the clad layer and different dendritic patterns.

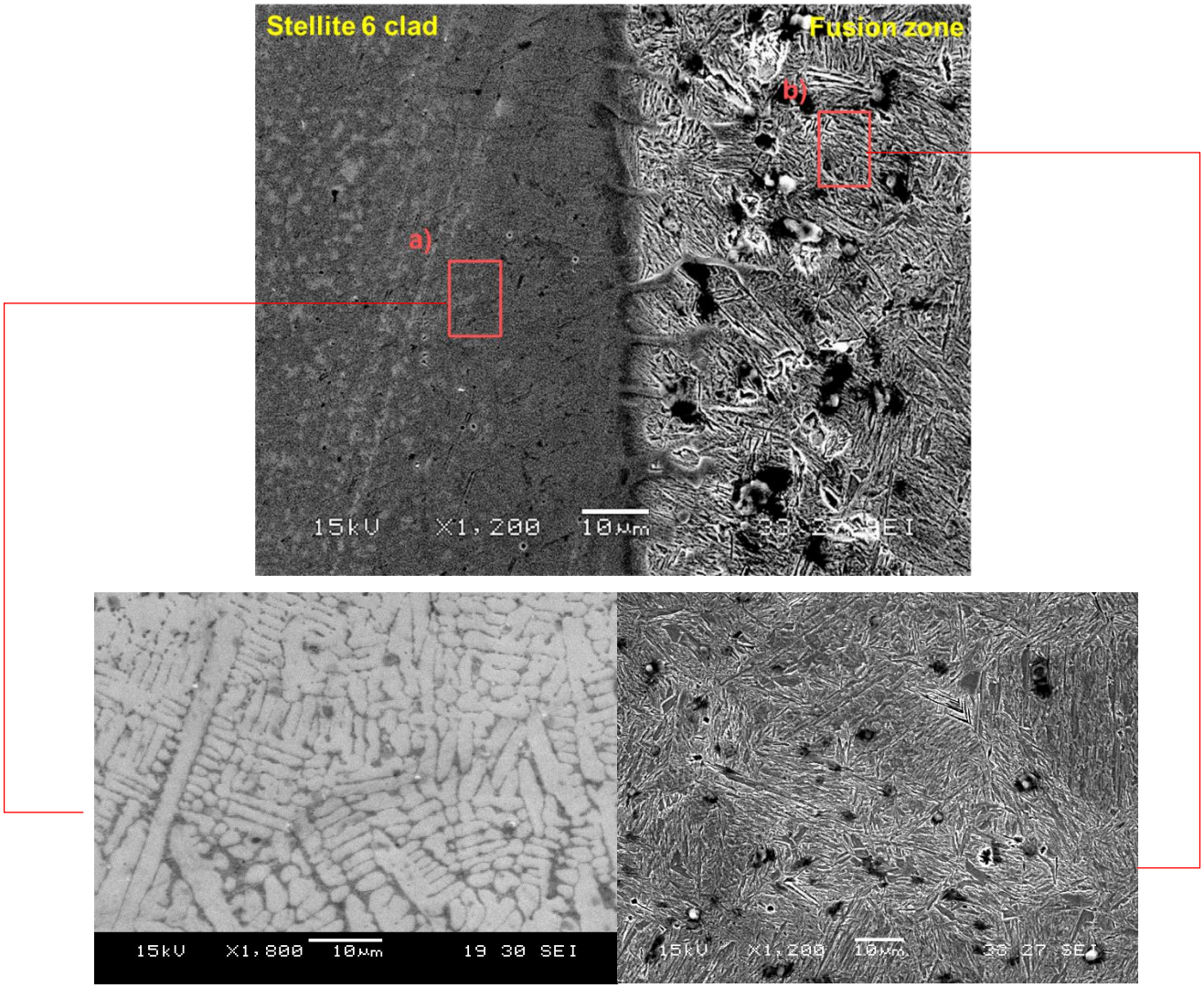

Figure 4-8: Interface between Stellite 6 clad layer and fusion zone, a) Columnar and dendritic phase of Co matrix b) Needle-like martensitic phase

Research on laser cladding of Stellite 6 have similarly proven that the dendritic structure is rich with cobalt in the form of α Co, whereas the dark coloured structures are carbide phases in the form of M_7C_3, $M_{23}C_6$, and Co_6W_6C, where M constitutes to Cr, Co and W [57, 134, 135].

The wear resistant property is thus influenced by carbon which forms the carbide phases with metals in Co-Cr alloy such as M_7C_3 (Cr) and W_6C (W) carbides. These carbides are affected by their solidification rate during the cladding process which in turn affects hardness [53, 136]. Results from the EDS measurements in Fig.4-9 further verify the presence of Co-rich dendritic and inter-dendritic mixture of carbide phases of Co, Cr and W, in the deposited cladding layer.

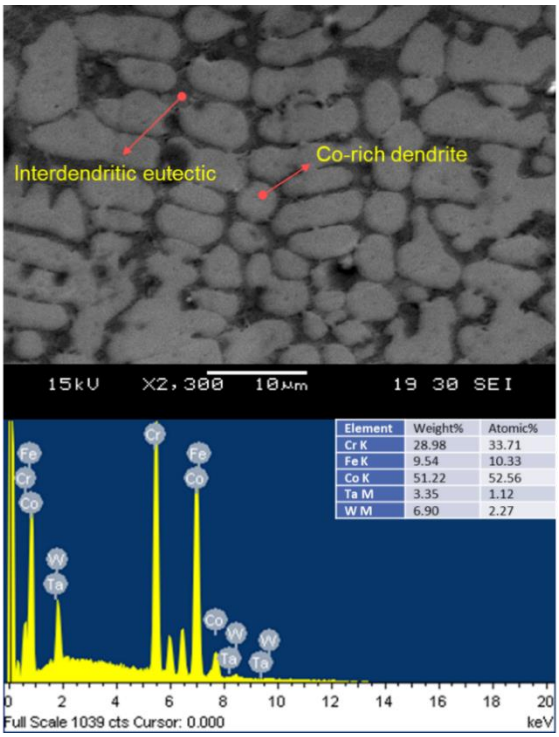

Figure 4-9: EDS compositional analysis of Stellite 6 cladding

Referring to Fig.4-10 below which shows the composition weightage across the clad rail cross section with the aid of a bar chart, it is evident that Stellite 6 cladding comprised primarily of elements Co, Cr, and W. The dilution of Stellite 6 by iron (Fe) is deduced to lower the hardness of cladding layer which in causes reduced corrosion and wear resistance during application in corrosive or wear prone environments. Therefore, the deposition of an inter-layer is often proposed to minimise dilution and mitigate hardness reduction [18]. A mixture of Co, Cr, and Fe elements are observed at the region close to the interface where % composition of Fe is larger as compared to Cr and Co.

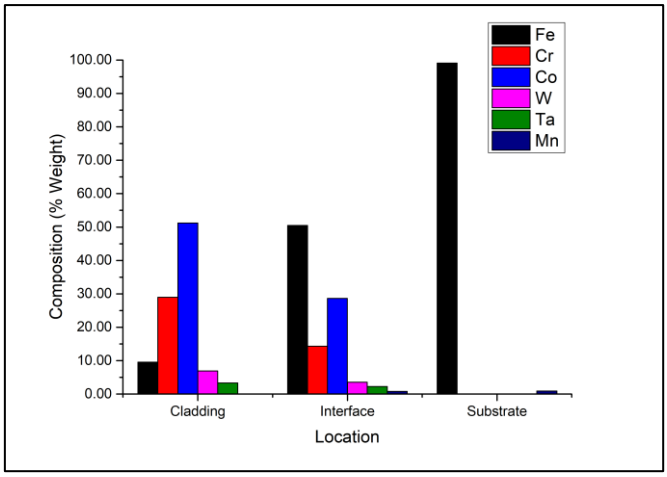

Figure 4-10: EDS analysis based on measurements along the clad-rail cross section

The effects of these phase transformation and observed microstructure from the clad to substrate region are then investigated with the microhardness indentation test results obtained.

4.4 Hardness Profile Distribution Across Cladded Rail Steel

The microhardness profile in Fig.4-11 showed an increasing hardness distribution from the interface to the cladding surface. This is due to the finer grain size at the cladding surface relative to at the interface where dilution of the Fe element is dominant. An average hardness of 420 HB was noted within the clad owing to the formation of the carbide hardening phases in the CoCr alloy matrix. This also proves that the alloying elements with primary carbide phases have a significant influence on the microstructure as well as hardness. Maximum hardness of 763 HB was observed at the HAZ, in the transition zone closer to the clad region due to the presence of the fine needle-like martensitic phase. The high hardness of the cladding as compared to base rail (325 HB) is reflective of the excellent wear resistance that is expected of Stellite 6 material albeit the presence of Fe dilution effect. However, the peak hardness values observed in the HAZ is not desirable and thus the cladding will have to be tested for delamination by brittle fracture in laboratory and on-track reliability tests.

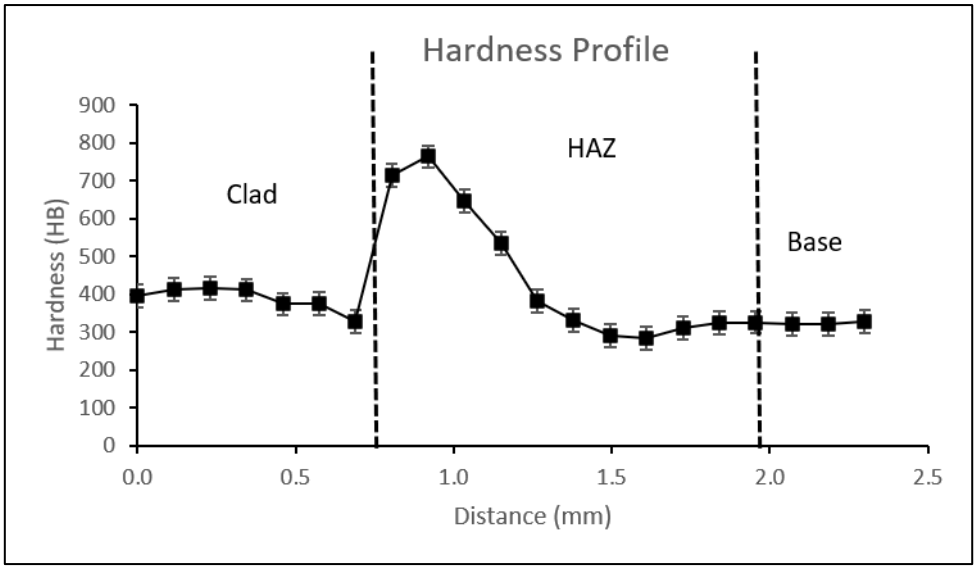

Figure 4-11: Hardness distribution profile across the clad rail cross section

The hardness distribution is reflective of the microstructural analysis and phase characterisation along the different regions of the clad-rail cross section from the deposited cladding layer, to the interface and the bulk rail steel substrate.

4.5 Chapter Summary

The material-process-performance characteristic study of laser cladding Stellite 6 clad material with R350HT rail substrate provides the following concluding remarks.

Laser cladding experimental method was developed with the following scope for metallurgical study: (a) Cross-section micrographic analysis of the cladded rail steel, (b) Cross-section microstructural analysis of the cladded rail steel, (c) Compositional analysis, (d) Hardness analysis across the clad-rail section.

The clad-substrate interface displayed clear metallurgical bonding with minimal dilution as Stellite 6 clad layers were deposited onto the rail head surface without any presence of defects. No cracking or delamination was observed which can be attributed to the initial pre-heating of the rail substrate to relieve thermal stresses. An in-depth assessment of the formation of clad interface characteristics and its relation to hardness is investigated.

The clad region showed columnar dendritic morphology which is in agreement with the earlier research observations of Stellite 6 microstructure. At the transition (fusion) zone, martensitic phase was primarily observed due to the rapid solidification and cooling during laser cladding process which can cause embrittlement. Results from the EDS measurements further verified presence of Co-rich dendritic and inter-dendritic mixture of carbide phases of Co, Cr and W, in the deposited cladding layer.

The hardness distribution was representative of the microstructural analysis and phase characterisation along the different regions of the clad-rail cross section from the deposited cladding layer, to the interface and the bulk rail steel substrate. However, the peak hardness values observed in the HAZ is not desirable and thus the cladding will have to be tested for delamination by brittle fracture in laboratory and track reliability tests with a running train.

Chapter 5 Wear Testing and Analysis of Laser Clad Material for Durability Study

The methodology for wear testing and analysis using a ball-on-disc setup is discussed. The laboratory scale testing simulates accelerated testing of wheel on rail wear. The present research however involves using an Al_2O_3 ball which is of extremely high hardness (1568 HB) to characterize the wear performance of laser clad material in comparison with the plain rail steel.

Wear characterisation is part of the scope to conduct durability studies of laser cladded rail steel and evaluate feasibility for laser cladding repair of localized rail head defects on critical rail components such as curves and crossing nose.

The motivation to investigate wear behaviour using a ball-on-disc setup and test methodology is discussed in Sections 5.1 and 5.2 respectively. The wear test performance of clad material and rail steel is measured in terms of wear volume, and wear coefficient derived from Archard's wear model. The results are evaluated and discussed in Section 5.3 and 5.4. The wear failure mechanism (Section 5.5) and work hardening behaviour (Section 5.6) of clad material is also examined. Concluding remarks from the chapter are summarised in Section 5.7.

5.1 Ball-On-Disc Wear Assessment

Ball-on-disc test setup is used to investigate the wear behaviour of the clad material in comparison to the rail steel substrate. This wear test setup is used to characterize sliding wear which is the more dominating type of wear in curves (on a high rail)

A schematic demonstrating the two types of contact for straights and curves is shown below in Fig.5-1.

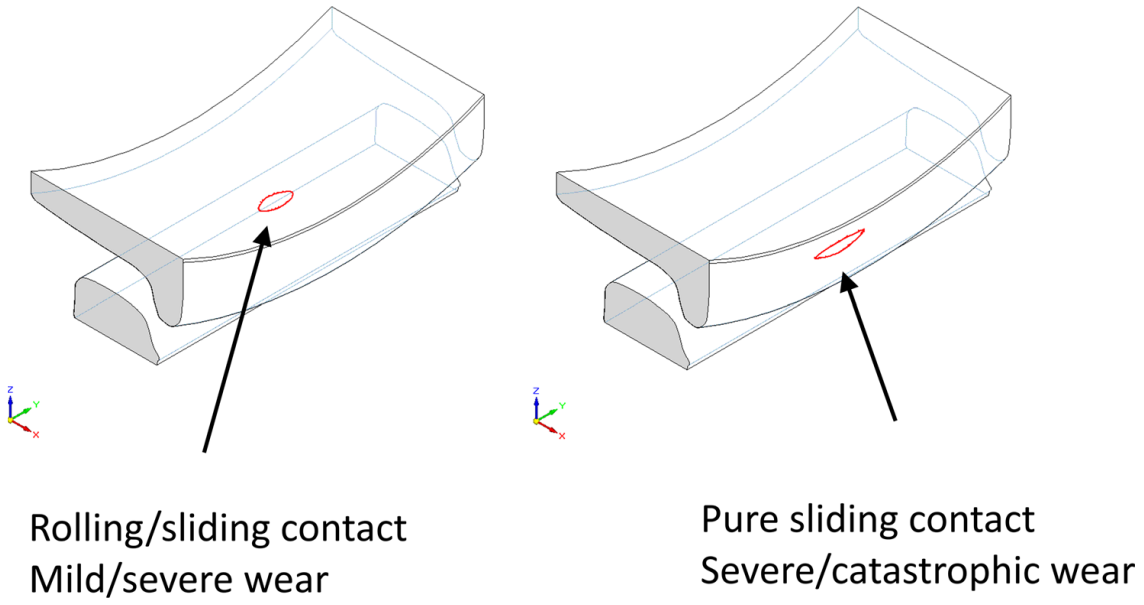

Figure 5-1: Schematic of two typical wheel-rail contact types: wheel tread-rail head contact (left); wheel flange-rail gauge contact (right) [137]

5.2 Wear Test Methodology

A laboratory scale ball-on-disc tribometer setup was used to conduct wear performance analysis of plain rail and laser cladded rail steel sections. The test procedure and sample dimensions were selected based on ASTM standards G99 [80].

The test was conducted at room temperature, under dry conditions. The extraction of disc samples from actual rail heads is illustrated in Fig.5-2 below.

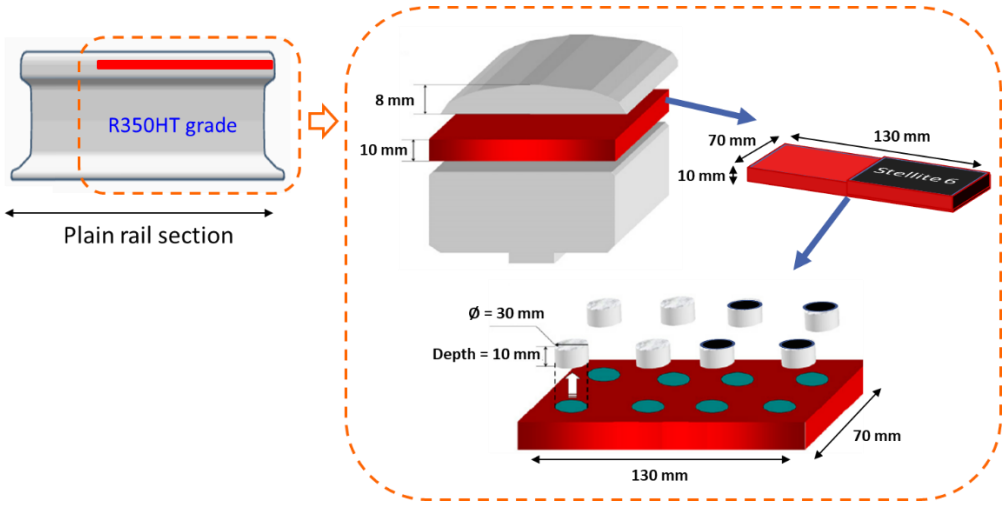

Figure 5-2: Schematic illustrating disc specimen extraction procedure

The extraction procedure involves removal of 8 mm thick top layer from rail head surface (to ensure uniformity in cladding thickness). Then 1 mm thick clad material (Stellite 6) is deposited on rail flat plane. Finally, small disc samples of 30 mm diameter and 10 mm thickness are cut out from the flat plate.

All disc specimens were polished to a mirror finish in accordance to the standards requirement of at least 0.8 µm surface roughness (Ra). The ball material selected is Aluminium Oxide (Al_2O_3) of 6 mm diameter and extremely high hardness of 1568 HB since negligible or minimum wear of the ball is desired.

The ball and disc samples were cleaned using acetone, followed by a rinse with ethanol and dried under warm air. A uniform load of 5 N and sliding velocity of 0.025 m/sec was applied, as the total sliding distance covered was 100 m.

The applied normal load of 5 N is equivalent to yielding a maximum contact pressure ≈ 1.3 GPa (derived from Hertzian Contact Theory), which is relatively comparable to the wheel rail contact pressure subject to the loading requirements of the railway system in Singapore.

While this procedure involves testing under pure sliding conditions and does not reflect rolling motion present in actual wheel-rail contact scenario, it is still valuable in investigating the clad material's wear behaviour relative to the parent rail steel. Preliminary wear assessment and characterisation prior to carrying out actual field trials on track is necessary for the development of a strategic laser cladding rail repair technique.

The test procedure was replicated for the R260 grade rail steel with and without cladding, and the results were analysed.

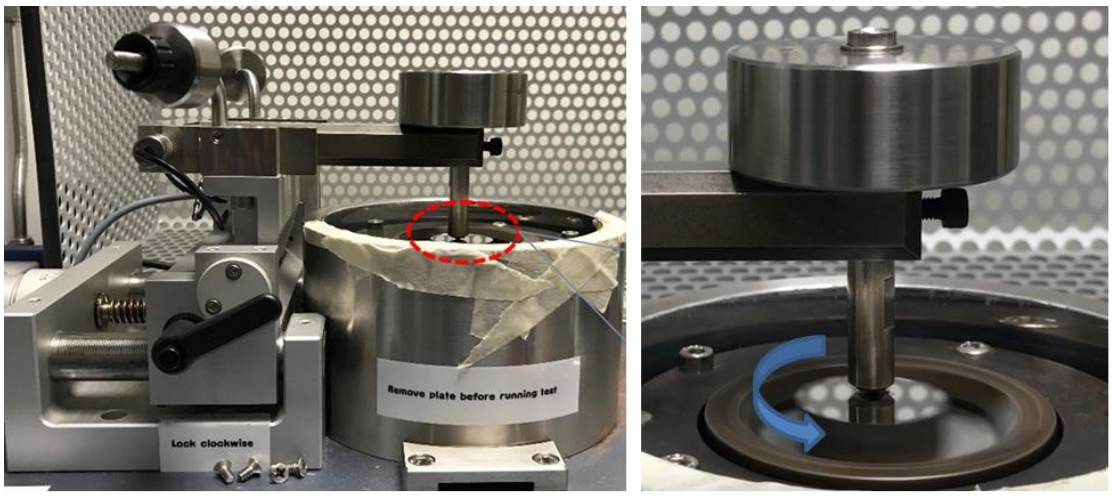

Figure 5-3: Ball-on-disc tribometer wear test setup

5.3 Wear Volume of Clad Material Vs Rail Steel

Fig.5-4 shows the wear tracks on the R350HT and R260 disc specimens for both with and without cladding which were analysed using an optical microscope.

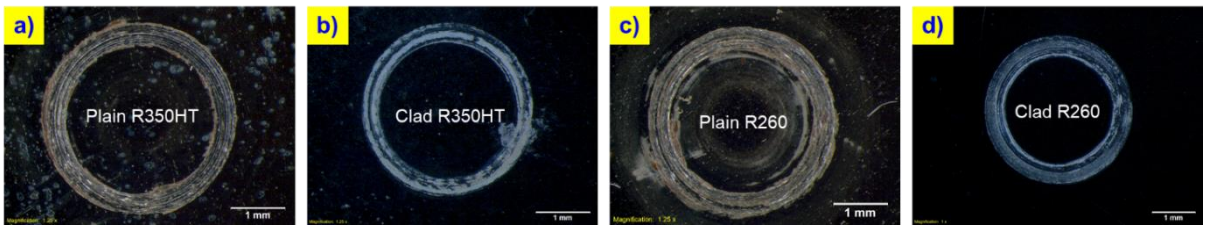

Figure 5-4: Optical micrographs of the wear track on each specimen

The track width was measured and used to evaluate total wear volume for both cladded and plain rail steel disc specimens in accordance to the wear volume formula from ASTM G99.

$$V_d = 2\pi R[r^2 sin^{-1}\left(\frac{d}{2r}\right) - \left(\frac{d}{4}\right)(4r^2 - d^2)^{\frac{1}{2}}] \quad (18)$$

Where V_d represents the disc volume loss in mm^3, R is the wear track radius (mm), d is the wear track width (mm), and r is the ball radius (mm).

The measured wear track width and wear volume based on Eqn (18) are shown in Table 7.

Table 7: Wear Track Width and Wear Volume

Wear Test Results		
Steel Grade	**Wear track width (µm)**	**Wear volume (mm^3) – ASTM G99**
R350HT	393	15.9 x 10^{-3}
R350HT with Stellite 6 clad	342	10.5 x 10-3
R260	455	24.7 x 10-3
R260 with Stellite 6 clad	355	11.7 x 10-3

As expected, the wear volume calculated for the plain rail steel disc specimens were predominantly larger in comparison to the cladded disc specimens. Both cladded R350HT and R260 exhibit similar wear with minimal difference in the volume loss.

The ASTM model to evaluate wear volume is dependent on three main parameters which are the wear track radius, track width and the ball radius.

This approach to determine wear volume can be regarded as an estimate and does not entirely reflect the actual volume loss of the disc specimens.

The Taylor Hobson surface profilometer was used to measure the wear scar depth by sliding a probe across the wear track. The surface topography in 2D and 3D along with the wear profile of the disc specimens are presented in Fig.5-5.

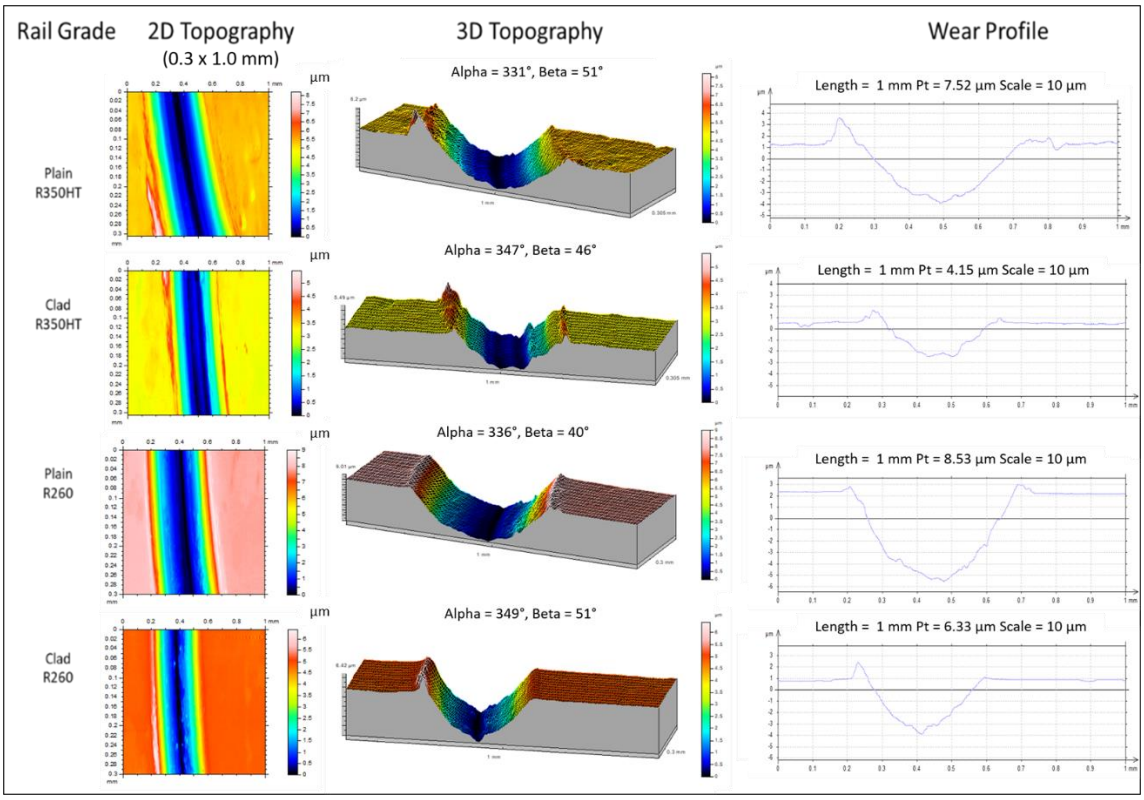

Figure 5-5: Surface topography and wear profile

The measured wear scar depth and wear volume are presented below in Table 8.

Table 8: Measured Wear Depth and Wear Volume

Disc Specimen	Wear depth (µm)	Wear volume (mm^3)
Plain R350HT	5.48	14.6×10^{-3}
Clad R350HT	3.10	9.8×10^{-3}
Plain R260	7.53	26.3×10^{-3}
Clad R260	4.00	12.2×10^{-3}

A comparison of the measured wear volume and the estimated wear volume based on the ASTM model is presented in Fig.5-6. While there are some variations between the two sets of data, it is to be noted that the ratio of volume loss is relatively consistent – Plain R350HT wear ≈ 1.50 times of Clad R350HT, Plain R260 wear ≈ 2 times of Clad R260.

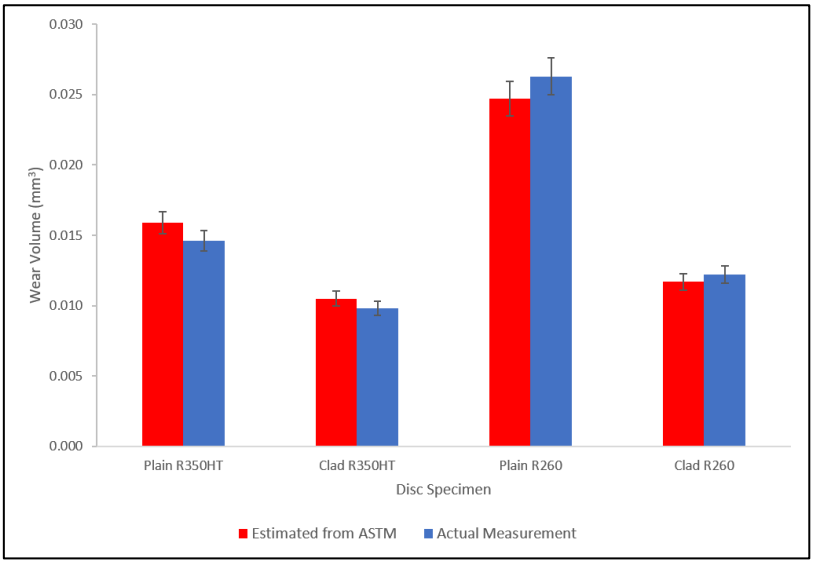

Figure 5-6: Wear volume loss of the disc specimens

With the known applied load of 5 N and sliding distance of 100 m, the wear rates can be determined for the cladded and plain rail disc specimens and is shown in Table 9.

Table 9: Wear Rate for the Cladding and Plain Rail Steel

Disc Specimen	***Wear rate (mm^3/N.m)***
Plain R350HT	2.92×10^{-5}
Clad R350HT	1.96×10^{-5}
Plain R260	5.26×10^{-5}
Clad R260	2.04×10^{-5}

5.4 Wear Coefficient of Clad Material Vs Rail Steel from Archard's Wear Model

The Archard's model is generally used to describe material loss and the dimensionless wear coefficient k, can be obtained from this model to characterize wear resistance of the specimen types above. The contributions of sliding velocity and contact pressure parameters are isolated to wear rate in the calculations and therefore provide a better understanding of the transitions in wear conditions.

$$V_{wear} = k\frac{Ns}{H}(mm^3) \tag{12}$$

The primary difference between the wear rate calculated above and the wear coefficient derived from Archard's wear model is that it takes into account the hardness of the softer contact body (disc specimen in this case) which is an influential factor in wear and tribology studies. The derivation of wear coefficients is an efficient tool that allows for rapid preliminary assessment of the wear problem based on experimental test trials between the contact bodies.

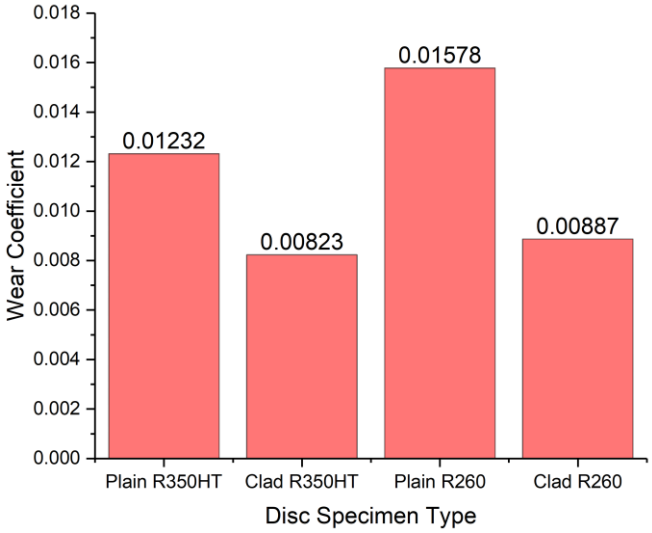

Figure 5-7: Wear coefficient k, for cladded rail and plain rail

The wear coefficients in Fig.5-7 are synchronous with the wear rates obtained wherein the k value for cladded specimens are approximately half that of the rail steel specimens. It is apparent that the wear rates and hence wear coefficients decrease significantly when the disc specimen has laser cladded layer deposited. It can be inferred that the microstructure and hardness of the cladded layer influences the wear resistance of rail steel. The higher wear coefficient indicates low wear resistance and the Stellite 6 cladded rail steel disc specimens exhibit superior wear resistance in comparison to the plain rail steel specimens.

The CoF, coefficient of friction plots with respect to the wear test cycles are shown in Fig.5-8. Referring to the CoF plots, there is a sudden peak in the values at the beginning which indicates the first point of sliding contact established between the two bodies as initial stage of wear process starts to occur. The initial rapid increase between 0.5 and 0.6 then stabilizes over time and gives rise to an average CoF of 0.51 and 0.49 for the cladded R260 and R350HT track respectively. The CoF observed for the plain rail steel specimens are slightly higher with an average of 0.56 and 0.57 for the R260 and R350HT track respectively.

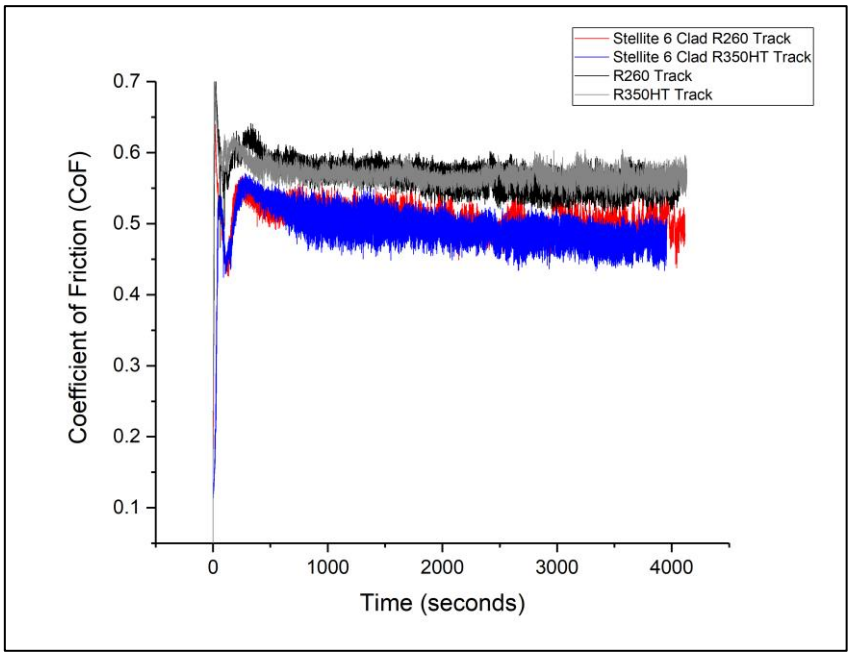

Figure 5-8: CoF vs Time Plot for both cladded and plain rail steel (against Al2O3 Ball)

The pure sliding test conditions allowed for preliminary assessment of wear in this laboratory-scale experimental test trials prior to the full-scale rail test studies. Similarly, previous research works have also proven feasibility with Clare demonstrating the scope of laser cladding to enhance rail wear service life of the standard R260 grade rail steel [7, 8]. Pore-free deposits and crack-free bonding was achieved while the wear performance and work hardening ability of Stellite 6 in comparison to the standard rail steel was evaluated. Lewis, et al then evaluated capability for rail repair by carrying out twin disc test trials to study wear and rolling contact fatigue (RCF) performance of laser cladded rail steel for which Stellite 6 displayed favourable wear characteristics among the several other clad materials examined in comparison with the standard R260 grade rail steel [6, 9].

Lai, Quan and Roy, Taposh, et al also achieved promising results from studies demonstrating laser cladding feasibility on hypereutectoid rail steels while investigating the effects of heat treatment on mechanical properties, wear and RCF performance of the cladded hypereutectoid rail steels [10-12, 66].

The wear behaviour and damage mechanisms are studied in the present research in Section 5.5 to further ascertain and examine the difference in wear coefficients and the wear resistant property of Stellite 6 and the R350HT grade rail steel material.

5.5 Wear Failure Mechanism of Clad Material Vs Rail Steel

The wear tracks were further analysed using SEM to assess and characterize the wear damage mechanism.

a) Stellite 6 Cladded Rail Steel

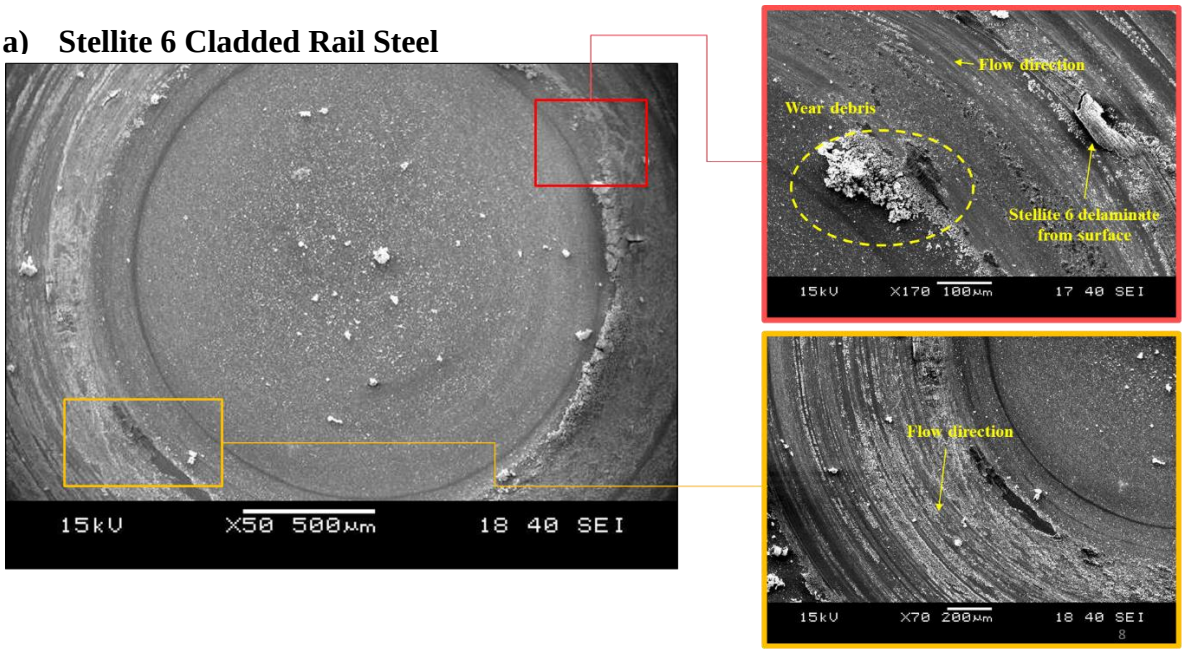

b) Plain Rail Steel

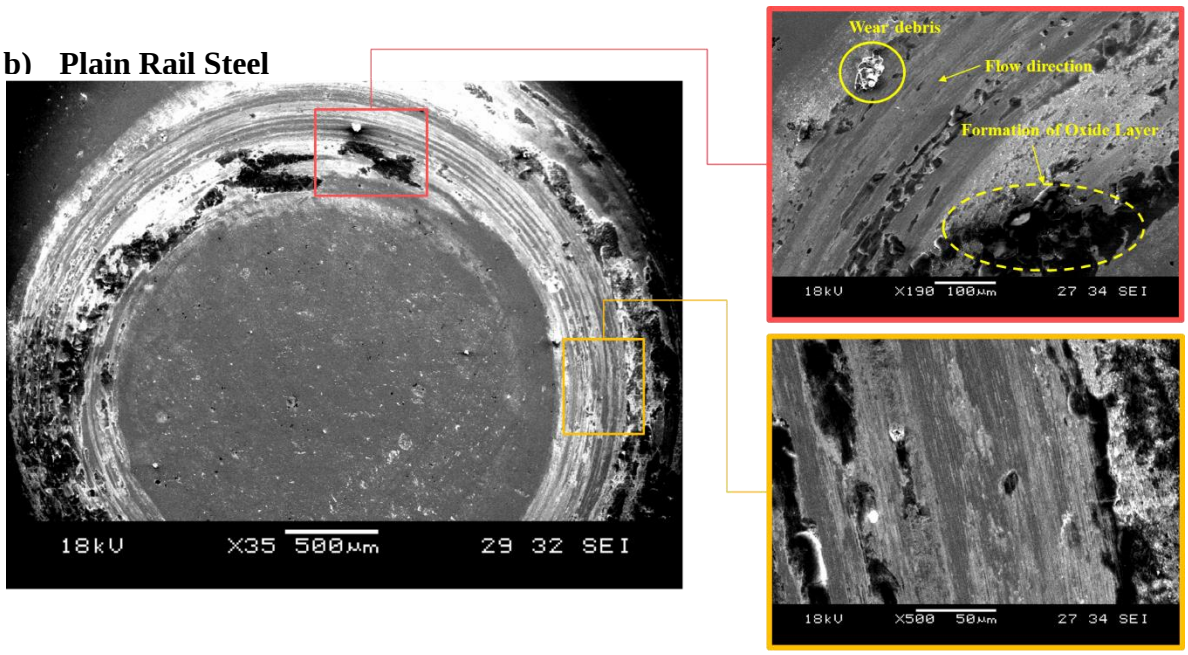

Figure 5-9: SEM images of cladded wear track section

Observations from the SEM images of the wear track sections show that both abrasive and adhesion wear are present. For the cladded surface, wear track is relatively uniform with some wear debris build-up on the circumference of the track. Delamination is identified as the dominant wear mechanism. Due to contact with the hard alumina ball surface, the Stellite 6 layer is observed to delaminate from the disc surface. Delamination occurs as the ball starts to plough into the disc surface over time with the uniform applied load. On the contrary, severe form of wear is observed on the surface of the plain rail steel surface. The abrasive grooves are more well-defined on the track and there are thick oxide layers formed at certain regions of the wear track. The wear damage mechanisms observed can be correlated to the wear performance of the cladding surface and rail steel substrate surface without cladding deposited. The difference in wear coefficients can be associated to the severity of wear conditions between the clad and rail steel which is representative of the wear resistance of Stellite 6 in comparison to the rail steel.

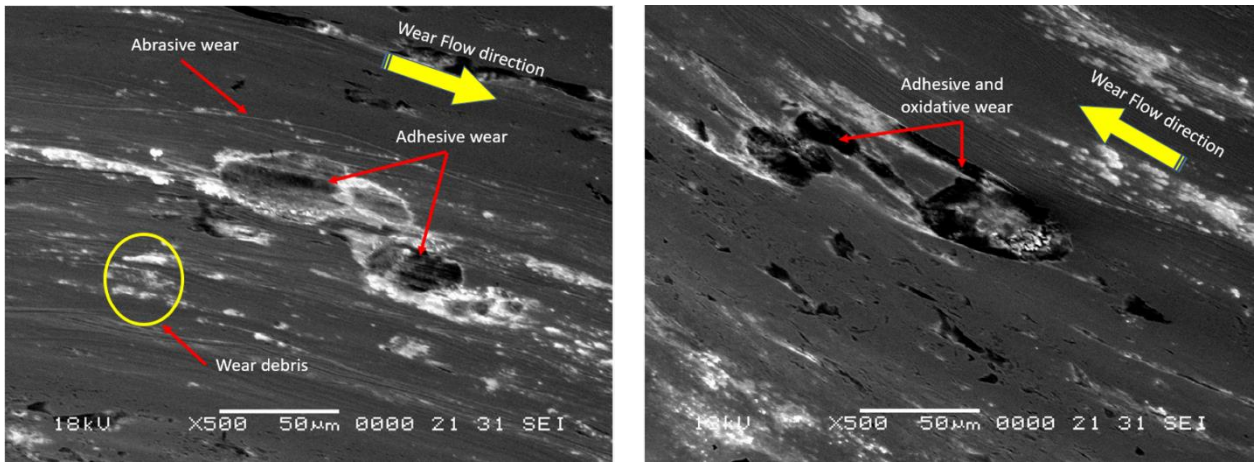

Figure 5-10: SEM images showing presence of abrasive, adhesive and oxidative wear mechanisms on wear track

5.6 Work Hardening Behaviour of Clad Material Vs Rail Steel

Work hardening occurs when there are plastic deformations on the surface of the rail. For the Ball-On-Disc tests, deformations occur each time the alumina ball goes around the track. This in turn alters the specimen's surface microstructure. With changes in microstructure, materials tend to return to its original state. However, due to metal's plasticity, it is unable to do so and thus, internal forces were formed, resulting in increased strength and hardness to the material [138-140].

Moreover, when new dislocations are formed, it also gives rise to tangles and jogs which restricts the mobility of the dislocations. With the immobility of the dislocations, it will thus give rise to hardness and strength to the material as well.

Hernández's et al concluded that by adopting the Ball-On-Disc experimental wear test method, the work hardening of rail steels can be evaluated and studied [83]. Likewise, Lewis et al investigated the work hardening effect of wheel and rail steel materials with the aid of twin disc wear test experiments and proved that rail surface hardness can be increased by up to 2.5 times of the bulk material hardness [139, 140].

As such, to validate the conclusion, hardness data of the wear specimens was recorded before and after the test trials with the Microhardness Tester.

Table 10: Hardness Data of Test Specimens

Brinell's Hardness (HB)	Initial	10,000 Cycles	50,000 Cycles	100,000 Cycles
R260	261	294	304	309
R350HT	367	371	373	373
Stellite 6	480	539	596	605

Complying with the ASTM standards, A370-18, the Vickers Hardness test was performed to determine the hardness of the wear test specimens [132]. The Vickers hardness data is then converted to Brinell's hardness for comparison. The values are tabulated and graphed in Table 10. It can be observed that hardness values generally increase over the number of test cycles implying that work hardening capability of the materials is evident. The hardness values were correlated with the total sliding distance in terms of the total number of wear test cycles and is plot in Fig.5-11 as shown.

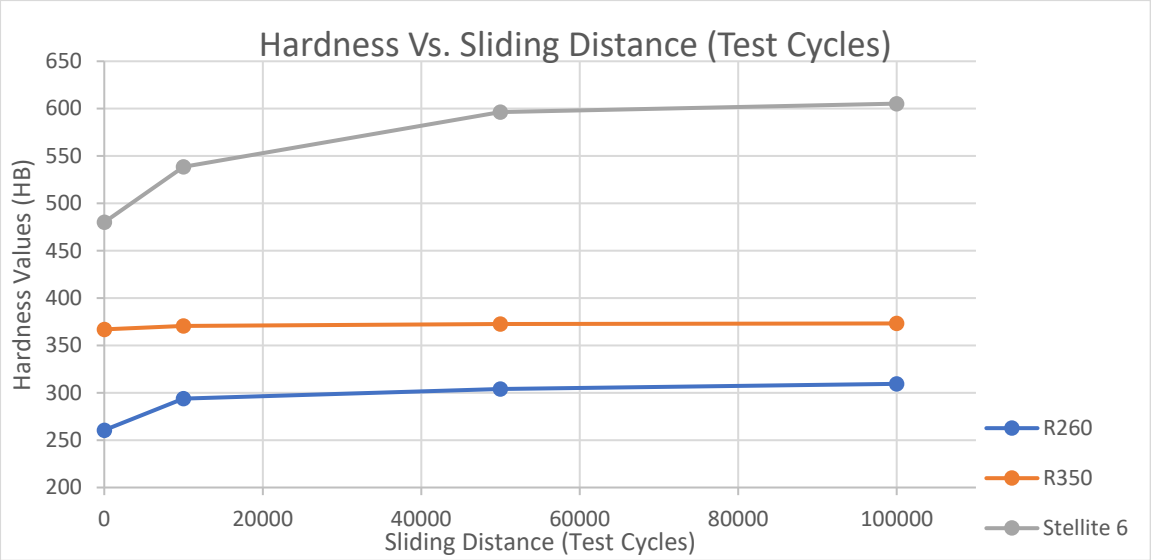

Figure 5-11: Hardness Vs Sliding Distance (in terms of no of test cycles)

5.7 Chapter Summary

The wear test results obtained from the ball-on-disc tribometer for durability study provides the following concluding remarks.

Wear volume of cladded R350HT is about 1.5 times less than the plain R350HT. Likewise the wear volume of cladded R260 is about 2 times less than the plain R260.

Overall, the cladded specimens exhibited wear volume significantly lower than the plain rail steel specimens. Wear for both the cladded R350HT and R260 is identical albeit a slightly higher wear seen for the latter.

Wear volume estimated using ASTM wear equation yielded similar results to actual wear measured using a surface profilometer. Wear coefficients obtained from the Archard's wear model prove the superior wear resistance of Stellite 6 cladding in comparison to the plain head hardened R350HT and standard R260 grade rail steel. Coefficient of friction for both the clad and plain rail is identical with minimal variation.

Adhesion and abrasion wear damage mechanisms were observed on the SEM images of wear track which are more prominent for the track on rail surface without cladding and thick oxide layers formed is an indication of rapid oxidation. As for the wear track on the cladded surface, delamination of the Stellite 6 cladding was present caused by ploughing of the harder contact alumina ball surface.

Work hardening ability of the rail steel grades R260 and R350HT were compared and assessed with respect to the Stellite 6 laser clad material. Plot of hardness data in correlation to the sliding distance in term of the total no. of wear test cycles showed general increasing trend of the hardness over the number of test cycles while ensuring steady-state wear is achieved.

Chapter 6 Shear Testing and Analysis of Clad/Substrate Material Interface for Delamination Study

The methodology for shear testing and analysis is discussed. The clad material/rail steel interface bond strength is evaluated and compared with the shear strength of the plain rail steel. The results from the shear testing and analysis will be used to characterize the clad/substrate material interface bond for assessment of delamination.

The design of shear test setup and methodology to investigate interface bonding between clad material and rail steel substrate is described in detail in Sections 6.1 and 6.2. The test results from the delamination study comprise of interface bond strength, failure & fracture analysis of the cladding layer which are discussed in Sections 6.3, 6.4, and 6.5. Concluding remarks from the chapter are summarised in Section 6.6.

6.1 Shear Test Setup

The interfacial bond strength between Stellite 6 clad material and the base R350HT rail steel was evaluated by conducting shear tests that conform with the American Standards ASTM A-264 [68]. A schematic illustration of the shear test setup is presented in Fig.6-1. The dimensions of the shear blocks and shear test samples were selected with reference to ASTM A-264.

The procedure to determine shear strength of cladded rail steel plate is as follows:

1) Preparation of tensile shear specimens which are then subjected to compression loading
2) Apply compressive load “F” on top of the shear test specimen such that fracture occurs along the interface region
3) Divide the load “F” by the shearing area to obtain shear strength

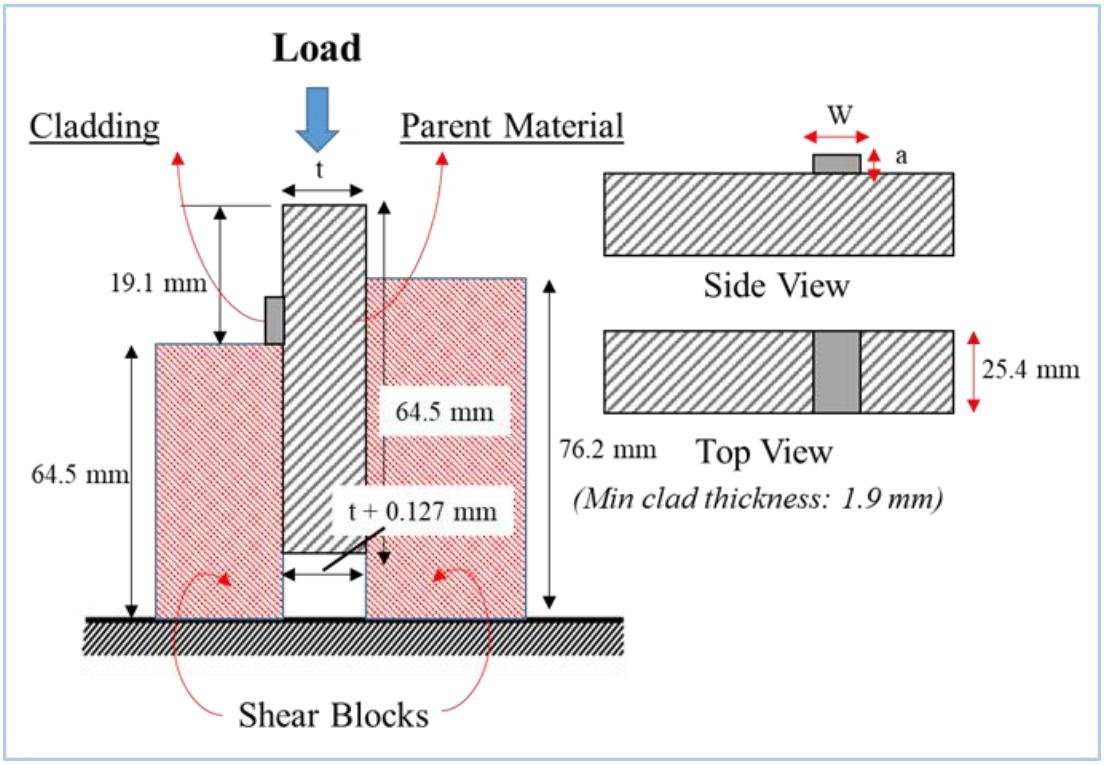

Figure 6-1: Schematic illustration of shear test setup in accordance to ASTM A-264

Since metallic materials in general are proven to exhibit shear strength of approximately 0.577 of their yield strength based on the von Mises Yield Criterion, the test results will then be used for comparison with the shear strength of parent metal to evaluate bond quality [141, 142].

The fracture mode type for this proposed test method is classified as “mode II: In-plane shear crack opening” and is shown in the illustration below in Fig.6-2, among the two other modes of fracture.

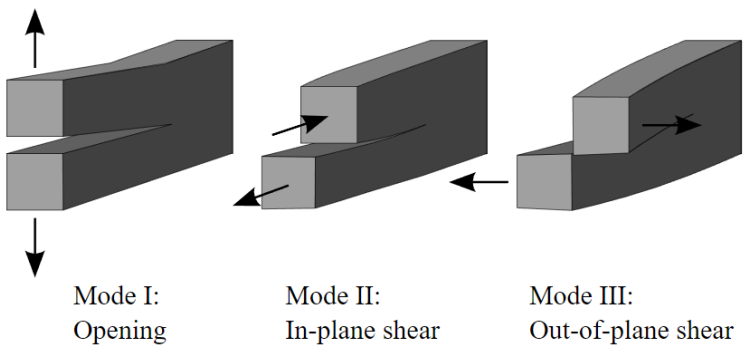

Figure 6-2: Three main modes of fracture classifications [143]

6.2 Shear Test Methodology

A small section of R350HT grade rail was cut into 5 separate segments and cladded with Stellite 6. Four specimens were deposited with 1 mm thick clad layer while an additional specimen was deposited with 2 mm thick cladding for comparative study. The shear test specimen dimensions are clearly illustrated in Fig.6-3.

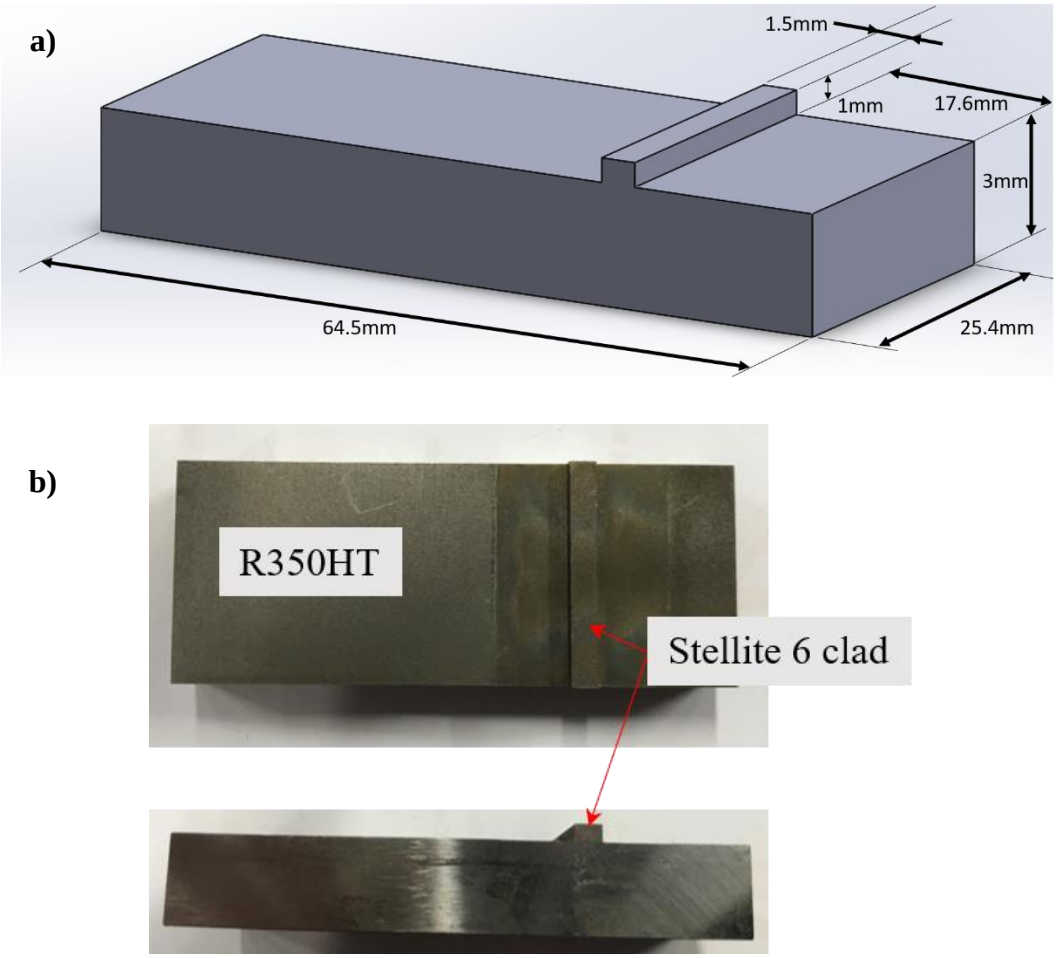

Figure 6-3: (*a*) Schematic showing shear test specimen dimensions, (*b*) Test specimen extracted from cladded rail steel section

The shear test experiment was conducted using a universal testing machine at room temperature of 23 °C under displacement-controlled test condition with loading rate selected as 1 mm/min. The fixture for the test was designed and fabricated from hardened steel, based on the ASTM A-264 standards. A schematic illustration of the test procedure is shown in Fig.6-4.

For the cladding interface bond strength analysis, the shear test condition was such that the shear direction conformed with the cladding direction, parallel to the interface line. The shear test specimens were subjected to compression loading by applying load “F” on top of the test specimens which were then sheared along the bonding interface upon completion of the testing process.

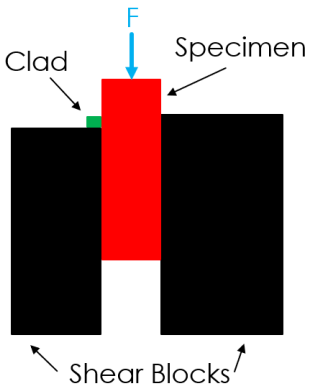

Figure 6-4: Actual shear test setup with specimen secured to fixture and loaded

6.3 Shear Failure Analysis

The load vs displacement plots for the specimens tested are provided in Fig.6-5.

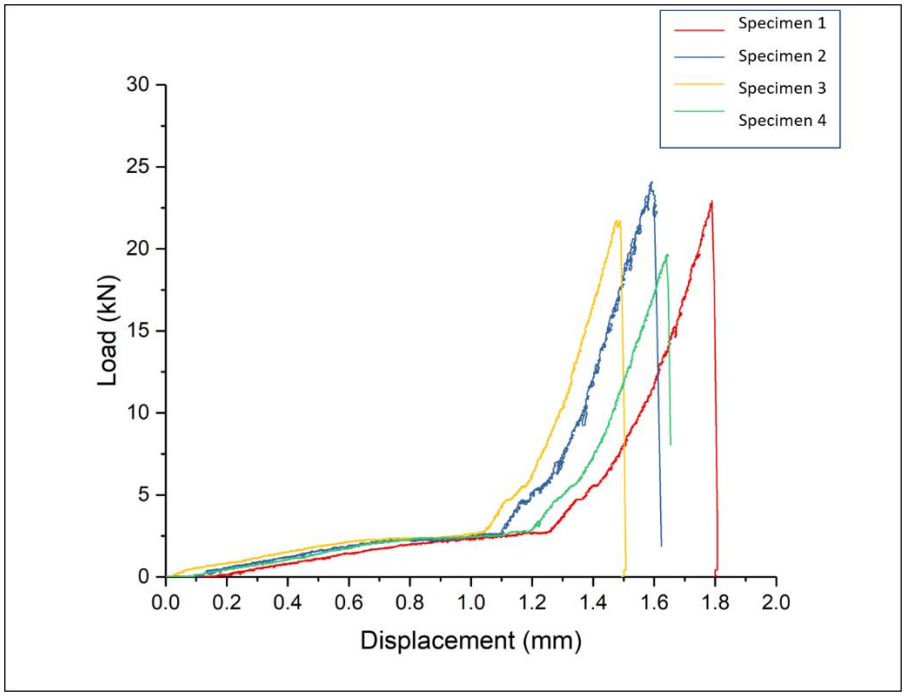

Figure 6-5: Load vs Displacement plot of the four shear test specimens

As the load gradually increases to about 2.5 kN, shearing starts to occur and thereafter as the load rises sharply and peaks at ≈ 20 kN where the specimens fail before load drops to zero. The minor variations in the load where shear begins and when the peak load shear failure occurs can be associated with the cladding quality. Fig.6-6 is further illustration of the shear stress at which the specimens fail. It is established that the shear strength is calculated as 57.7% of yield strength based on Von Mises Yield criterion. The average shear strength of the cladded specimens is evaluated to be approximately 581±25 MPa which corresponds to ≈ 76 % of the yield strength and 32 % higher than the shear strength of R350HT rail steel. The average shear strength is also significantly higher than the minimum of 140 MPa as specified in the ASTM A-264 standards.

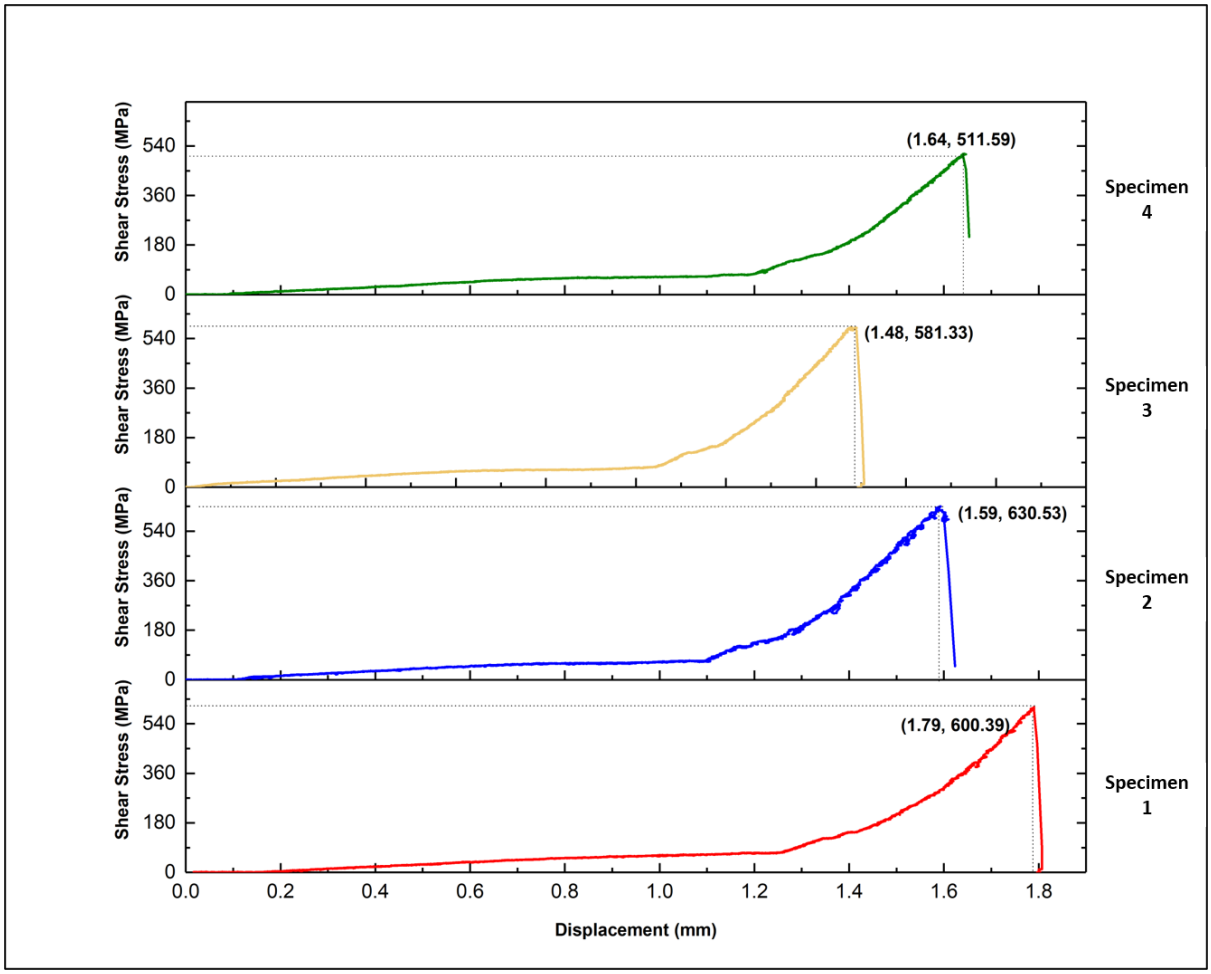

Figure 6-6: Shear vs Displacement plot of the four shear test specimens

According to a similar shear test study conducted by Rao et al on the assessment of interfacial bond strength of cladded plates, the shear bond strength was evaluated to be 22 % higher in comparison to the shear strength of the parent metal [141].

6.4 Clad Material-Rail Steel Interface Bond Strength

Results obtained from the shear test experiment are presented in the following Table 11 below. The test results indicate that the shear strength evaluated for all the Stellite 6 cladded specimens exceeds that of corresponding properties of R350HT rail steel, thereby verifying the existence of strong metallurgical bond between the cladding layer and rail substrate material. Preliminary assessment indicates that delamination is unlikely to occur when cladded rail track is subjected to train load due to the strong interfacial bond. This proves that there is sufficient capability to meet the performance requirements in laser cladding repair & remanufacturing of rail steel.

Table 11: Shear Test Results Summary

Specimen	Shear Area (mm^2)	Maximum Shear Load (kN)	Shear Strength (N/mm^2)	Time to Failure (sec)	Cladding thickness (mm)
1	38.17	22.92	**600**	91	1
2	38.19	24.08	**631**	93	
3	37.40	21.74	**581**	90	
4	38.43	19.66	**512**	88	
5	76.60	43.36	**566**	102	2

Repeatability of the shear test trials to verify the shear bond strength showed identical results as shown in the shear stress vs displacement plot in Fig.6-7.

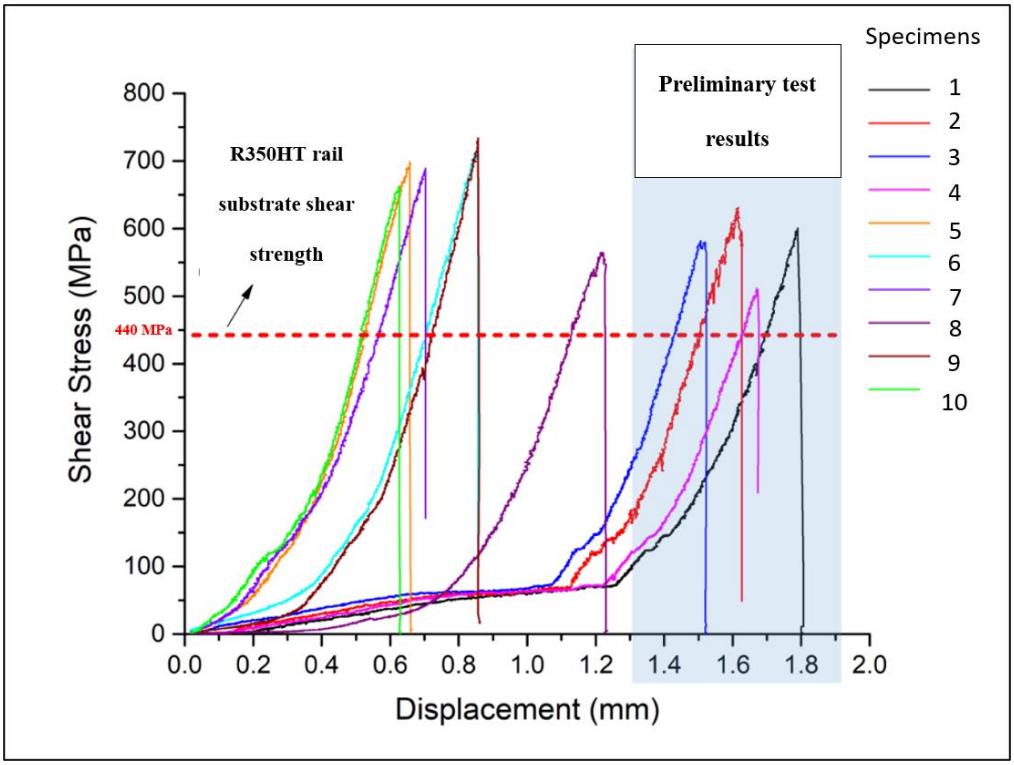

Figure 6-7: Shear stress vs Displacement plot

6.5 Shear Fracture Analysis

Images of the failure location and the fracture surface morphology after shear test are presented for analysis. Fig.6-8 to 6-12 shows the photographs along with LSM optical micrographs of the fracture surfaces of the sheared test specimens. The shear strength test specimens were examined to fracture at the interface bond line and complete fracture of the cladding from the base rail steel plate was observed for all except one specimen. It has to be noted that this break-up that occurred during the shearing process indicates total detachment of the clad layer from the rail steel substrate leading to interfacial delamination. The initial shear crack is originated at the bond interface, as the shear crack then primarily tears from the bond interface and then propagates within the rail steel substrate side where the strength is lower than that of the cladding layer side. The dominant cracks then propagated in the direction parallel to the applied loading.

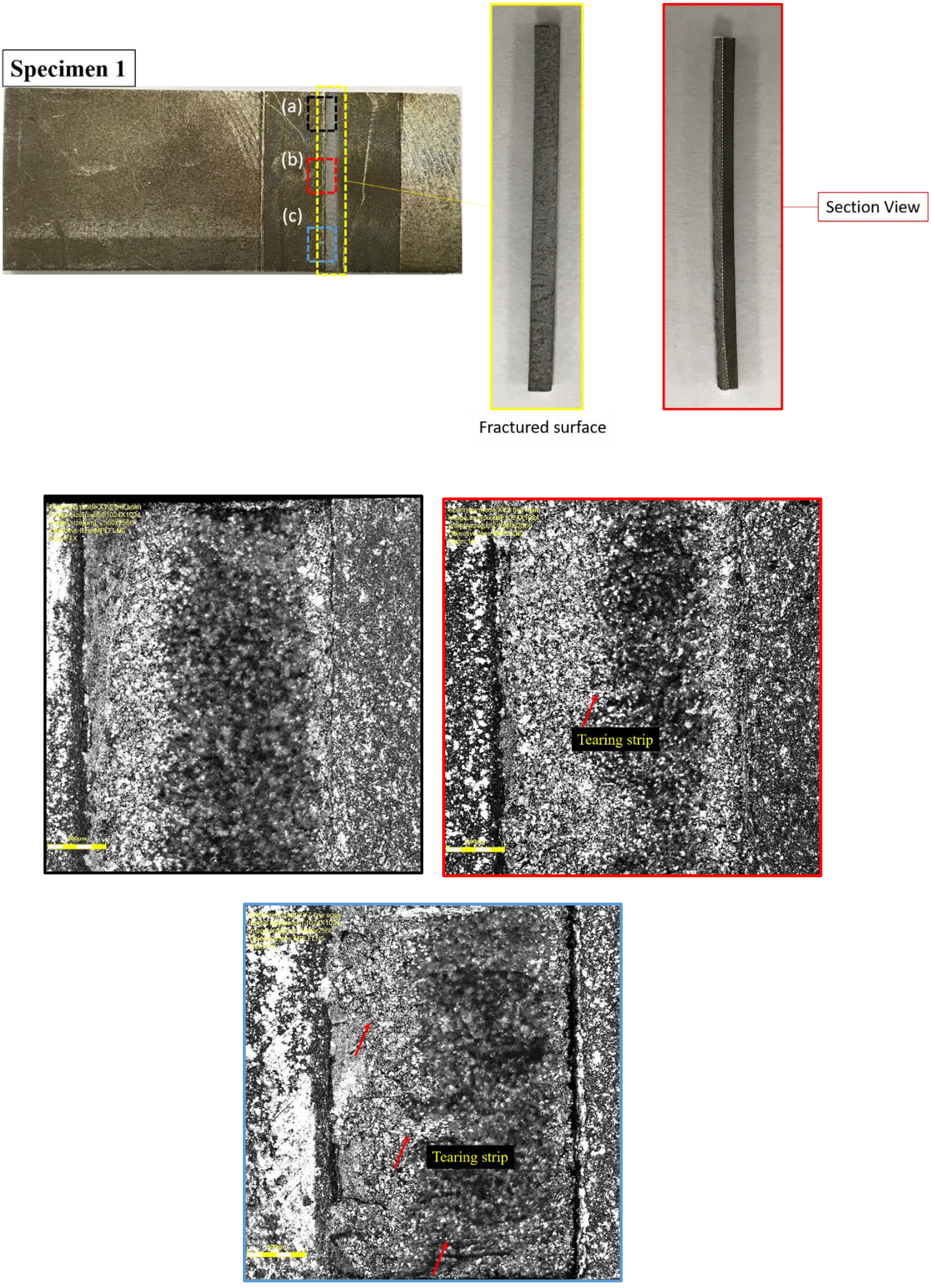

Figure 6-8: Optical micrographs – fracture surface morphology of shear test specimen (1)

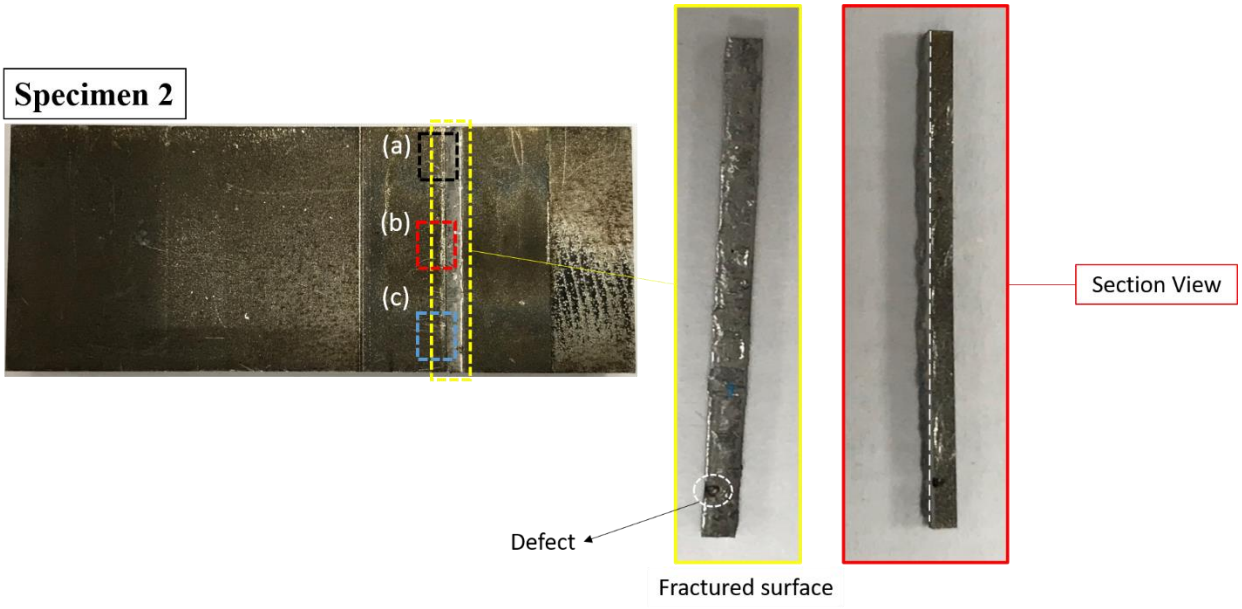

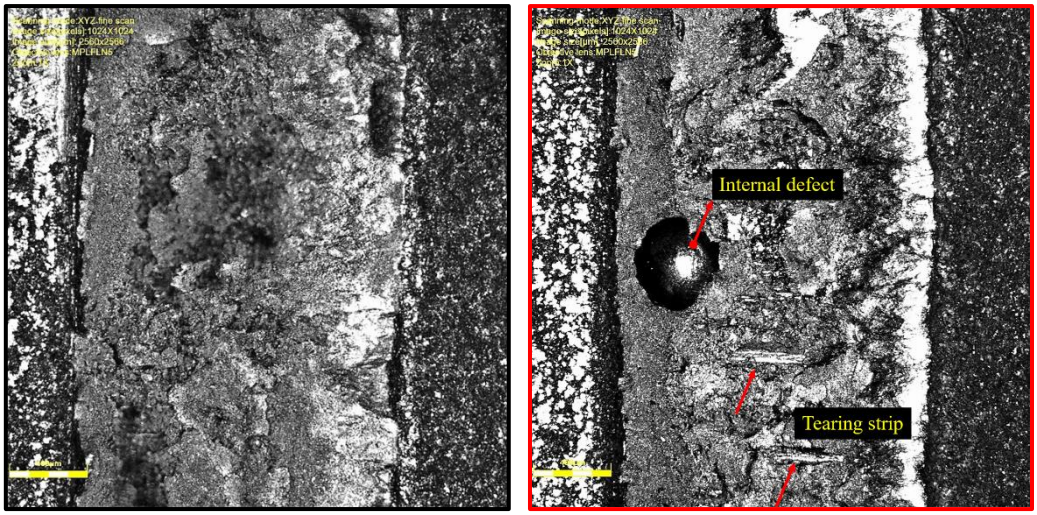

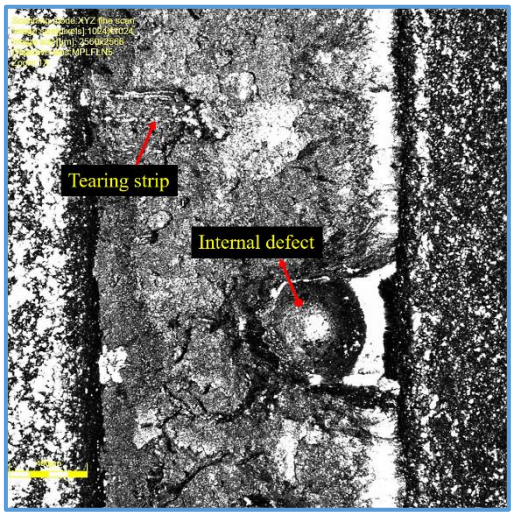

Figure 6-9: Optical micrographs – fracture surface morphology of shear test specimen (2)

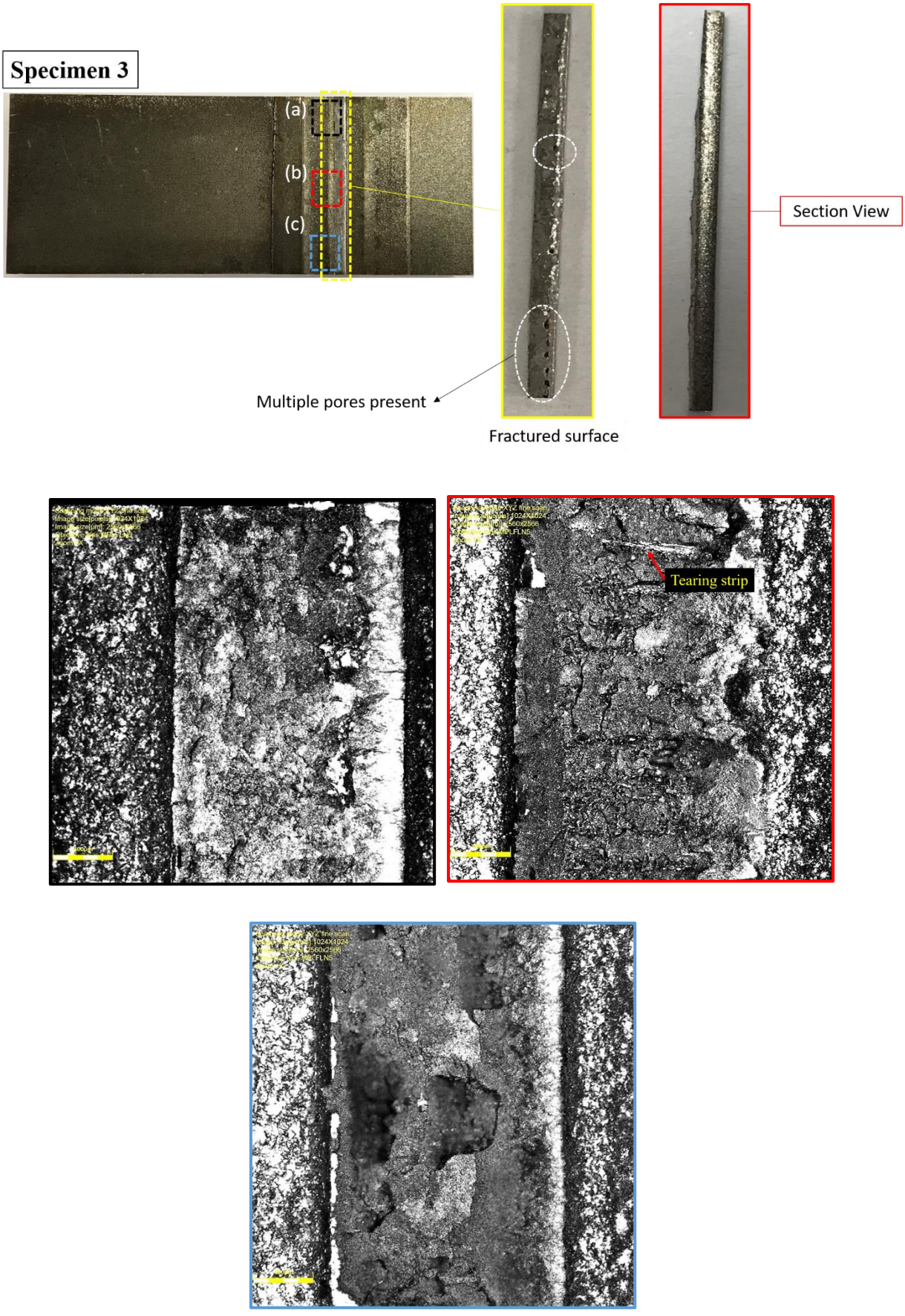

Figure 6-10: Optical micrographs – fracture surface morphology of shear test specimen (3)

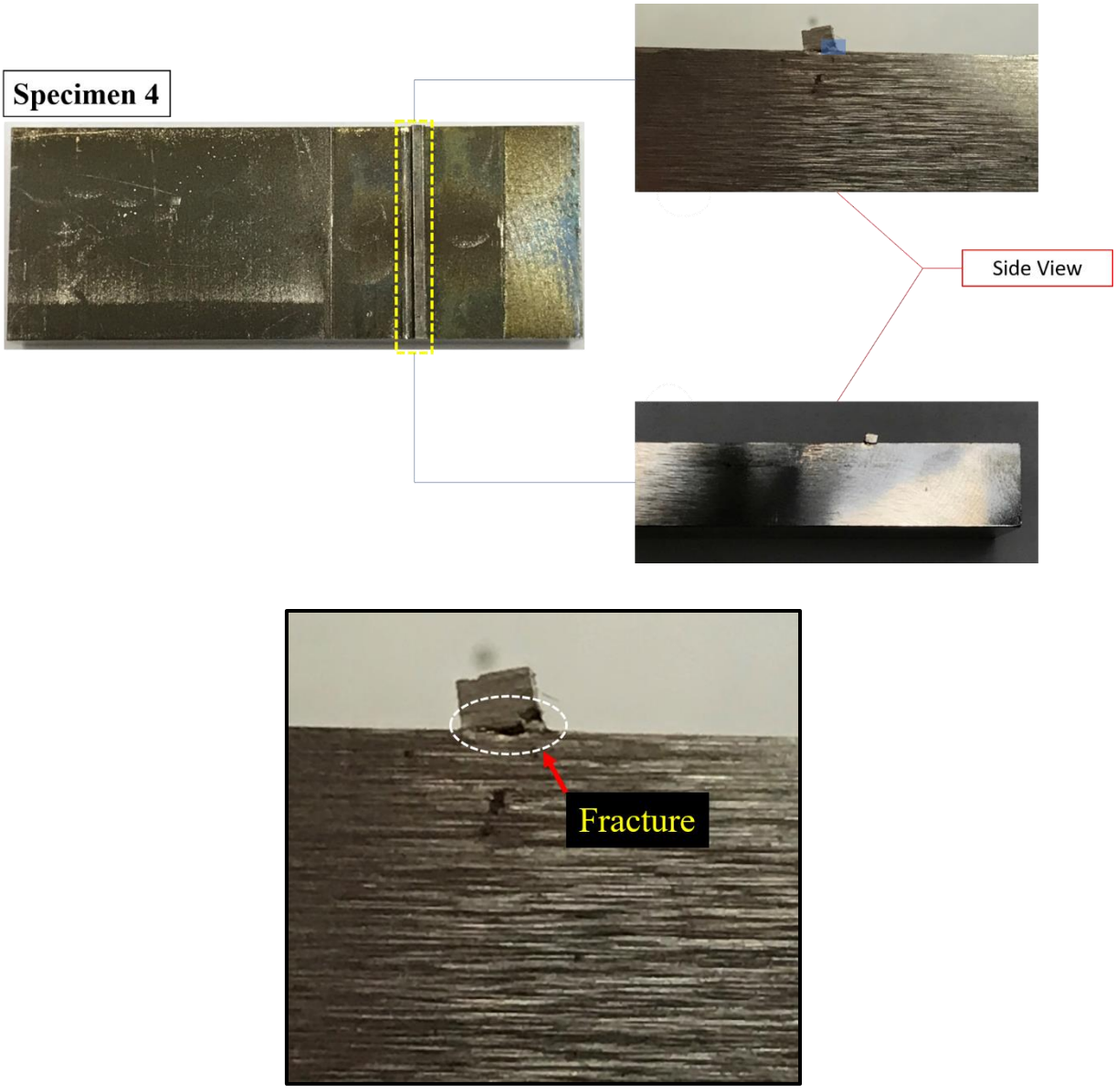

Figure 6-11: Optical micrographs – fracture location of shear test specimen (4)

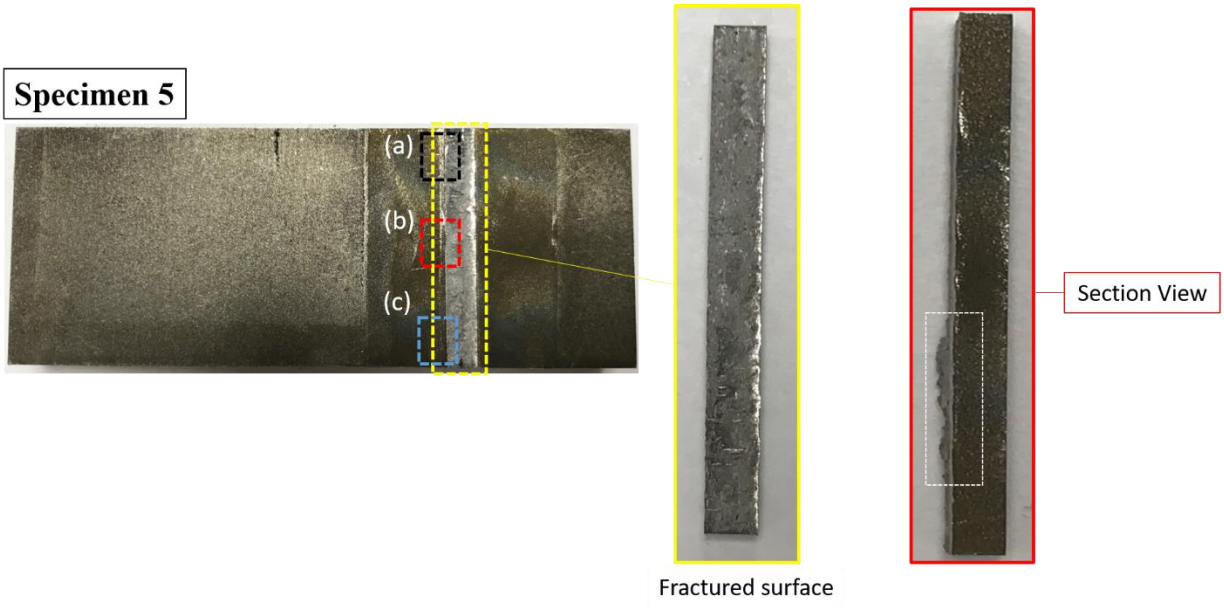

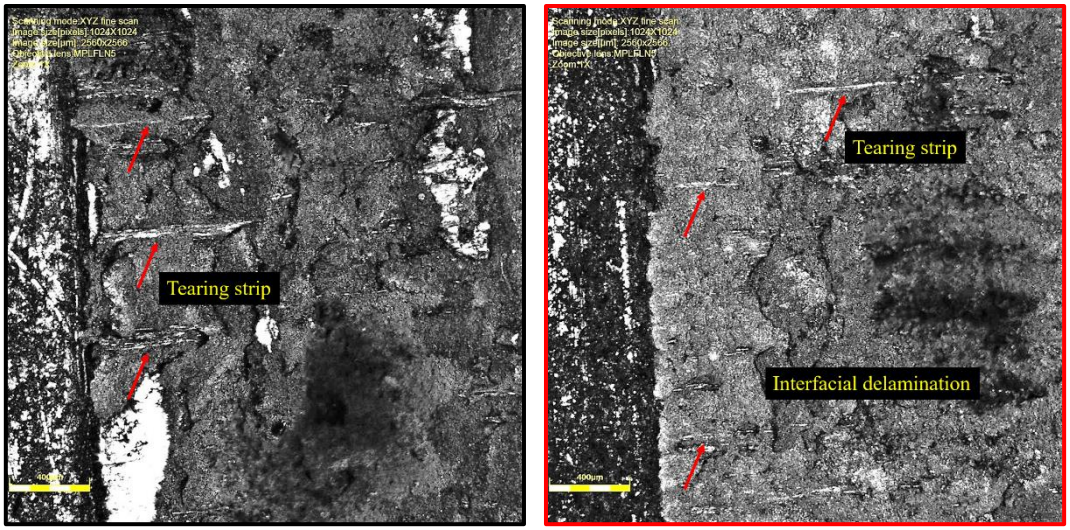

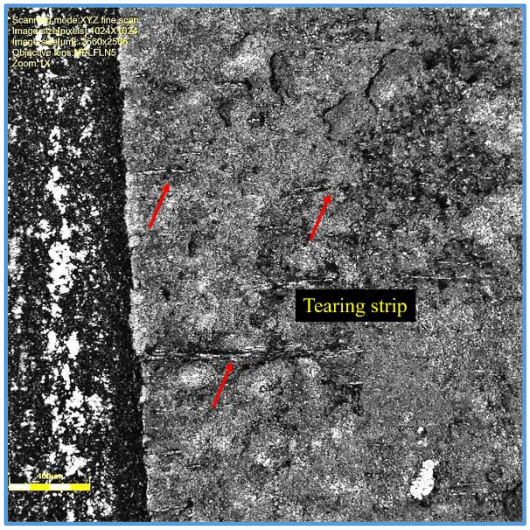

Figure 6-12: Optical micrographs – fracture location of shear test specimen (5)

Based on the study of the optical micrographs and analysis of the fracture surface morphologies of the specimens, it is evident that shear initiated along the edge where the specimen was loaded. The crack was developed in the substrate metal but did not reach the bond interface line as examined from the LSM images, particularly in Fig.6-8 where the smooth crack surface implied a clean break during failure. Fig.6-9 shows non-uniform fracture of the surface which is also closer to the interface line in comparison to the failure of specimen (1). Multiple pores are present near the clad interface in Fig.6-10 where the fracture is observed to have occurred even closer to the bond interface line. The porosity could have also resulted in a lower shear bond strength relative to the other two specimens (1) and (2). In Fig.6-11, the tested specimen shows fracture initiating in the cladding rather than at the interface or the rail substrate. The additional test specimen (5) which was deposited with 2 mm thick cladding layer (Fig.6-12) showed fracture occurring at the interface with minimal amount of base material still attached at the cladding interface. Tearing marks can be seen that were generated from the point of shear. Interfacial delamination was the primary mode of fracture that occurred due to the pure shear phenomena.

The results and observations from the analysis are consistent with the research findings of Zhu et al where the main fracture site was observed in the parent metal side as the crack initiated and propagated along the bond interface line [144]. The interface exhibited good bonding quality in majority of the test specimens examined.

6.6 Chapter Summary

The shear test experiment results obtained from the methodology proposed and developed for delamination study provides the following concluding remarks.

Shear load (stress) Vs Displacement plots were derived for which shear failure of the clad material specimens occurred. Preliminary assessment indicated that delamination is unlikely to occur when cladded rail steel is subjected to train load due to the strong interfacial bond. Shear strength from the test results exceed 57.7% of yield strength of R350HT rail steel based on Von Mises Yield criterion. The shear strength test specimens were examined to fracture at the interface bond line and complete fracture of the cladding from the base rail steel plate was observed for all except one specimen. The crack was developed in the substrate metal but did not reach the bond interface line.

Shear initiated along the edge where the specimen was loaded as tearing marks were observed, generating from the point of shear. Interfacial delamination was the primary mode of fracture that occurred due to the pure shear phenomena.

The interface bond strength assessment allowed improved understanding of the shear failure damage mechanism of the cladded test specimens. With the optical micrographs pointing to fracture occurring at the rail substrate site and not at the interface bond line, the bond quality from the laser cladding process is favourable for on-track full-scale reliability test trials.

Chapter 7 Reliability Assessment and Full-Scale Testing of Laser Cladded Rail Track

Upon completion of the material-process-performance characteristic study of laser cladded rail steel, the research focus involved full-scale reliability test trials of laser cladded rail steel specimens on railway track. The rail specimens were laser cladded and installed on both test track and mainline track environment to evaluate cladding reliability and performance when subjected to actual running train load conditions. The purpose of the reliability test trials is to further investigate and confirm laser cladding rail repair feasibility that has been studied at the laboratory level and can be considered as a strategic approach to assess on-track viability of laser cladding repair.

The approach of conducting laser cladding repair of rail head defects which involves extracting specimens from the railway track and carrying out repair trials off-site in a laboratory environment prior to reinstalling the specimens on the track for service from an operational perspective is first investigated.

The design of a comprehensive full-scale reliability test program of laser cladded rail steel on track is elaborated in Section 7.1. The results from inspection and monitoring to investigate reliability and performance of the laser cladded rail track is examined and post-extraction analysis of the cladded rail steel specimens are discussed in Sections 7.2 and 7.3 respectively. Concluding remarks from the chapter are summarised in Section 7.4.

7.1 Full-Scale Reliability Test of Laser Cladded Rail Steel on Track

7.1.1 Preparation of Laser Cladded Rail Steel Specimens for Installation on Track Environment

The full-scale test trials involved cladding procedure of Stellite 6 clad 1-m length on two 6-m long R350HT rail specimens. The cladding process comprised of several intermediary stages that include milling, pre-heat treatment of the rail surface, and post grinding of the cladded surface. In the following Fig.7-1 to 7-5 below, the cladding procedure is described with labelled schematics. The selected clad length of 1 m is divided equally from the centre line.

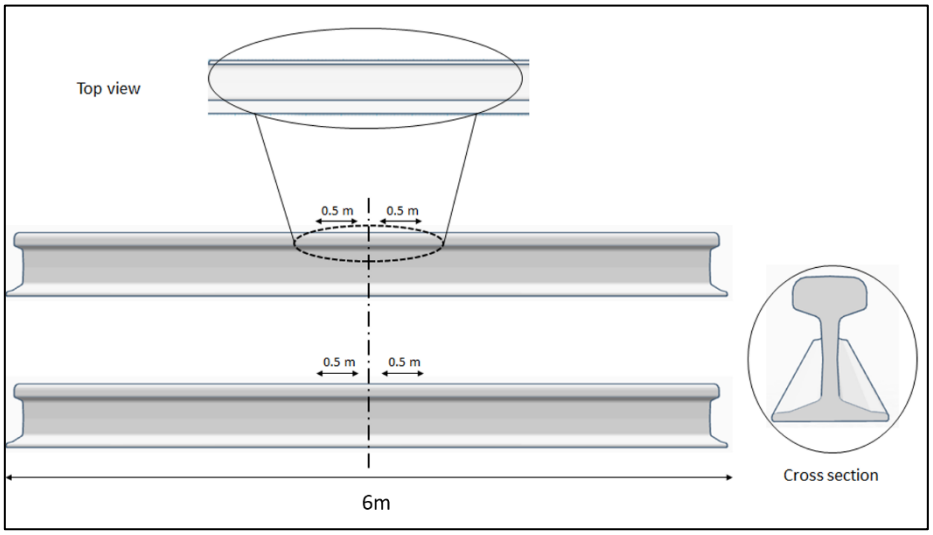

Figure 7-1: Schematic of two 6-m long rail specimens with 1-m clad length defined

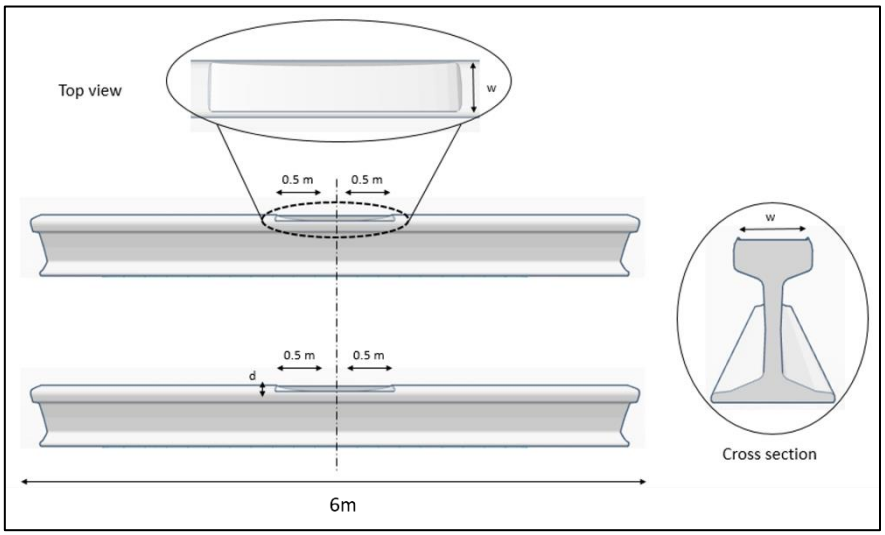

Figure 7-2: Schematic illustration of the material removal from rail surface by milling

The purpose of milling as illustrated in Fig.7-2 is to grind off the top rail surface to remove the first layer of material for preparation of a flat and clean surface prior to the cladding process. Material removal depth and width (approx. full rail head width) are specified as *d* (1 mm) and *w* (70 mm) respectively. Pre-heat treatment of the rail specimen at 200 °C for an approximate 10-minute duration ensured moisture removal from the surface which can affect the clad quality. A 4-kW diode laser source is used with laser spot size of 5 mm diameter for the deposition of two cladding layers on the rail head surface. Clad thickness and width are specified as *t* (1.5 mm) and *w* (70 mm) respectively as shown in the schematic below in Fig.7-3. The cladding area is denoted by the dark shaded zone. The cladding process to complete the 1 m clad length trials is estimated to be ≈ 25 minutes for each layer (Fig.7-4).

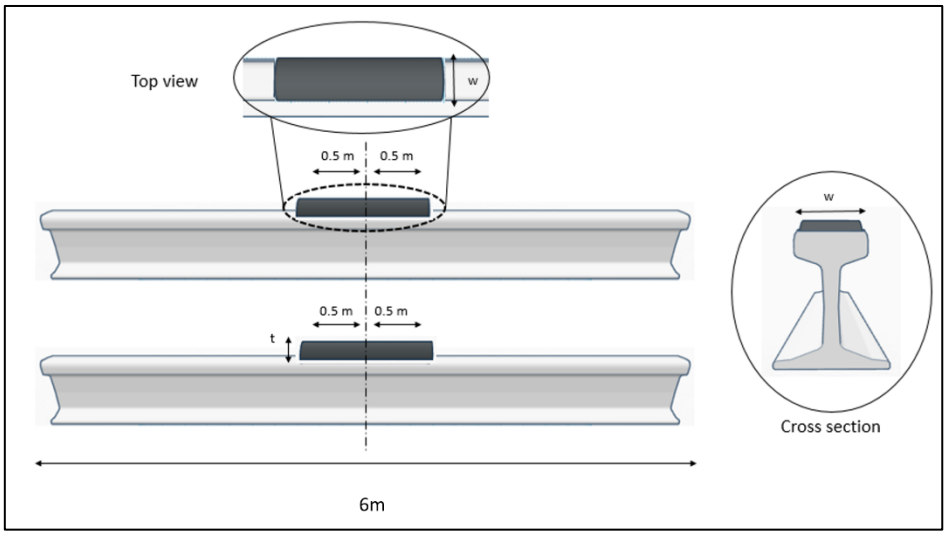

Figure 7-3: Schematic showing the clad zone on the rail head surface

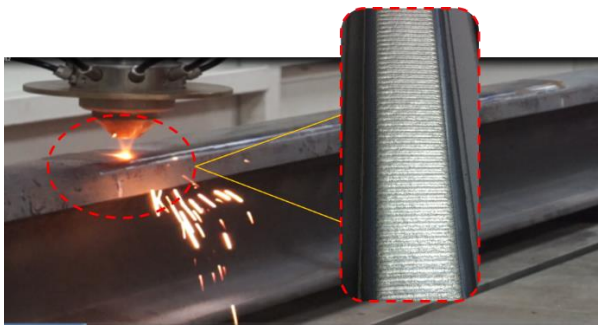

Figure 7-4: Laser cladding process of rail head surface

Post grinding of the cladded rail specimens after the cladding process removes the excess clad material deposited such that the cladded rail profile conforms with the rail head profile as per service standards. The schematic representation and actual cladded surface upon completion of cladding process is as shown in Fig.7-5 and 7-6 respectively.

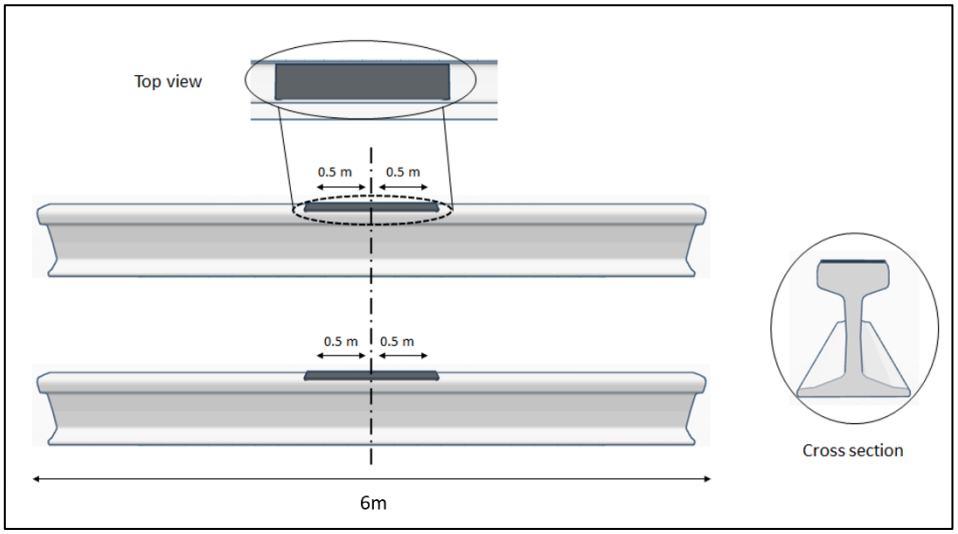

Figure 7-5: Completed clad profile after post grinding

Figure 7-6: Actual clad surface after post grinding

7.1.2 Reliability Assessment of Laser Cladded Rails for Installation on Track Environment

The cladded rail specimens were welded back onto the test track at Bishan depot (BSD) for actual train run tests for reliability study of the cladded track. There were two specific types of tests conducted which are the normal brake test and emergency brake tests. The aim is primarily to evaluate durability of the cladding layer deposited and inspect for presence of any cracks or delamination. The overall test flow of the full-scale reliability trials on the cladded rail track is summarized in Fig.7-7.

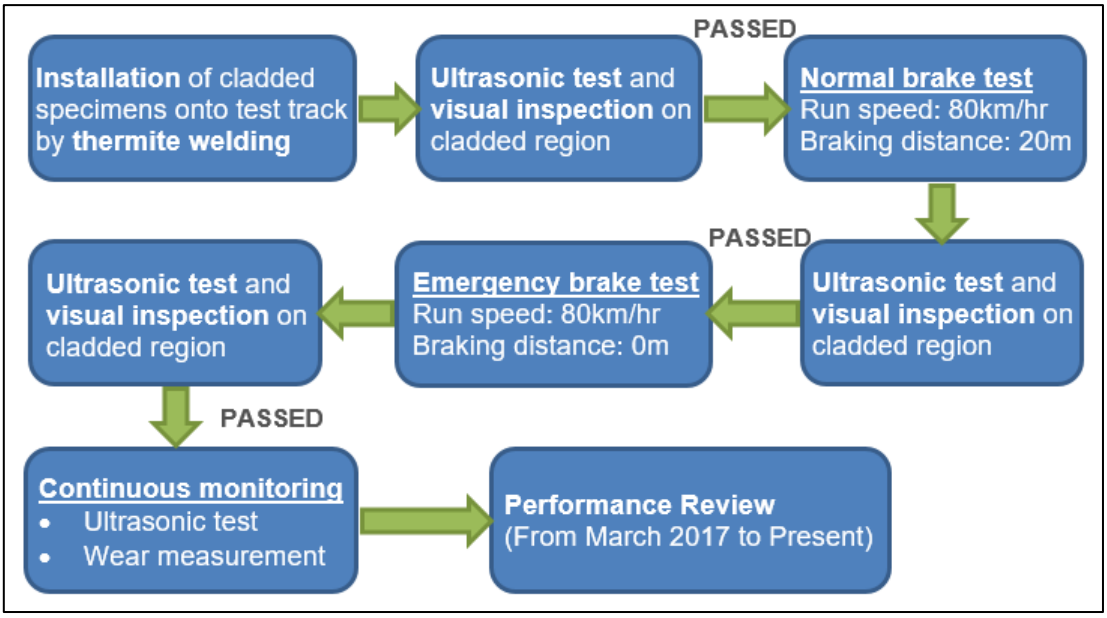

Figure 7-7: Reliability test flow of the full-scale cladded track trials

The cladded rail specimens first installed on March 2017 on the BSD test track (Fig.7-8) were subjected to several modes of inspection and monitoring before and after the train running and braking tests. Initial examination through visual inspection were positive as no obvious signs or indications of wear and damage on the clad surfaces were observed. Ultrasonic test (UT) inspection technique was adopted to further examine and detect for presence of cracks and delamination of the clad.

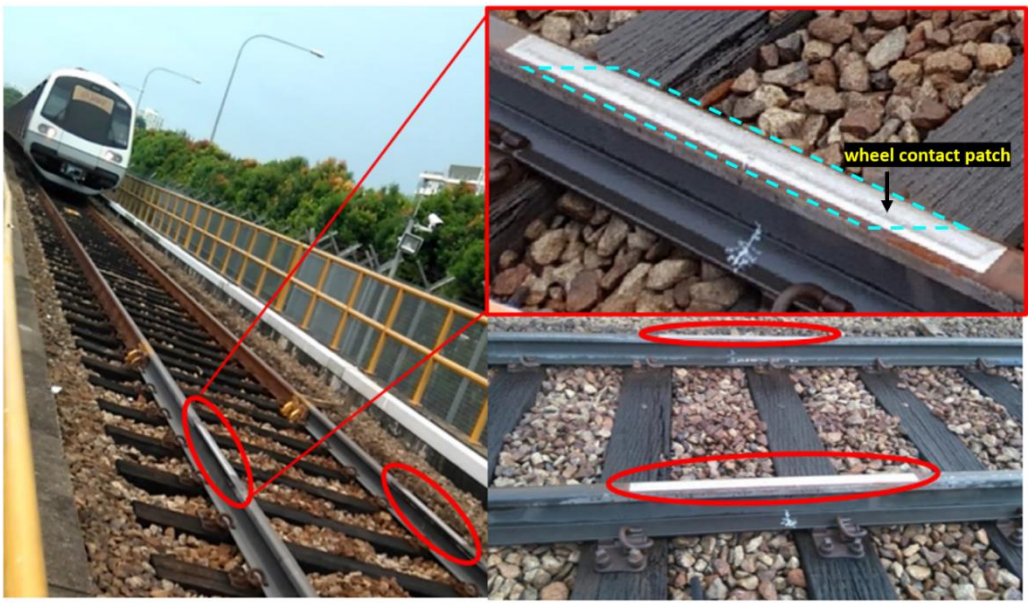

Figure 7-8: Cladded rail specimens on BSD test track

7.2 Performance Monitoring and Inspection of Laser Cladded Rail Steel

Intermittent monitoring and inspection cycles to evaluate the reliability of cladded rails for an approximate 1-year trial duration period was planned. Inspection methods in the form of UT, visual and 3D scanning were selected for reliability assessment of the cladded track specimens. The results and observations are summarised and presented in Table 12 below.

Table 12: Inspection Results of Cladded Rail Specimens

Inspection Period (1 Year)	**UT Inspection**	**Visual Inspection**	**3D scan Inspection**
March 2017 – April 2018	No indications were detected. Cladding layer did not develop any cracks or exhibit delamination	No obvious signs or indications of wear and damage on the clad surfaces were observed	Smooth and uniform wear transitions and mild wear were observed within a tolerance limit of 0.3 mm.

During the 3D scan inspection measurement on-site, the cladded surfaces were cleaned and fitted with markers to capture the surface scan data. Wear map of the cladded rail steel specimens were analysed based on the superimposed surface scan data obtained before and after the specimens were subjected to train induced loads over the 1-year inspection period. Both specimens exhibited smooth and uniform transitions in wear were observed and minimal material loss along the scan data showed mild wear within a tolerance limit of 0.3 mm as shown in Fig.7-9.

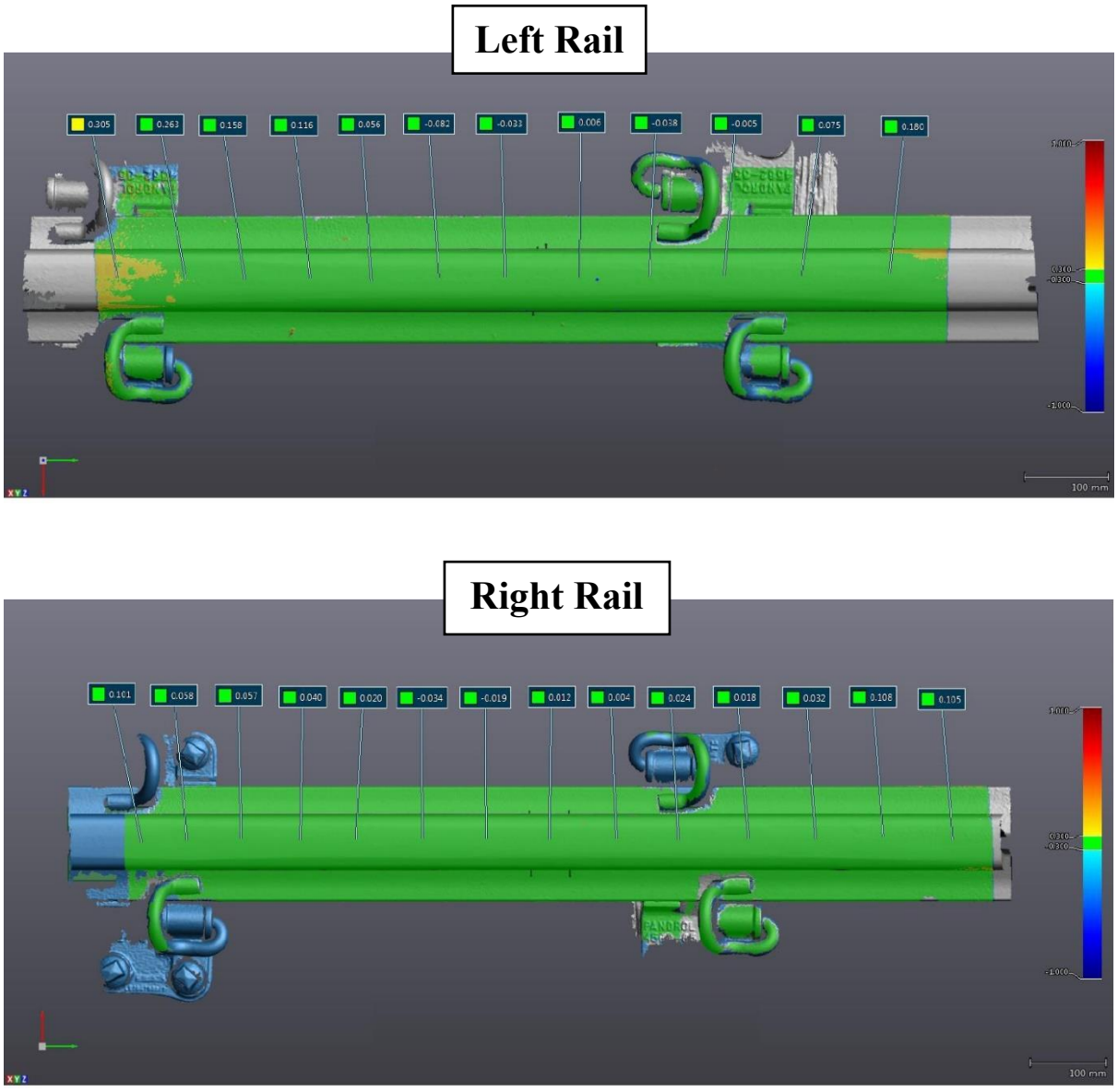

Figure 7-9: Wear map obtained from 3D surface scan data of cladded rail track

Visual inspection of the cladded rail track specimens showed that the cladded section remained intact as no obvious indications of cracking or delamination of the cladding layer were present. Fig.7-10 presents two sets of visual inspection results captured during the monitoring period.

Figure 7-10: Visual inspection of laser cladded rail specimens on test track

While the cladded rails at the test track are still in active service subject to train runs, the current full-scale reliability test trial study serves only as a preliminary assessment to evaluate cladding layer durability and delamination. The test track environment is subjected to low train traffic which also constitutes to low train load and may not be a definitive indicator of the cladded track wear performance which is minimal. Therefore, the next phase of study involved progress to extend the laser cladding reliability trials on mainline track environment.

7.3 Post Extraction Analysis of Laser Cladded Rail Steel

Upon successful implementation of material-process-performance studies on the laser cladded rail specimens both in laboratory and on-site Bishan depot test track trials, the next phase of study involved replicating the initial test trial methodology and install the two straight, parallel 6 m long rail specimens with cladding length of 1 m each on the mainline track for reliability assessment. The cladded rail specimens were installed at Redhill-Tiong Bahru [Chainage 25512 – 25518] on 28th February/1st March 2019. Fig.7-11 below shows the two cladded rail specimens of clad layer thickness 1 mm installed on the track.

Figure 7-11: 2-clad rail specimens installed at Redhill-Tiong Bahru [CH 25514L & CH 25514R]

During the allocated 12-month reliability trial period, the cladded specimens were monitored and assessed based on visual and ultrasonic testing inspection for cracks and delamination. The frequency of monitoring was limited to only 3 sessions [6th March 2019, 17th May 2019, 10th March 2020] due to track access constraints.

As part of the latest monitoring and inspection session on March 2020, it was identified that the cladded specimens had underwent rail profile grinding operations predominantly at the transition region between the clad and parent rail. It has to be also noted that upon installation of the cladded specimens on the track, initial profile grinding was performed at the transition region to mitigate slight differences in rail profile and maintain uniformity.

Upon completion of the 1-year trial duration, the laser cladded rail specimens were then extracted out for post-extraction studies and analysis. During rail replacement work, one of the cladding sections was cut out, about 300mm from the original edge. A thermite weld was then formed at this cut point. An illustration of the cladded specimens prior to extraction is shown in Fig.7-12.

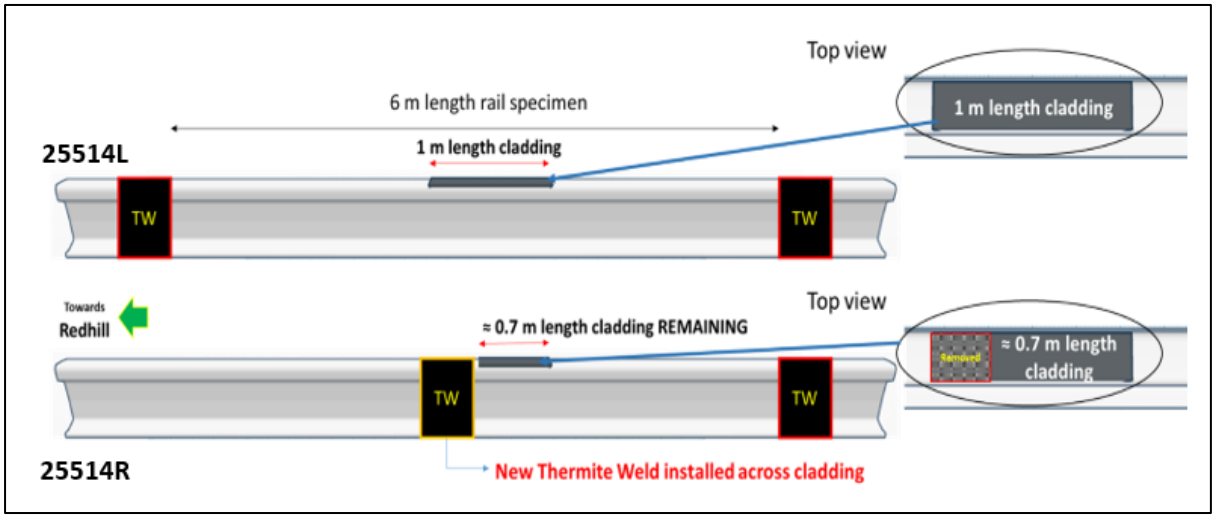

Figure 7-12: Schematic illustration of the cladded specimens prior to extraction

The extracted specimens in Fig.7-13 were then subject to further testing and analysis which included non-destructive testing (NDT), cross-section study at the transition region between the clad material and parent rail to check for any clad toe cracking, and clad-parent rail material integrity study to check for any delamination.

The type of analysis methods adopted are as follows: [A] Non-Destructive Testing (NDT), [B] X-Ray Tomography and [C] Laser Scanning Microscopy.

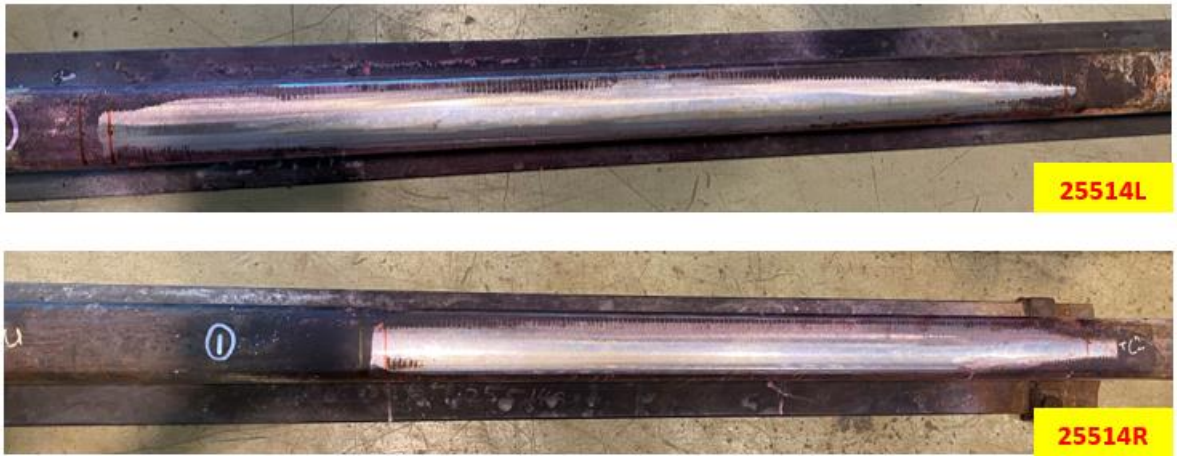

Figure 7-13: Cladded specimens extracted from the mainline track

7.3.1 Non-Destructive Testing (NDT) Analysis

The scope of NDT inspection performed on the cladded rail specimens (25514L and 25514R) to detect defects present in the cladding layer includes Ultrasonic Testing (UT), Penetrant Testing (PT), & Magnetic Particle Testing (MPT). Specifications of the NDT are provided in Table 13.

Table 13: NDT Technique Specifications

Ultrasonic Testing (UT)	Penetrant Testing (PT)	Magnetic Particle Testing (MPT)
Sensitivity was taken on the 1st hole (5 mm FBH) of the rail head in the rail calibration block to a height of 50% of full screen height (50 % of FSH). Equipment used: Doppler ANYSCAN 30	Dye Penetrant Testing was performed on entire clad surface. Chemicals used: Chemetall water washable penetrant (Chekmor 240) with LD7 developer	Magnetic Testing was performed at rail to clad interface. Chemicals & Equipment used: Permanent yoke (4034) White contrast – Nabakem MP 35 Black Magnetic Ink – Nabakem SM 15

The NDT testing was carried out in collaboration with TUV SUD PSB Pte Ltd, a certified & qualified testing services provider. The analysis procedure is of certified standards ensuring accurate results are determined. Based on the UT inspection results obtained, the indication depths detected and clad thickness measured for both the specimens in Fig.7-14 are reflected below in Table 14.

Table 14: UT Indication Depths & Clad Thickness Measurement

S. No	Long Rail (25514L)				Short Rail (25514R)			
	Location, mm (from End A/B)	Depth @ Max. Amplitude, mm	Max. Depth, mm	Clad Thickness, mm	Location, mm (from End A/B)	Depth @ Max. Amplitude, mm	Max. Depth, mm	Clad Thickness, mm
1	0 (End A)	0.57	3.93	0.405	5 (End A)	0.49	2.20	0.460
2	35 (End A)	0.74	3.26	1.150	206 (End A)	0.55	2.60	0.995
3	163 (End A)	1.37	3.92	0.805	259 (End A)	1.78	4.24	1.100
4	463 (End B)	0.98	2.52	0.615	432 (End B)	0.43	3.12	1.200
5	415 (End B)	0.48	2.70	0.625	374 (End B)	1.65	4.31	1.195
6	343 (End B)	1.24	3.07	0.855	204 (End B)	0.43	3.08	0.780
7	300 (End B)	1.43	2.61	0.800	104 (End B)	0.69	4.14	0.880
8	135 (End B)	1.22	3.44	0.450	95 (End B)	0.67	3.02	0.700

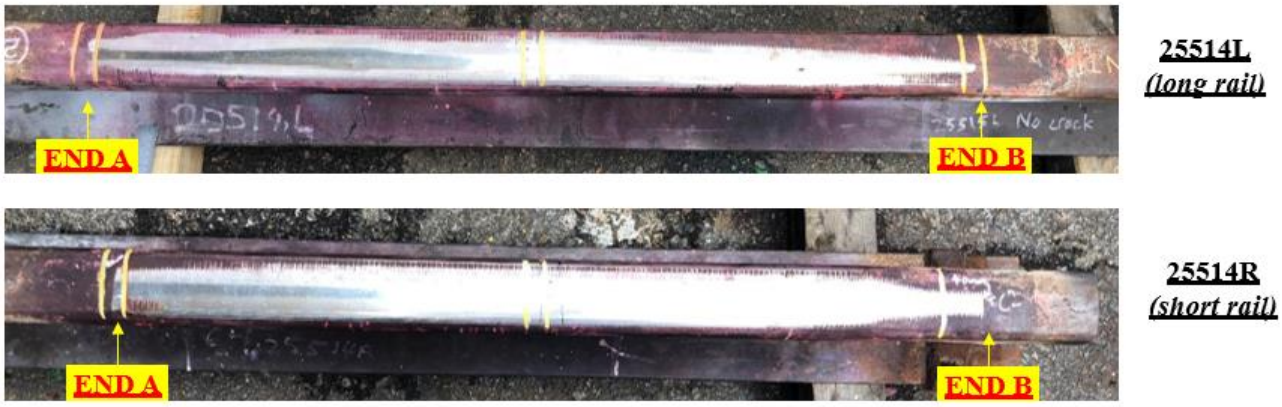

Figure 7-14: UT inspection of the extracted specimens

The PT inspection results are shown in Fig.7-15 where several surface indications were observed on both rail specimens particularly at the interface region between the clad material and parent rail (for the 25514L specimen). However, no cracks or indications were detected along the interface in MPT for both the cladded specimens in Fig.7-16.

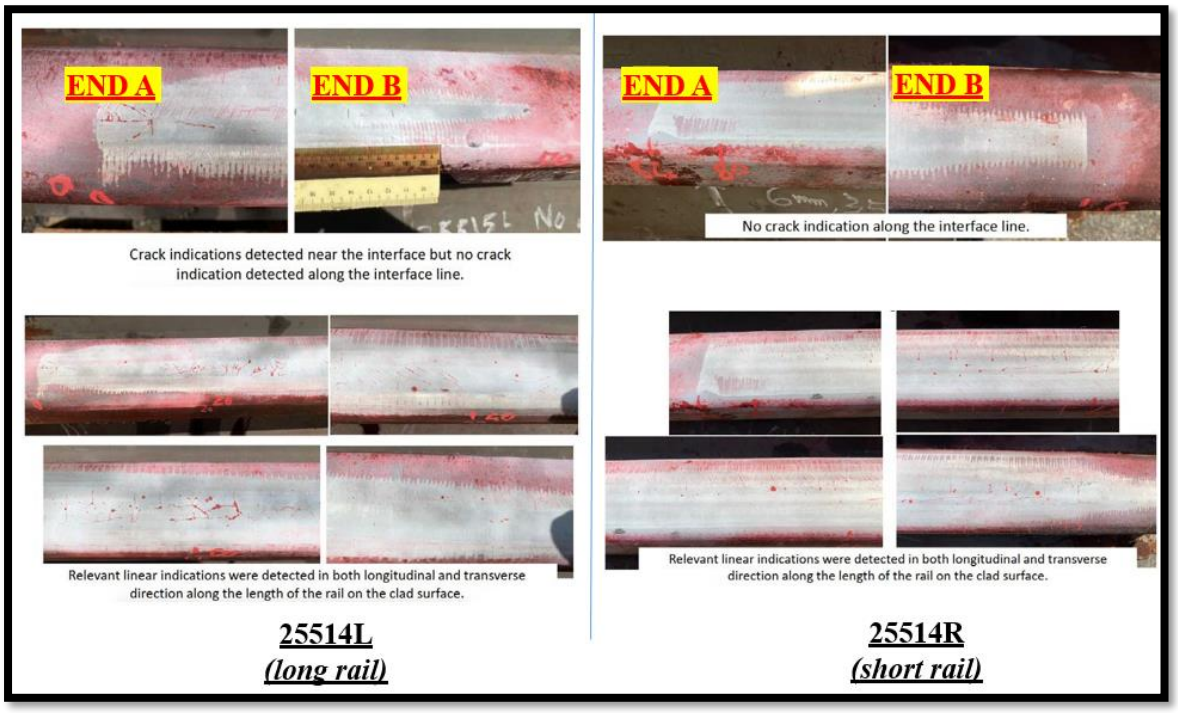

Figure 7-15: PT Inspection results of extracted specimens 25514L & 25514R

Figure 7-16: MPT Inspection results of extracted specimens 25514L & 25514R

Although the results obtained from NDT inspection & analysis showed that several indications were present on the cladded surface of both the rail specimens, it is not distinctly evident if the cladded sections developed any cracks or exhibit delamination due to train induced loads.

Additionally, severe profile grinding operations carried out over the course of the trial period would have significantly affected the reliability assessment. This was also supported by visual inspection of the extracted specimens in Fig.7-17 which showed a “Christmas tree” like shrinking effect of the cladding towards the transition region at both ends of the specimen. Hence, further cross-sectioning study and analysis is required to verify the actual conditions of the cladded track.

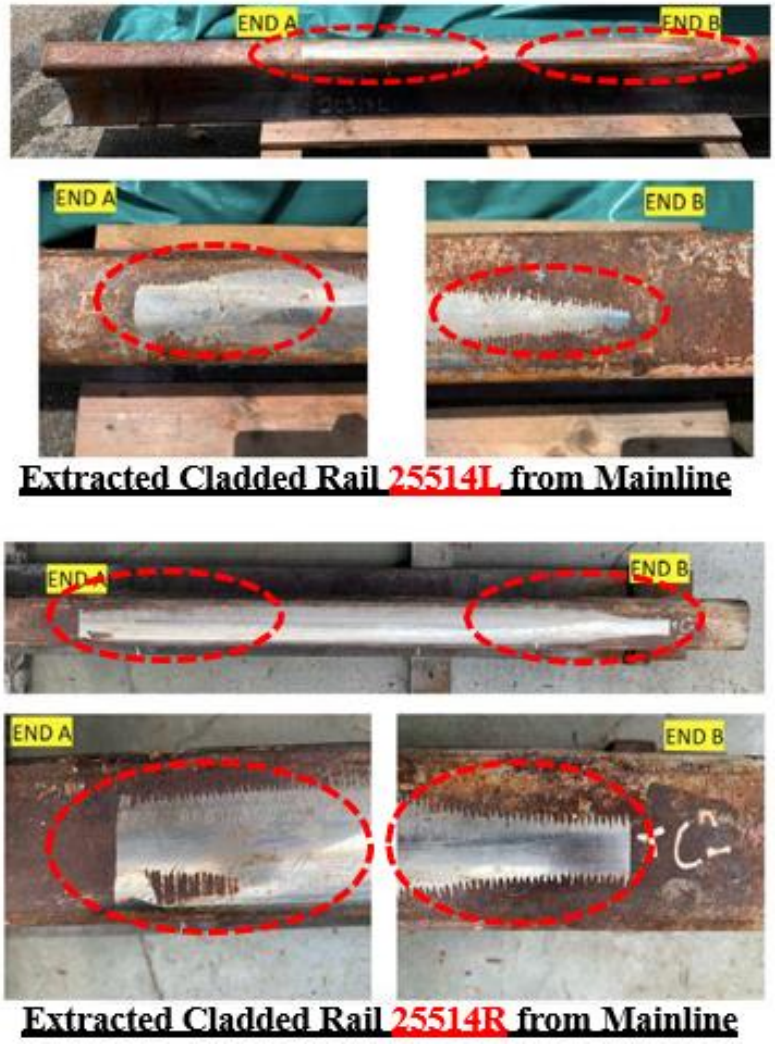

Figure 7-17: Visual Inspection of 25514L and 25514R at the transition region

7.3.2 X-Ray Tomographic Analysis

The purpose of conducting cross-section study is to further assess the clad-parent material integrity, particularly at the transition region. 20-mm rail sections were sliced from the two cladded rail segments (25514L and 25514R) and the wire-cut procedure is illustrated in a schematic in Fig.7-18. The cut-out points were located at 10 mm off the left and 10 mm off the right from the centre-line of clad-rail transition region as indicated below.

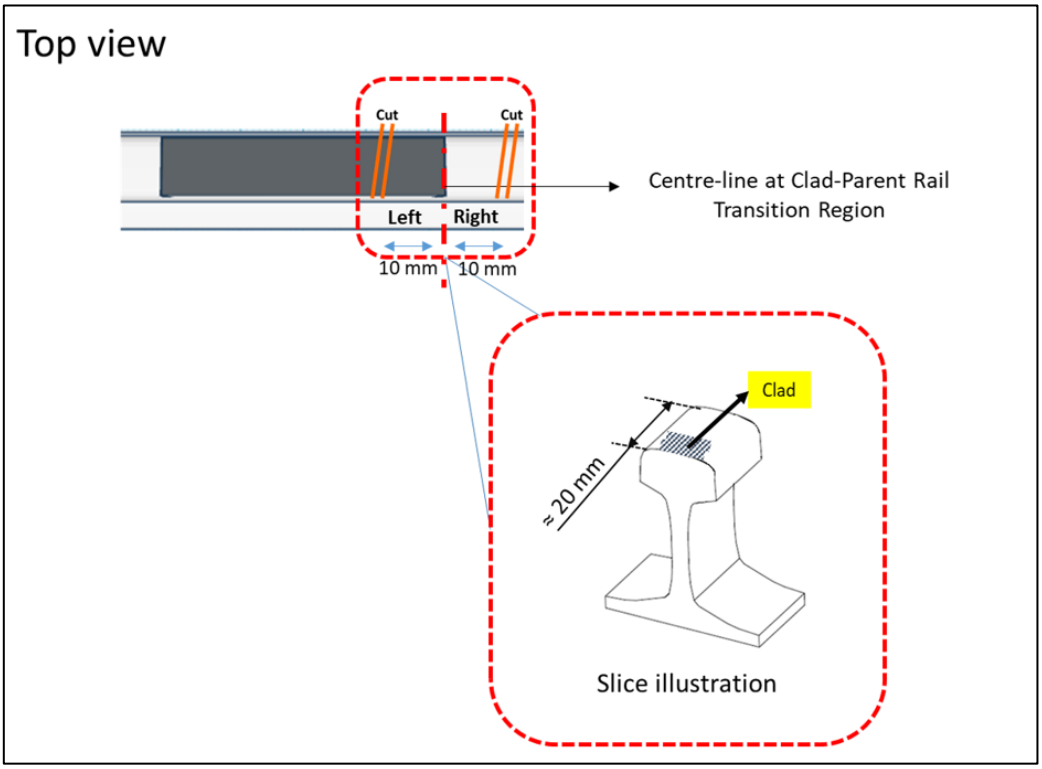

Figure 7-18: Cut-out of 20 mm rail section slice

Five 20-mm rail slices were extracted from the cladded rail segments as part of the cross-section inspection study. The slices were then labelled accordingly as shown in Figure 7-19.

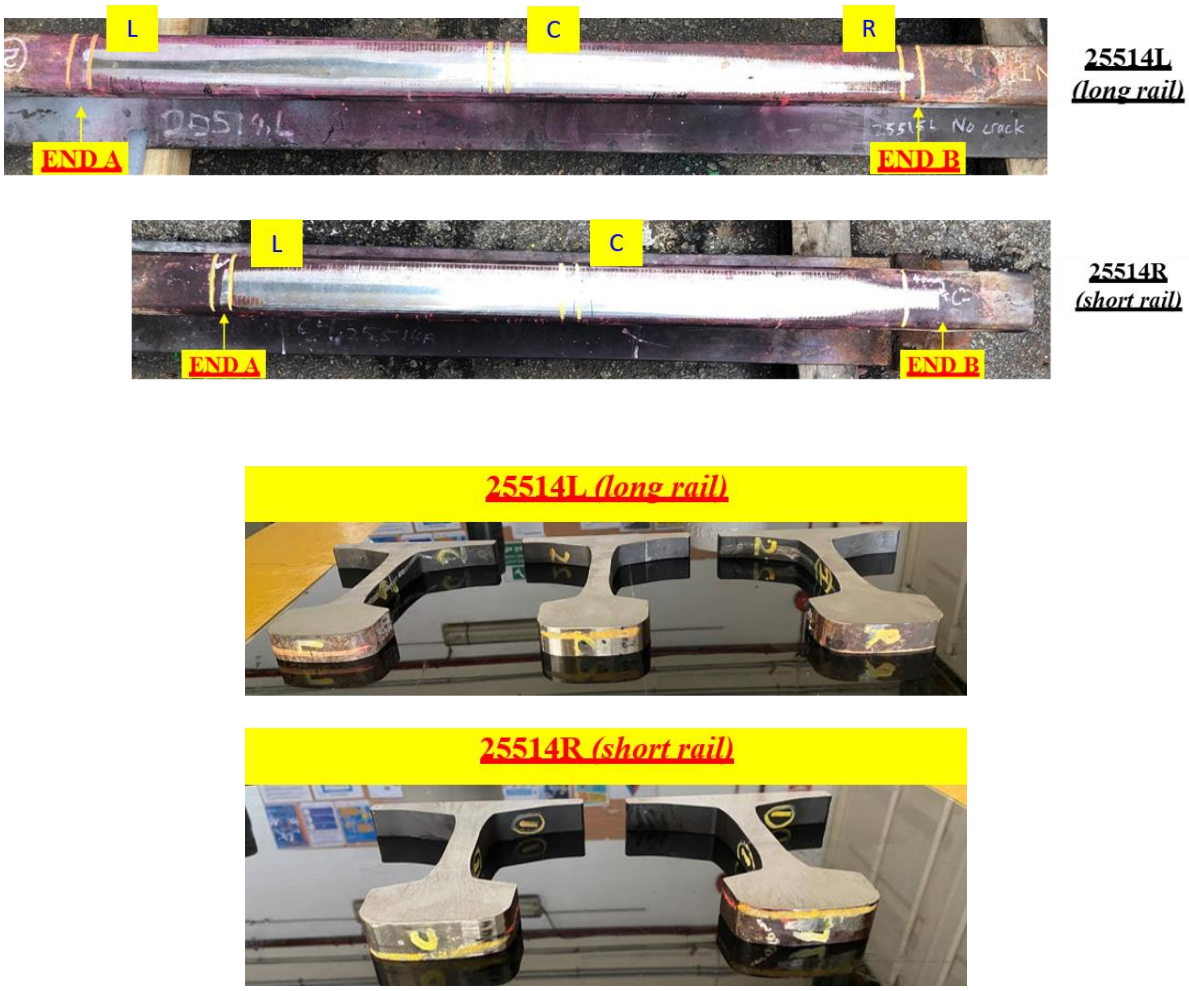

Figure 7-19: Slices “L”, “C”, “R” from 25514L and “L”, “C” from 25514R

X-ray tomography analysis was performed on slice “C” of the 25514L cladded rail segment to check for clad toe cracking and clad layer inspection. The X-ray tomography also known as computed tomography scan or CT scan is an advanced imaging technique that uses computer processed combinations of multiple X-ray measurement data captured at different angles to create tomographic images of a specimen. This technique allows for cross-section inspection of the rail slice where any defects present such as pores or cracks will be reflected in the scan image. The CT scan instrument and sample setup is as shown in Fig.7-20.

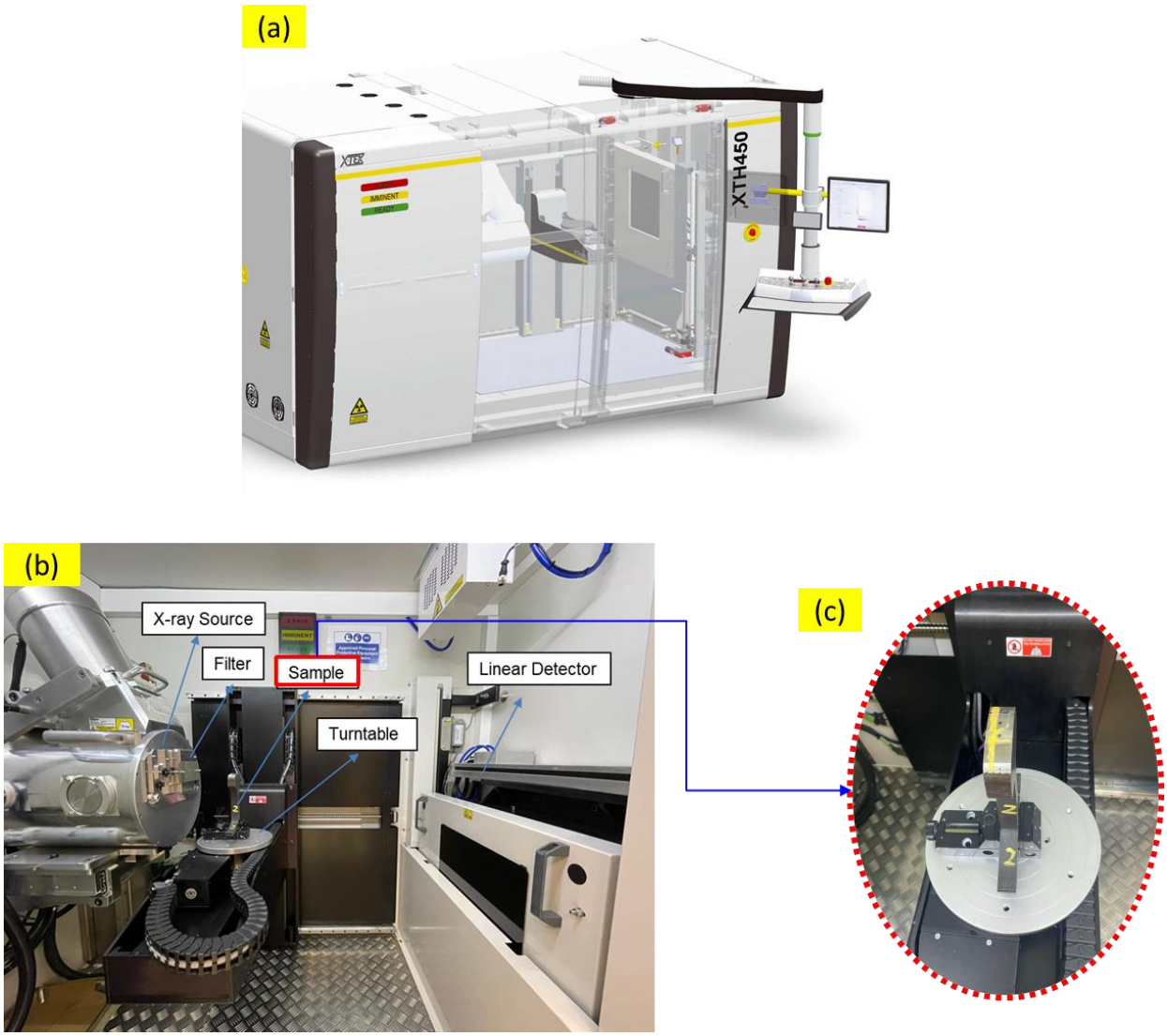

Figure 7-20: (a) XTH450 X-ray inspection machine, (b) Scan setup, (c) Close-up view of the sample position w.r.t X-ray source

The rail sample was rotated in a 360 ° clockwise direction throughout the measurement process as the X-ray image and CT slices are generated using a Curved Linear Detector Array (CLDA). The CLDA optimises the collection of X-rays by eliminating scatter phenomena that typically corrupt 2D radiographs of most metal components. For every scan, 0.08 mm of the CT slice is produced as it took approximately 12 hours to develop scan image of the full rail head-width of 2 mm thickness.

The CT scan parameters used are provided in Table 15.

Table 15: CT Scan Parameters

Parameters	Variables
System	Nikon X TH 450 lc
Detector	Curved Linear Detector Array (CLDA)
Beam Energy	430 kV
Power	89.9 W
Spot Size	0.08 mm
Voxel Size	0.079 mm
Exposure	2.4 sec
Projections	720 frames

The 3D rendering of 2-mm thick rail head section X-ray scan image is attached as shown in Fig.7-21 and the observations are such that no cracks were present in the clad layer. Only minor pores were detected on the surface of the clad which can be classified under laser cladding process related porosity defects.

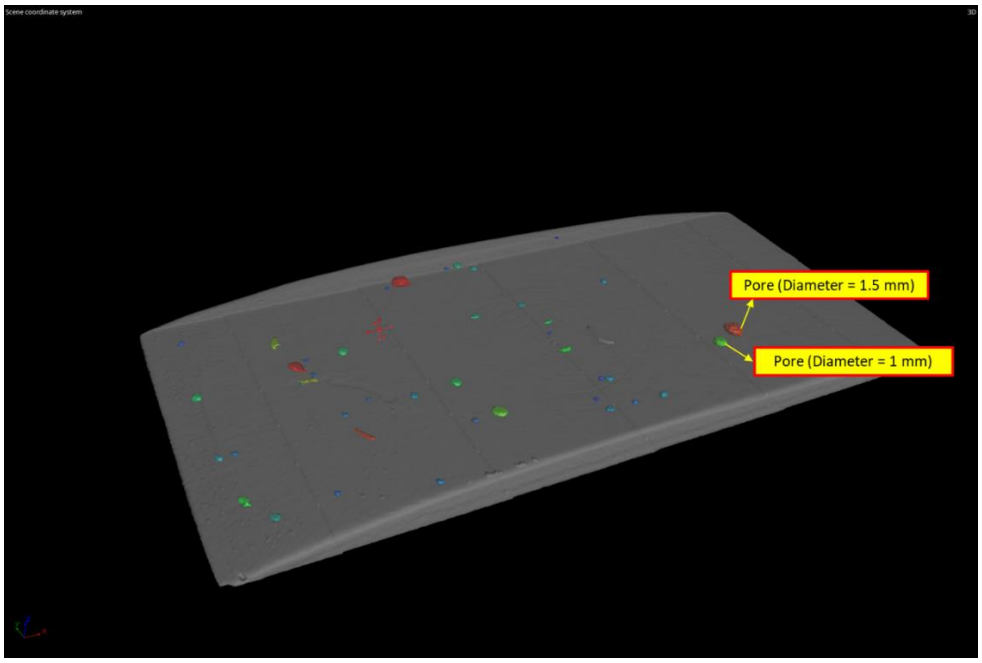

Figure 7-21: 3D rendering of 2-mm thick rail head section X-ray scan image

The defect density was then calculated using an advanced deep learning Volume Graphics (VG) local contrast algorithm in order to analyse and quantify these porosity defects. The porosity characteristics are presented in a chart below in Fig.7-22.

Based on the material volume and defect volume obtained, the defect density is evaluated as approximately 0.157 % which is relatively insignificant compared to the overall clad material volume. This proved that the cladding is of superior quality with only minor porosity defects observed which can be mitigated by carrying out further process optimisation studies.

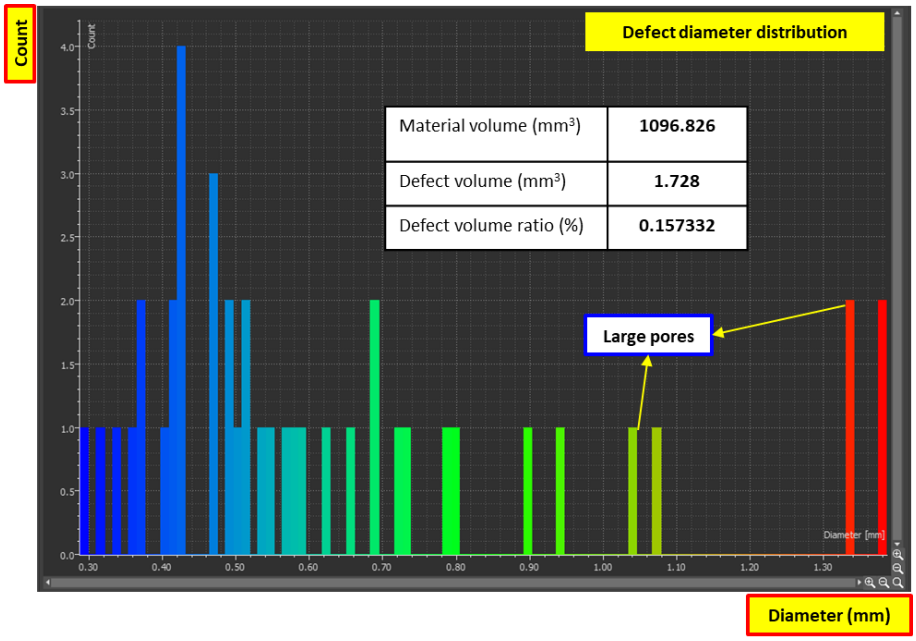

Figure 7-22: Porosity characteristics chart derived from deep learning VG local contrast algorithm

In addition to the crack assessment and defect density analysis, the wear of cladding layer was also investigated by measuring the clad thickness across the rail head section. The measurement data is presented in Fig.7-23. Initial cladding layer thickness prior to service is 1 mm.

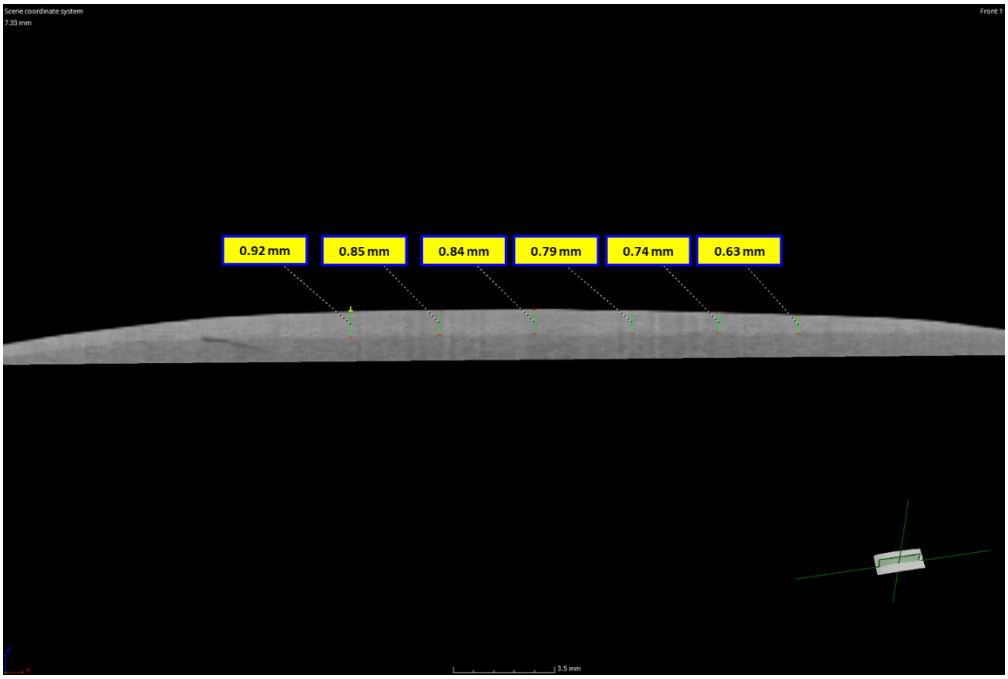

Figure 7-23: Cladding thickness measurement across rail head section

It can be concluded that the results obtained from the X-ray tomographic analysis proved to be highly valuable in the clad-parent material integrity assessment based on the following observations. No clad toe cracks or delamination of cladding layer present with only minor porosity defects were present on the surface of the clad as the defect density (0.157 %) evaluated is insignificant compared to the overall clad material volume. Mild wear of the cladding layer was observed with an average wear ≈ 0.205 mm as the clad thickness varied from 0.92 mm to 0.63 mm.

While the overall clad quality can be further improved by carrying out appropriate process optimisation studies, the cladding layer did not exhibit delamination nor develop any cracks when subject to train loads during the 12-month trial period.

7.3.3 Laser Scanning Microscopic Analysis

Results from the X-ray tomographic analysis were then supported and verified by using a laser scanning microscope (LSM) – OLYMPUS LEXT OLS4100 (LSM) to examine the cladded rail cross-section. The analysis was again performed on slice "C" of the 25514L cladded rail segment. Fig.7-24 shows the cross-section micrograph as observed using the LSM.

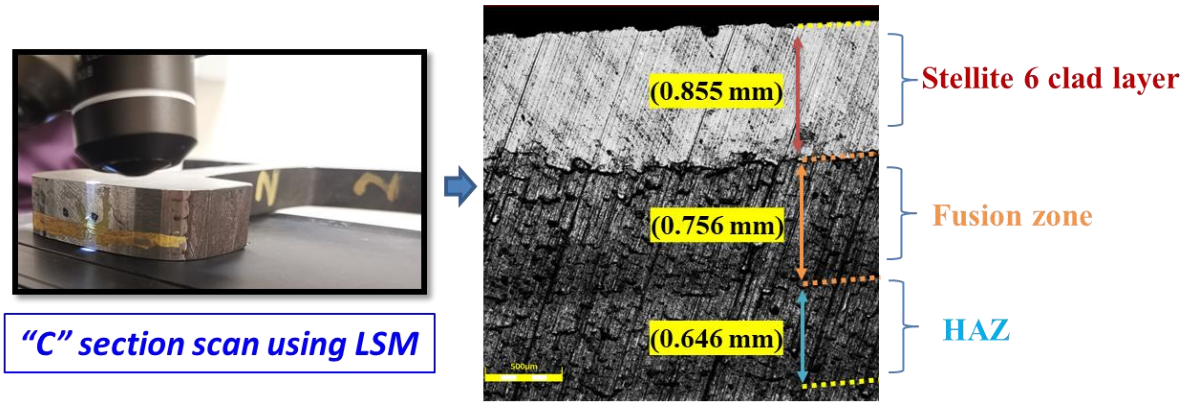

Figure 7-24: Cross-section laser scanning microscopy inspection results across the centre of rail head surface

The clad rail cross section can be ideally characterized with the presence of four main features which are the deposited clad layer, fusion (transition) zone, heat affected zone (HAZ) and the bulk material (substrate). The Stellite 6 cladding layer, fusion zone, and HAZ observed across the centre of rail head surface from the scan image exhibits a clear metallurgical bond with no cracks present. The clad thickness at the centre of the rail section is ≈ 0.855 mm.

The cladding layer thickness was then measured across the rail head profile to evaluate wear and is shown below in Fig.7-25. The average clad thickness of 0.756 mm is identical to that obtained in the clad thickness measurements from the X-ray tomographic analysis – 0.795 mm.

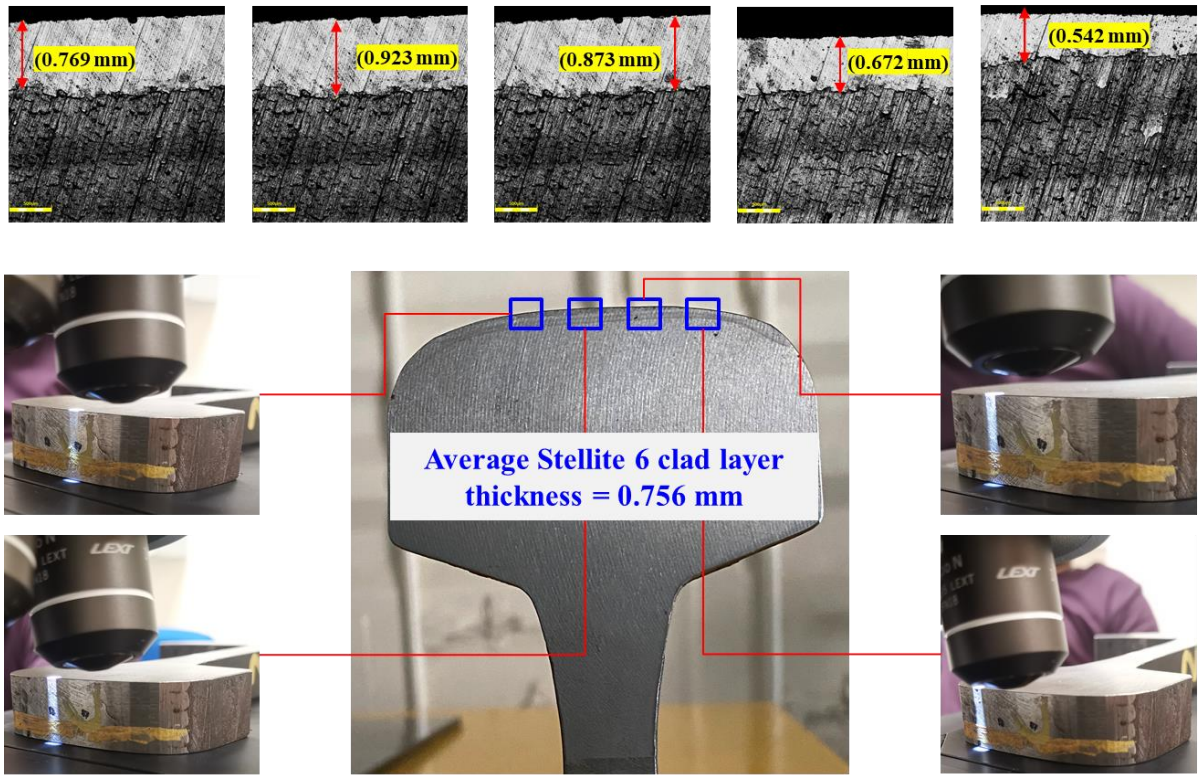

Figure 7-25: "C" rail slice clad thickness analysis using LSM

The cross-section study performed using LSM is supportive of the results obtained from X-ray tomographic analysis.

It has to be noted that in order to ensure a fair and reliable assessment of the clad-parent material integrity during the extraction analysis, specimens "L" and "R" of the 25514L rail segment, and specimens "L" and "C" of the 25514R rail segment were excluded from the study. This is due to the following reasons:

- Rail replacement works carried out on the 25514R rail segment means it is not feasible to make any valid conclusions from the "L" and "C" rail slice specimens
- Severe rail profile grinding operations, particularly at the transition region had affected the clad surface integrity between the clad material and parent rail. It is not feasible to make any valid conclusions from the "L" and "R" rail slice specimens of the 25514L rail segment

7.4 Chapter Summary

The reliability assessment and full-scale test trials of the laser cladded rail track to study the durability and delamination of cladding layer provides the following concluding remarks.

Laser cladding procedure is developed for full-scale test trial of the cladded rail steel specimens on track. The specimens were then installed on BSD test track environment for performance assessment and reliability studies. Inspection methods in the form of ultrasonic testing UT), visual and 3D scanning were adopted and the results were analysed.

Visual and UT inspection of the specimens was positive as the cladding layer remained intact with no obvious indications of cracking or delamination of the cladding layer present. Wear map obtained from the 3D scan measurement data showed both specimens exhibiting smooth and uniform transitions in wear with minimal material loss along the scan data indicating mild wear.

While the cladded rails at the test track are still in active service subject to train runs, results from the trial study served only as a preliminary assessment since the test track is subjected to low train traffic corresponding to low train load and may not be an accurate gauge of the minimal cladded track wear performance. Hence, the next phase of study focused on extending the laser cladding reliability trials on mainline track environment.

The objective of laser cladded rail steel reliability test trials on mainline track environment was likewise to determine if the cladded sections would develop interface cracks leading to delamination or notable service wear behaviour over a 12-month period under the typical East-West Line revenue traffic.

Results obtained from NDT inspection & analysis showed that several indications were present on the cladded surface of both the rail specimens. there was no conclusive evidence to determine if the cladded sections developed any cracks or exhibit delamination due to train induced loads. The X-ray tomographic analysis proved to be highly valuable in the clad-parent material integrity assessment. Critical observations from the analysis include:

(1) No clad toe cracks or delamination of cladding layer present

(2) Only minor porosity defects were present on the surface of the clad as the defect density of 0.157 % is relatively insignificant compared to the overall clad material volume

(3) Reasonable clad wear of 0.205 mm as the cladding thickness varied from 0.92 mm to 0.63 mm

Cross-section study performed using the LSM was supportive of the results obtained from the X-ray tomographic analysis. The Stellite 6 cladding layer, fusion zone, and HAZ observed across the centre of rail head surface from the scan image exhibited a clear metallurgical bond with no cracks present. The average clad thickness of 0.756 mm was identical to that obtained in the clad thickness measurements from the X-ray tomographic analysis – 0.795 mm.

While the overall clad quality can be further improved by carrying out appropriate process optimisation studies, the cladding layer did not exhibit delamination nor develop any cracks when subject to continuous train loads on the mainline track during the 12-month trial period.

To conclude, the reliability test trials and extraction analysis proved successful implementation of the cladded rail specimens on the mainline track environment subject to prudent monitoring and rail grinding operations is required.

Chapter 8 Implementation of a Portable, Modular Laser Cladding System for Rail Repair Applications

Laser cladding know-how on Stellite 6 material-process-performance characterisation study was conducted and proven feasibility for implementation of full-scale reliability assessment of the laser cladded specimens on both a test track and mainline track environment.

The development of a portable and modular laser cladding system design is investigated for implementation of mobile, on-site laser cladding repair operations of railway components on track. The application of laser cladding process for localised repair of rail head defects on track has potential to improve and prolong the rail service life while mitigating total rail replacement works.

The prospect of localised rail head defects repair is explored in Section 8.1. The design and development of a portable laser cladding system and implementation for rail repair operations is discussed in Section 8.2 and proposed as a design solution in the form of technical disclosure filing in Section 8.3. Results from the preliminary laser cladding repair trial studies on a simulated track setup are then analysed in Section 8.4. Concluding remarks from the chapter are summarised in Section 8.5.

8.1 Localised Rail Head Defects for Repair

Rail steel defects are regular features and majority of these defects can lead to very expensive and time-consuming total rail replacement events. Many of these defects are repairable surface rail head defects as shown in Fig.8-1. These rail head defects can be removed and potentially restored back to original rail head profile with an on-site portable, modular laser cladding system. Consistent and routine laser cladding repair helps to improve and prolong the rail head life of rail track that developed localized severe rail defects or cracks that may require total rail replacement.

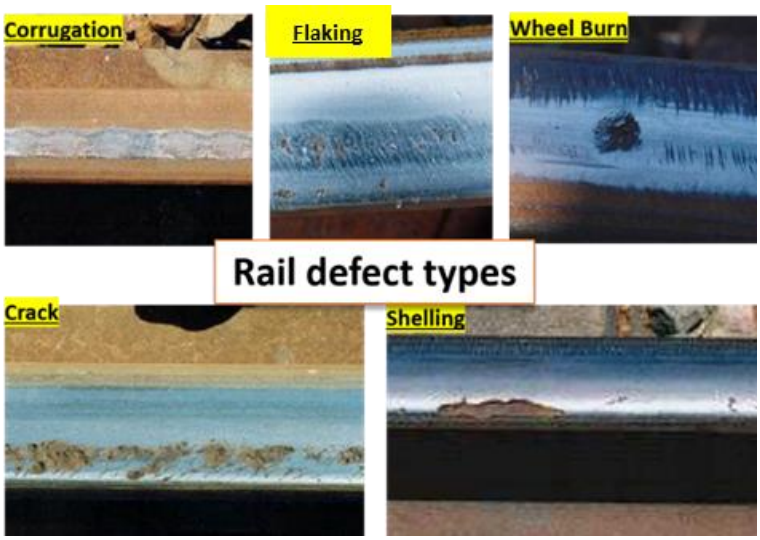

Figure 8-1: Localised rail head defects for repair [13]

In addition to the running rail head surface defects, the rail component that experiences the highest rate of failure is the crossing nose due to the high impact and wear combined with shearing stress that often result in constant maintenance and replacement. Below are some instances of commonly occurring crossing nose defects in Fig.8-2.

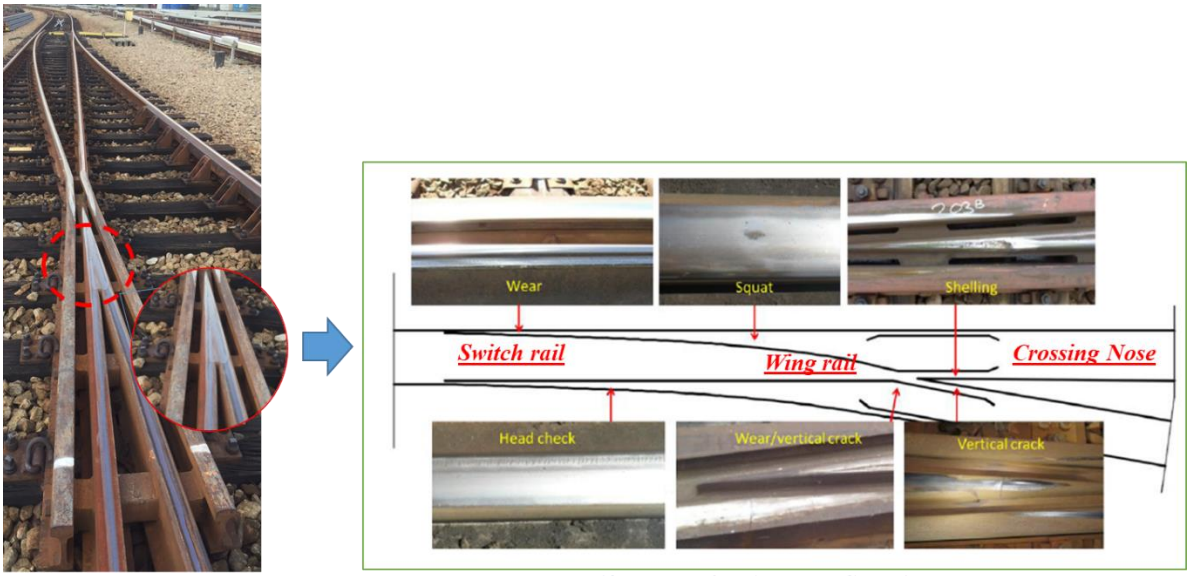

Figure 8-2: Illustration of the different crossing nose defects: a) Shelling, b) Transverse crack, c) Spalling and d) Plastic deformation [145]

Defects such as chip-off, shelling, cracks, squats, and head checks are predominantly observed in the crossing nose, whereas severe wear is present on the wing rail. Due to the geometrical rail discontinuity, the crossing nose is subjected to high impact forces. The combined effect of large impact and differing geometry of the crossing rail sections contribute to significant damage of the crossing rail during contact leading to reduced service life.

To mitigate the costly and time-consuming operation of total replacement, the on-site portable laser cladding system is well placed to repair worn and chipped off nose sections of crossings and switch steel elements. Laser cladding repair work on crossings & switches has valuable potential for research [146].

Existing research have investigated and proven feasibility to implement laser cladding technology for rail component repair, with the most notable research work compiled and are presented in Fig.8-3 below. The research of carrying out laser cladding repair of rail component surface defects in a laboratory or a workshop environment have shown substantial promise.

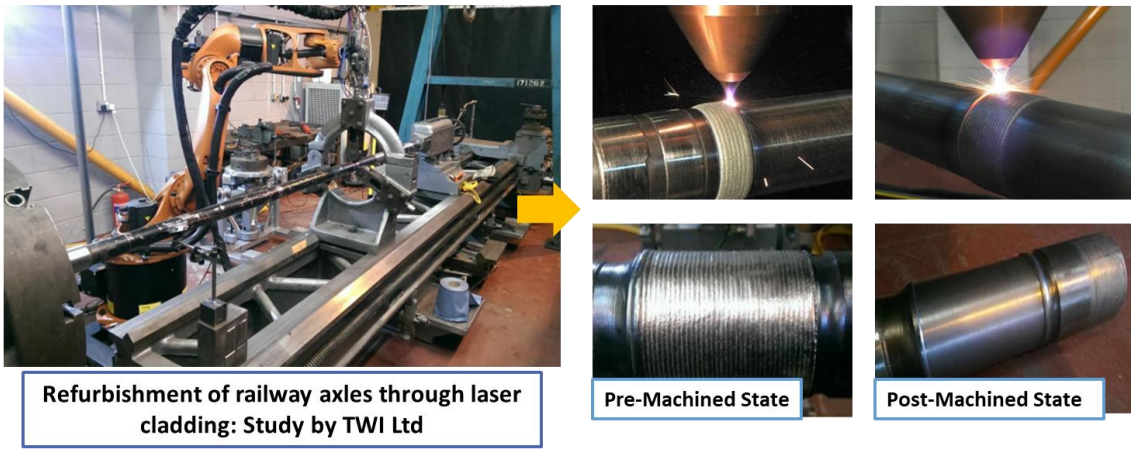

Figure 8-3: Laser cladding for rail repair research [6-9, 65, 129, 147-150]

8.2 Portable Laser Cladding Machine Design

A portable, modular laser cladding system is designed and developed with the capability of on-site of repair of railway track components. The laser cladding machine features a modular design comprising an assembly of components which are configured on three (3) deployable cage-trolleys allowing it to perform remote and on-site laser cladding repair operations on railway components including but not restricted to railway tracks, turnouts and crossings.

The trolley cage enables the trolleys to be hoisted via a crane, lifting or launch device, in order to be lifted, carried, and deployed on the rail track on the trolley track wheels. Once deployed, the trolleys can be further maneuvered manually to the cladding area to perform the laser cladding operation.

The complete portable modular laser cladding system must include a laser module, robotic arm, cladding head, power feeder, gas tanks, cooling system and 3-phase AC-generator. This encompasses all the functional components of a robotized cladding system and the necessary equipment to do simple maintenance of the portable modular laser cladding system and the storage to carry the tools, equipment, and consumables required for the work.

The configuration of the track trolleys in Fig.8-4 is as follows:

- Trolley 1: robot arm with cladding head, heat exchanger to cool down the cladding head, control cabinet to house the laser module/laser controller/robot controller, and powder feeder with two hoppers
- Trolley 2: main chiller for the laser module, argon gas cylinder with cage, electrical distribution cabinet, and reels for laser cable/water hose/gas hose storage
- Trolley 3: AC Generator for the power supply to the system components

Trolley 1

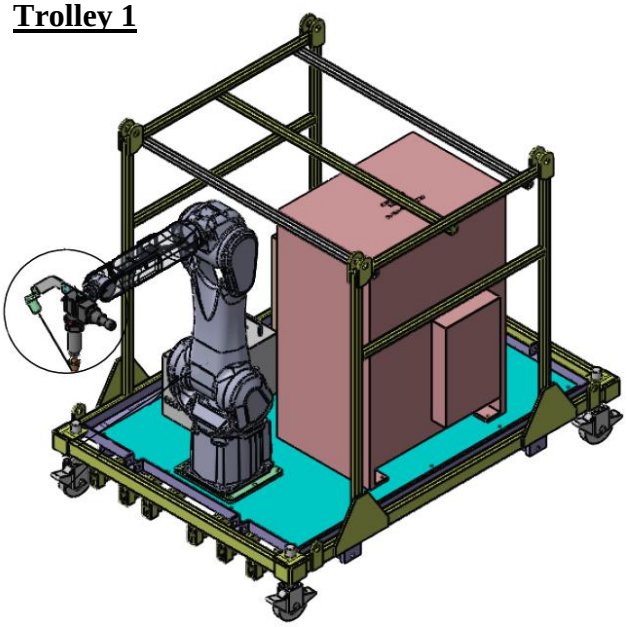

Trolley 2

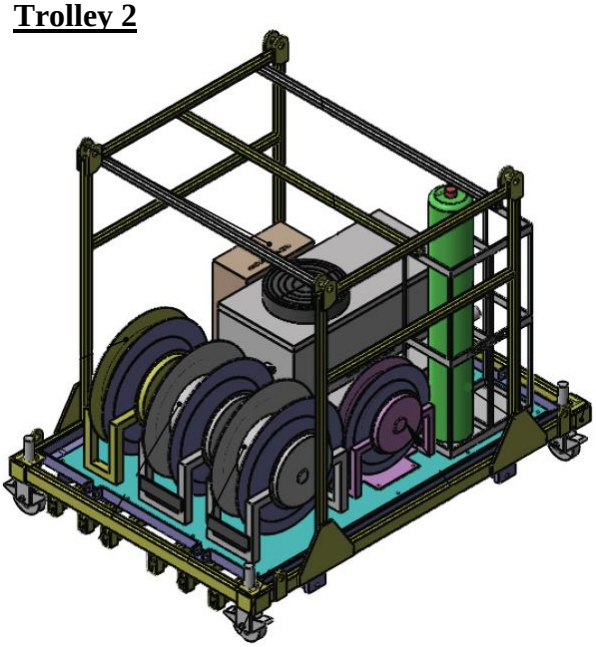

Figure 8-4: Laser cladding machine design CAD models [Track Trolleys 1 and 2]

Another main component includes a laser shielding device to protect the environment against dangerous radiation of laser light emitted from the laser cladding operation. It has to be a laser safety Class 4 shielding device and conform to the National Environmental Agency (NEA) Radiation Protection Acts and its Regulations.

8.3 Patent Filing and Publication

The development of a portable, modular laser cladding system is proposed as design solution to carry out mobile, on-site laser cladding repair operations of railway components on track in the form of a technical disclosure filed and published as a Singapore patent under the SMRT-NTU research project contribution. Two technical disclosures were filed and the provisional patents granted are as follows:

- Laser Cladding Repair System for Rail Track and Crossing [Application No - 10201803946X, Filed on 10/05/2018]

- Modular Laser Cladding System on Railway Trolley Launched from Well-Wagon or Train Gantry Vehicle [Application No - 10201903373T, Filed on 15/04/2019]

A Singapore patent was also filed and published for the state-of-the-art "Modular Laser Cladding System" design for portable on-site rail repair applications on railway track:

- Modular Laser Cladding System [Application No – 10202003426T, filed on 15/04/2020, Published on 27/11/2020]

The tender to develop the Portable Modular Laser Cladding System was awarded on October 2019. The Cage-Trolley structural system was certified for structural integrity and safety by a Professional Engineer (PE)**.** Fabrication and commissioning of the system was completed on September 2020.

8.4 Portable Laser Cladding System Deployed for Preliminary Rail Repair Trial Study

The portable laser cladding system was set on a simulated track setup as shown in Fig.8-5 and preliminary trial studies were conducted to demonstrate laser cladding repair on rail steel.

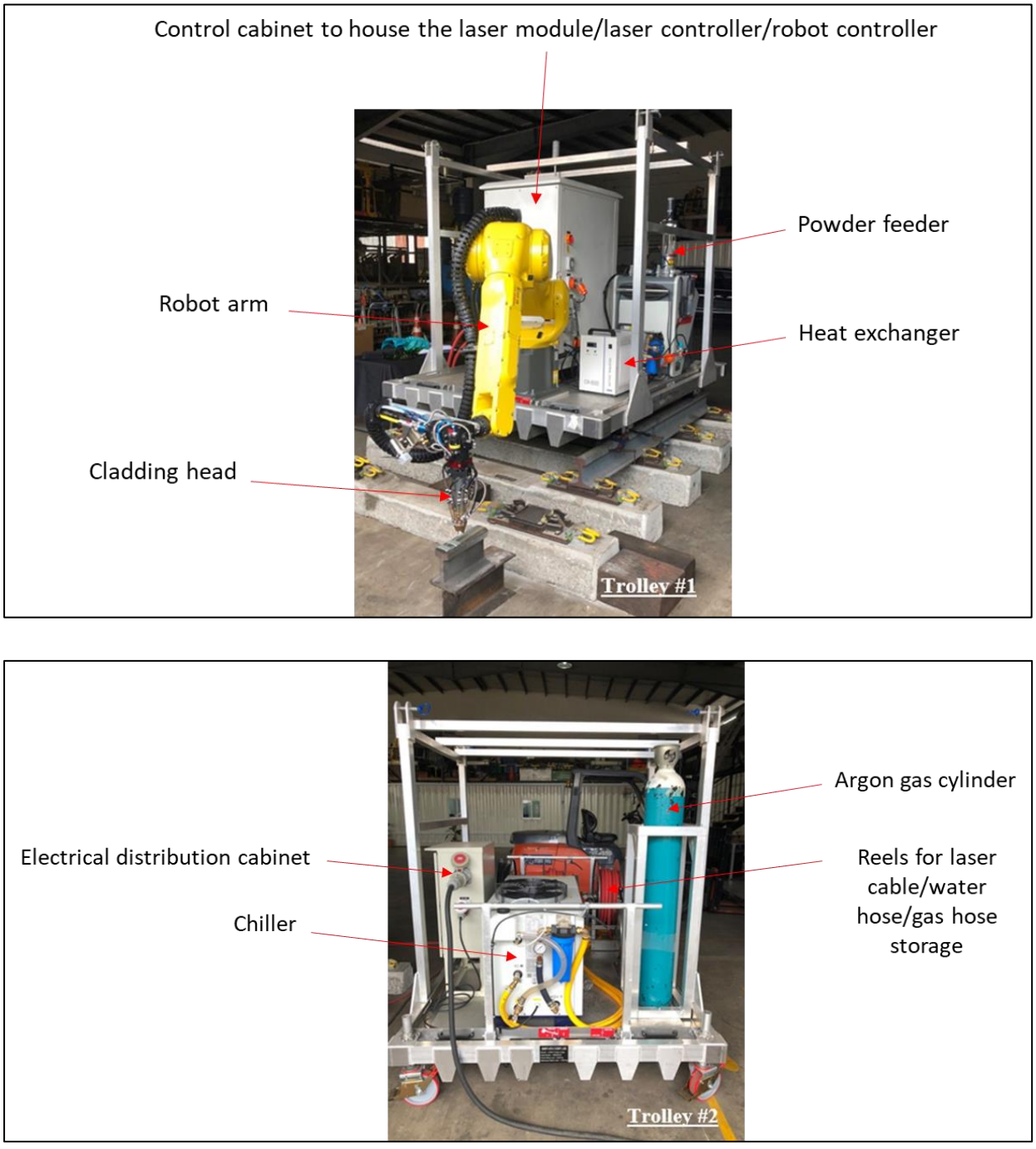

Figure 8-5: Portable modular laser cladding system for simulated on-track rail repair studies

Besides the assembly of the main components on track trolley 1 and 2, the laser cladding system was supported by a generator for power supply and a laser shield device for protection against the laser beam during the cladding operation. The complete configuration of the portable laser cladding system is presented in Fig.8-6.

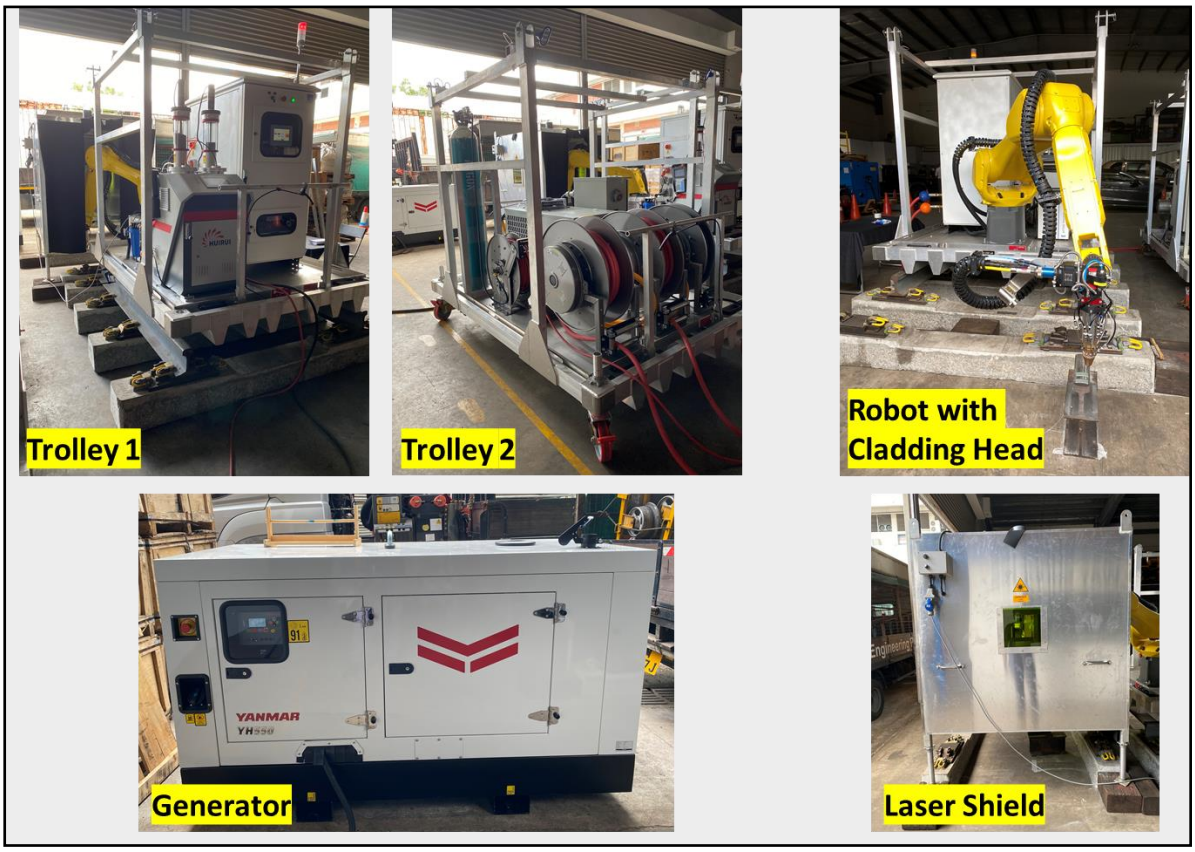

Figure 8-6: Complete setup of the portable laser cladding system

Rail steel specimens were cladded with Stellite 6 and Inconel 625 selected as part of the cladding repair trial study. Inconel 625 is identified as a suitable buffer layer between the more wear-resistant Stellite 6 clad material and the rail steel substrate. Thawari, Nikhil, et al had demonstrated the positive impact on mechanical and microstructural properties by incorporating Inconel 625 material as buffer layer in the deposition of Stellite 6 cladding on SS316 substrate [151].

Three specific types of studies were conducted to investigate the cladding quality of Stellite 6 and Inconel 625 on the R350HT rail substrate as demonstrated in Fig.8-7 below.

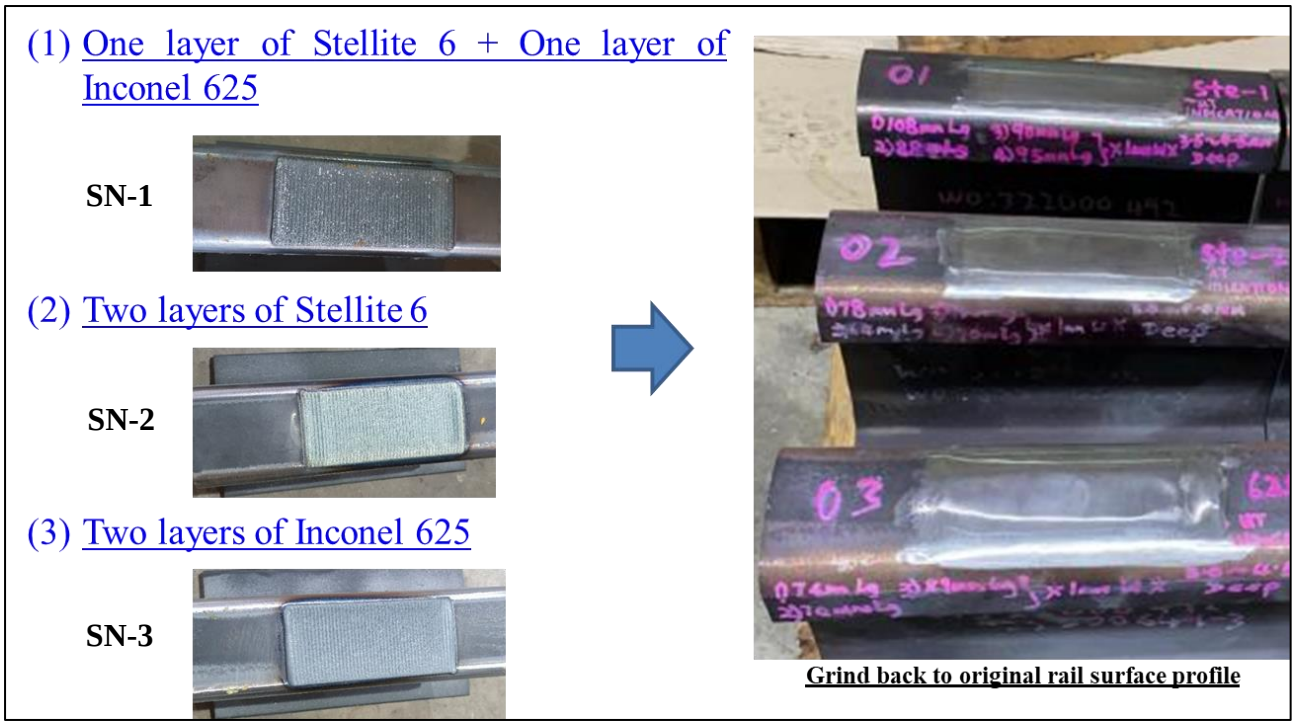

Figure 8-7: Rail steel repair study using the portable laser cladding system

The cladding area selected was 100 mm by 72 mm (full-rail head width). Two cladding layers were deposited each of thickness 1 mm with 3-mm clad bead size (laser spot diameter). The as-clad specimens were then grind back to original rail surface profile prior to investigating the clad quality.

The scope of inspection performed on the cladded rail specimens to examine defects present in the cladding layer includes non-destructive testing (NDT) and hardness test analysis. Results from the liquid penetrant test of the 3 specimens are shown in Fig.8-8.

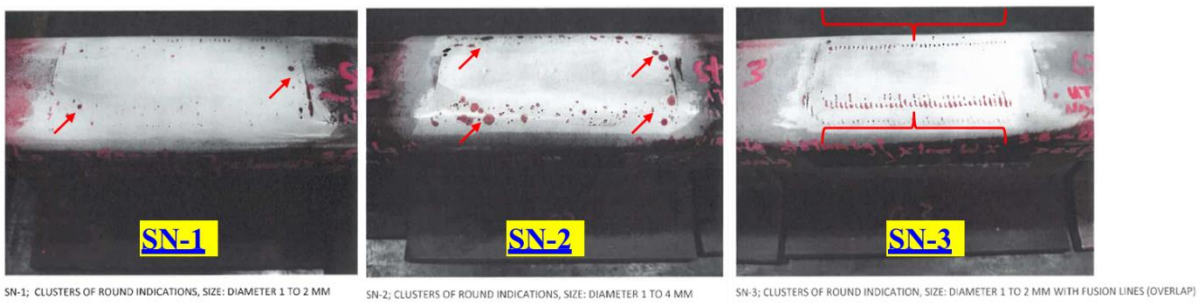

Figure 8-8: Penetrant test results

Clusters of round indications observed denotes round porosities along the boundaries of the clad region on SN-1 and SN-2 whereas interrun porosities were observed along the boundaries of the clad region on SN-3. Minimal porosity was observed on Specimen 1 (SN-1) – one layer of Stellite 6 and one layer of Inconel 625.

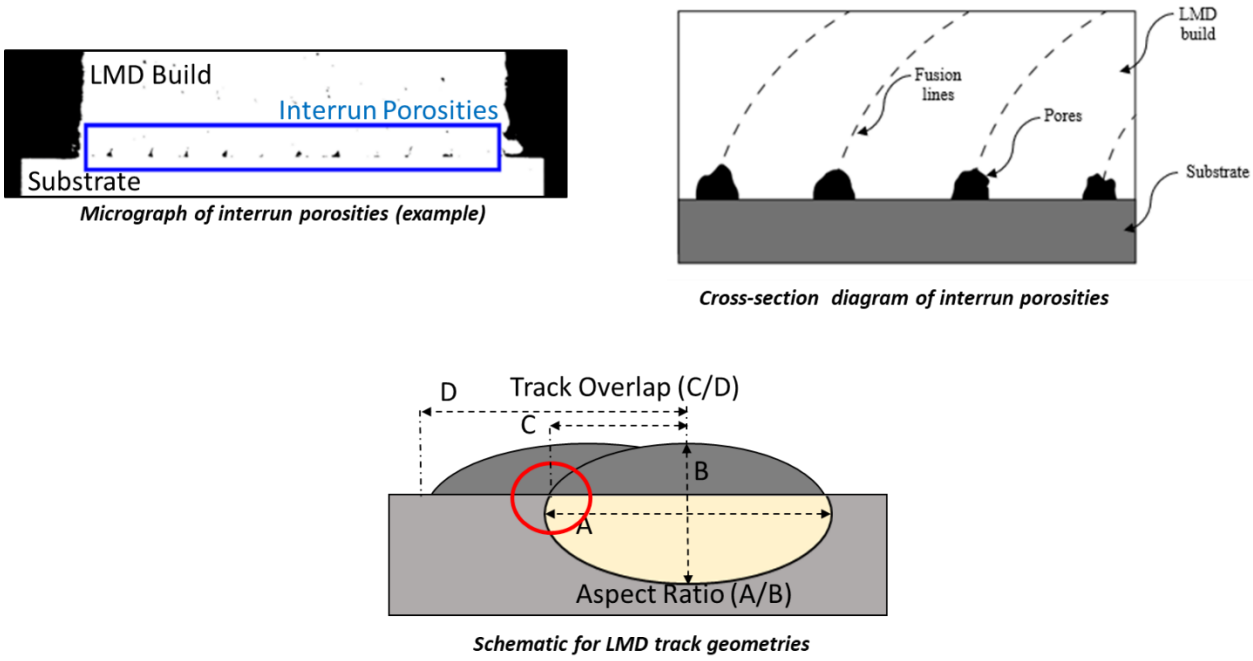

Figure 8-9: Interrun porosity defect characterisation [152]

With respect to Fig.8-9, interrun porosity defects can occur when (1) aspect ratio of clad bead is too low (A/B), (2) track overlap is too high (C/D), or when there is (3) lack of powder pre-heating. Interrun porosities are a result of poor powder flow access or lack of fusion. The 60 % track overlap and 19 g/min powder flow rate may be on the high end of the process input.

Results from the ultrasonic testing (UT) inspection analysis showed that four longitudinally oriented linear indications were observed on all 3 specimens. The linear indications are perpendicularly oriented to the raster scan clad deposit pattern and are located at the substrate-clad interface as illustrated in Fig.8-10.

Rapid thermal expansion and contraction may have caused cracking to occur at the solidification phase especially when the heat energy input is extremely high. Typically, solidification cracking does not occur in LMD processes due to the small melt pool relative to welding [153].

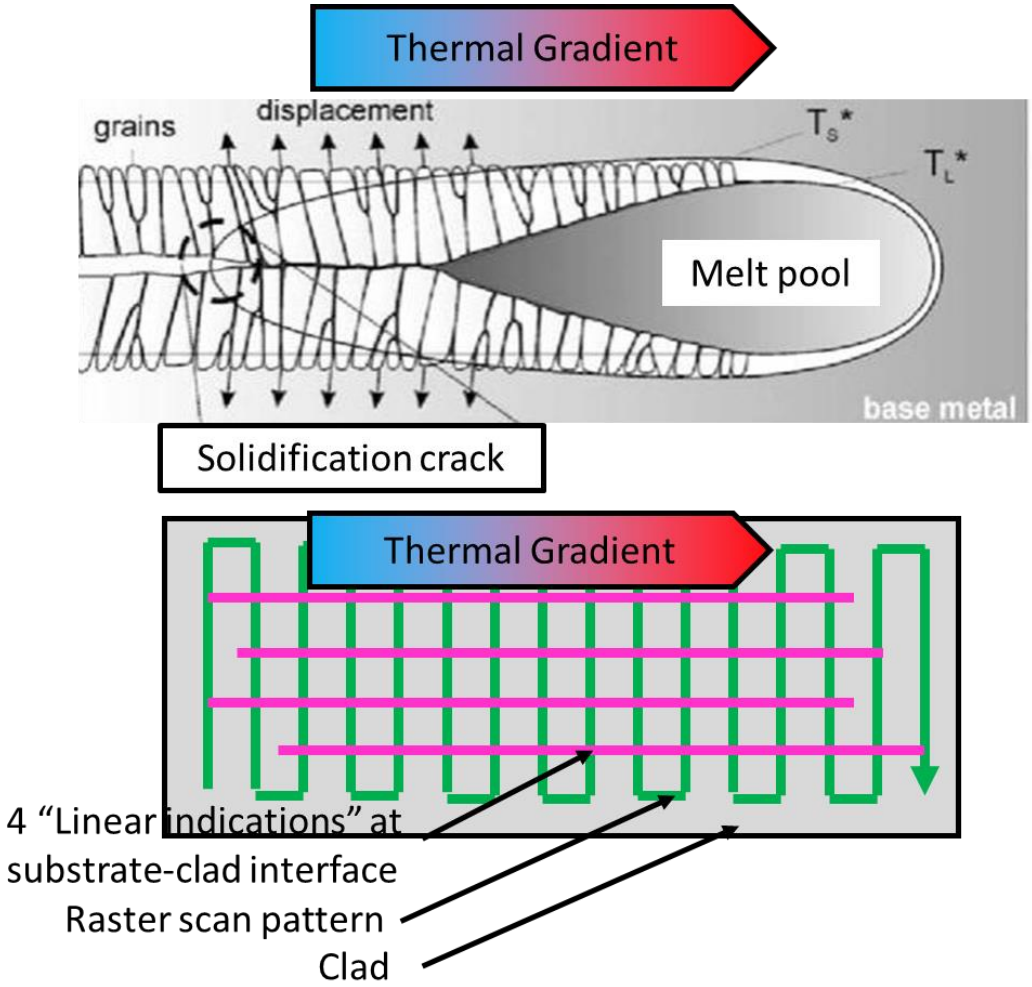

Figure 8-10: Illustration of the linear indications on the substrate-clad interface [153]

Since LMD is considered as a rapid additive manufacturing technique due to the large melt pool (relative to other AM techniques) and fast scan speed (1000 mm/min), it is possible for solidification cracking to occur perpendicular to the raster scan pattern. The laser power for the preliminary study was 2.4 kW which is approximately 1.5 to 3 times higher than the typical working range of LMD processes.

The hardness test results and the test locations on sample surface are presented in Table 16 and Fig.8-11 below.

Table 16: Hardness Data of the 3 Types of Cladded Rail Steel Specimens

SN/Location	Hardness Test Results (HBW)		
	A	B	C
SN-1 (Stellite 6 + Inconel 625)	315 ± 1	313 ± 1	317 ± 1
SN-2 (Stellite 6)	386 ± 8	378 ± 8	404 ± 8
SN-3 (Inconel 625)	221 ± 1	219 ± 1	218 ± 1

Figure 8-11: Hardness test locations on sample surface

The hardness values observed for the SN-1 and SN-2 is ≈ 1.46 and 1.78 times larger than that observed for the SN-3 specimen which is reflective of the wear resistant characteristics of the Stellite 6 and the softer Inconel 625 cladding is ideal for deposition as a buffer layer. The slight deviation (18 %) in hardness between SN-1 and SN-2 is due to inconsistency in the surface profile caused by the grinding process.

To conclude results from the preliminary trial study, the porosities and indications observed from the inspection results were mainly due to laser cladding process-related defects that can be mitigated via process parameter optimisation.

Process study was then conducted to investigate optimal cladding parameter settings using the robotised cladding system for rail steel repair. The optimised laser cladding parameters for SN-1x: One layer of Stellite 6 and one layer of Inconel 625, is shown below in Fig.8-12. A lower laser power setting was used to resolve linear indications that were observed in the inspection results. The track overlap and powder flow rate were also modified to mitigate the porosity defects. The refabricated clad specimen based on the optimised parameter settings is shown in Fig.8-13.

OLD Settings:

Parameter	Value
Laser Power	2.4 kW
Track Overlap	60%
Scan Speed	1000 mm/min
Powder Flow Rate	19 g/min
Pre-heating	Inconel 625: 100**°C** Stellite 6: 150**°C**

***NEW Settings:**

Parameter	Value
Laser Power	2.4 kW → 1.8 kW
Track Overlap	60% → 50%
Scan Speed	1000 mm/min
Powder Flow Rate	19 g/min → 14 g/min
Pre-heating	Inconel 625: 100**°C** Stellite 6: 150**°C**

Figure 8-12: Optimised cladding parameters for Stellite 6 and Inconel 625

Figure 8-13: SN-1x, refabricated specimen with optimised parameter settings (one layer of Stellite 6 and one layer of Inconel 625)

Similar to the previous trial study, the scope of inspection comprised of NDT and hardness analysis to evaluate clad quality and examine for presence of defects or interface cracks.

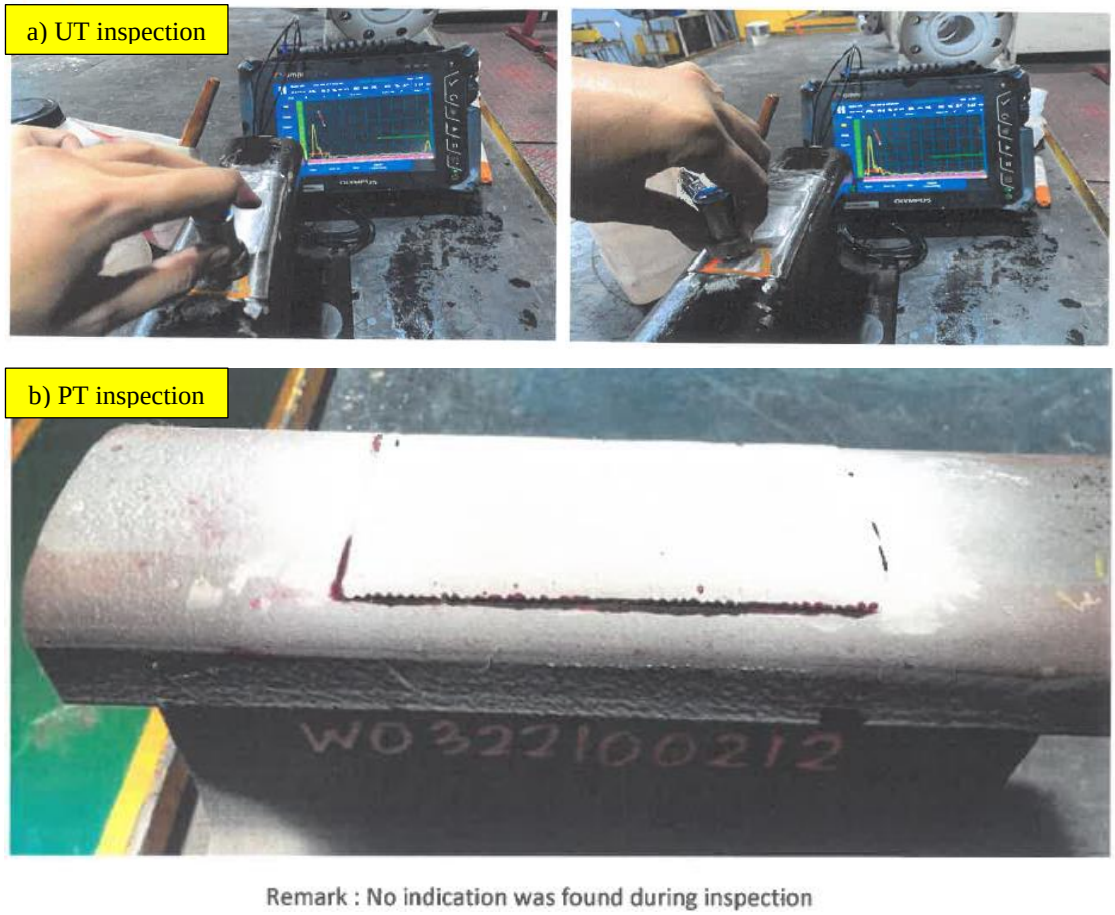

Figure 8-14: a) UT inspection and b) PT inspection of SN-1x specimen

Referring to Fig.8-14, although the UT inspection results showed an indication between the cladding material and parent rail, further analysis conducted from liquid penetrant test (PT) showed no cracks or indications.

The hardness data for the SN-1x specimen are presented in Table 17 below. The test results show consistency of the laser cladded material hardness with less than ±10% variation in term of surface hardness, with the test locations on sample surface as shown in Fig.8-15.

Table 17: Hardness Data of SN-1x Specimen

Location	1	2	3	4	5
Hardness (HBW)	571	545	505	488	554

Figure 8-15: Hardness test locations on sample surface

The re-fabricated SN-1x specimen with optimised laser cladding parameters for deposition of one layer of Stellite 6 and Inconel 625 as a buffer layer showed that clad quality with minimal porosity defects and indications on clad surface is achieved.

8.5 Chapter Summary

The development of a portable, modular laser cladding system design solution was studied for mobile, on-site laser cladding repair operations of railway components on track in the form of a technical disclosure filing. The preliminary trial studies conducted using the portable, modular laser cladding system demonstrated capability for rail steel repair on a simulated track setup. The process studies focused on selecting Inconel 625 as a buffer layer combined with the Stellite 6 cladding layer on the R350HT rail steel substrate. The cladding parameters – laser power, track overlap, and powder flow rate were modified to mitigate porosity defects and linear indications present due to rapid solidification.

Chapter 9 Conclusions and Recommendations for Future Research Scope

9.1 Conclusion

This thesis describes in detail the current objectives and novel aspects of laser cladding research achieved for rail steel repair and reliability assessment.

The research study focused mainly on laser cladding characterisation, durability, delamination and reliability performance of laser cladded rail steel specimens. Experimental characterisation of laser cladding on rail steel is studied to evaluate feasibility for laser cladding repair of localized rail head defects on critical rail components such as rail steel at curves and crossing nose.

Based on the research objectives investigated earlier, the following conclusions can be made as follows:

1. Rail wear degradation study and analysis using maintenance service data was investigated. Rail sections at R300 and R500 radius curves were of particular interest of study due to the increased tendency for failure from severe wear. Wear out failure was observed for all the rail sections at R300 and R500 radius curves with the β value larger than 1. The characteristic life (η) of 30 and 28 years for high rails at both set of radius curves is relatively shorter in comparison to the low rail sections. The longest life of 47 years was observed at the low rail of the R500 radius curve. The extrapolated service wear life model from Zarembski provided an alternative method to correlate wear in terms of Load Vs MGT, Load Vs Time, and Load Vs Train Cycles as compared to the Wear Vs Depth plots in the Weibull model analysis. The wear life model conforms with the railway system loading requirements in Singapore where nominal wheel load is between 8 to 16 tons.

2. Experimental characterisation of laser cladding Stellite 6 clad material with R350HT rail steel substrate was studied involving detailed cross-sectional analysis. The clad-substrate interface from the micrographic analysis showed clear metallurgical bonding with 14.4 % dilution as the Stellite 6 clad layers were deposited onto the rail head surface without any presence of defects. No cracks or delamination was observed at the interface which can be attributed to the initial pre-heating of the rail substrate to relieve thermal stresses.

Microstructural evolution across the rail, interface and clad was studied and characterized and initial observations from the LSM images showed that the clad region comprised of dendrite phase rich in cobalt phase with inter-dendritic mixture of Co, Cr, W carbide phases. Martensitic phase is dominant at the transition (fusion) zone which is formed during the instantaneous solidification and cooling phase of the cladding process. The heat transfer changes that take place during melt pool creation combined with the pre-heat treatment prior to cladding result in finer pearlite structure at the HAZ compared to the R350HT substrate. The EDS results also verify the presence of Co-rich dendritic and inter-dendritic mixture of carbide phases of Co, Cr and W, in the cladding layer.

The hardness profile distribution evaluated across the clad-rail section showed an average hardness of 420 HB within the clad owing to the formation of the carbide hardening phases in the CoCr alloy matrix. The peak hardness of 763 HB observed in the HAZ is not desirable and thus further studies involving shear analysis and on-track reliability trials were required to investigate failure of the cladding layer due to embrittlement.

3. Wear testing and analysis using the ball-on-disc tribometer setup for durability study of Stellite 6 clad material and R350HT grade rail steel was conducted. The wear analysis was also conducted on standard R260 grade rail steel for comparison. The cladded disc specimens exhibited much smaller wear than the unclad rail steel disc specimens. The wear volume of R350HT disc specimen was approximately 1.5 times than that of the Stellite 6 cladded disc specimen. Likewise, a two times larger wear was observed for the R260 disc specimen. The wear volume estimated using ASTM wear equation (from G-99) yielded similar results to the actual wear measured using a surface profilometer. Wear coefficients obtained from the Archard's wear model also proves the superior wear resistance of Stellite 6 cladding in comparison to the head hardened R350HT and standard R260 grade rail steel. The SEM images of the wear track sections were then examined to identify presence of both abrasive and adhesion wear damage mechanisms during the wear test run. The abrasive grooves were more well-defined on the wear track of the unclad rail steel disc specimens with thick oxide layers formed. The wear track on the cladded disc surface is relatively uniform with some wear debris build-up on the circumference of the track. Delamination of the Stellite 6 cladding was present at certain regions of the track caused by ploughing of the harder contact alumina ball surface.

Work hardening behaviour of the rail steel grades R260 and R350HT was also investigated and compared with the Stellite 6 laser clad material. The plot of hardness data with respect to the sliding distance showed general increasing trend of the hardness over the number of test cycles while ensuring steady-state wear is achieved.

4. The experimental methodology for shear testing and analysis was developed to investigate the clad/substrate material interface shear bond strength for assessment of delamination. The shear load (stress) against displacement plots were derived when shear failure of the clad material specimens occurs. Shear strength from the test results was greater than 57.7% of yield strength of R350HT rail steel based on the Von Mises Yield criterion.

Among the specimens tested, complete fracture of the cladding from the base rail steel plate was observed for all except one specimen. Shear initiated along the edge where the specimen was loaded as tearing marks can be seen that were generated from the point of shear. Interfacial delamination was the primary mode of fracture that occurred due to the pure shear phenomena. Preliminary assessment indicated that delamination is unlikely to occur when cladded rail is subjected to train load due to the strong interfacial bond based on the shear strength evaluated and fracture analysis.

5. A comprehensive reliability test program was developed such that 1-mm thick Stellite 6 cladding layer was deposited on R350HT rail steel specimens prior to installation on running rail tracks to investigate reliability and performance when subjected to actual running train loads. Periodic monitoring and inspection were conducted to evaluate the reliability of cladded rails for an approximate 1-year trial duration period as the specimens were subjected to NDT, visual and 3D scan inspection. The 3D surface scan data showed material wear loss of 0.1 mm while the specimens passed the UT and visual checking. The reliability assessment of the cladded rail specimens on the test track was then replicated for study on the mainline track environment. Post extraction analysis of the cladded specimens include NDT inspection and analysis which revealed several indications present on the cladded surface of both the rail specimens. Results from the x-ray tomographic analysis concluded that no clad toe cracks or delamination of cladding layer was present. Minor porosity defects were observed on the clad surface which made up of 0.157 % defect density and is negligible when compared to the overall clad material volume. The average clad thickness of 0.756 mm from the LSM cross-sectional study is identical to that obtained in the clad thickness measurements from the X-ray tomographic analysis – 0.795 mm. The reliability test trials and extraction analysis proved successful implementation of the cladded rail specimens on the mainline track environment while ensuring consistent monitoring and careful rail grinding operations.

6. A portable and modular laser cladding system for simulated on-track studies was designed and developed. The cladding system comprised of the assembly of the main components on cage-track trolleys #1 and #2, with power supplied using a generator and a laser shield device for protection against the laser beam during the cladding operation. The robotised cladding system is capable of performing remote laser cladding repair operations on railway components including but not restricted to railway tracks, turnouts and crossings. The fabricated system was utilised to conduct laser cladding trial studies with Stellite 6 on R350HT rail specimens and Inconel 625 as buffer layer. Two layers of cladding, each of 1 mm thickness was deposited on the rail head surface for preliminary assessment. A clad length of 100 mm with the full rail head width was covered. The penetrant test results revealed clusters of round porosities along the boundaries of the clad region on the SN-1: 1 mm of Stellite 6 and 1 mm of Inconel 625, and SN-2: 2 mm of Stellite 6 deposited specimens. The SN-3: 2 mm of Inconel 625 deposited specimen had interrun porosities along both the longitudinal edges of the clad surface. The high track overlap (60 %) and powder flow rate (19 g/min) parameter were deduced to have caused the formation of these interrun porosities. Further analysis from the ultrasonic inspection showed linear indications oriented in perpendicular direction to the raster scan clad deposit pattern. These indications were attributed to the excessive energy input during the solidification phase. The 1.46- and 1.78-times high hardness of SN-1 and SN-2 in comparison to the SN-3 specimen demonstrates wear resistant characteristics of the Stellite 6 and the softer Inconel 625 cladding is ideal for deposition as a buffer layer.

Process study involving optimised laser cladding parameters with lower laser power, track overlap and powder flow rate was able to achieve clad quality with only minor porosity and indications. Encouraging results from the simulated on-track studies proved that remote laser cladding repair of rail components has significant potential for research.

9.2 Recommendations for Future Research Scope

The current research work investigated feasibility of implementing laser cladding technology for rail repair and service life extension by developing strategical-approach based objectives supported with experimental characterisation and reliability assessment studies of laser cladded rail specimens. Moreover, the development of a portable modular laser cladding system for on-site localised repair of rail head defects has broadened the scope for research to a significant extent. Some of these extended work scope for future research are as follows:

1. Further process-related studies including parameter optimisation are required using the portable modular laser cladding system to develop cladding methodologies for rail repair implementation on the track.

2. Other premium cladding powder material alloys can be evaluated for rail repair feasibility such as AISI 4340 steel – due to its homogeneity with the rail steel substrate in terms of carbon composition, Additional cladding materials that have potential for laser cladding repair of rail steel substrates include: Stellite 21, Stainless Steel (304, 316L and 434 grades) [154, 155].

3. With rail crossings identified as high value components with highest susceptibility to failure due to high impact stress and wear at the nose region. Common carbon steel crossings and cast manganese crossings are two of the prevalent crossing types used in Singapore's railway tracks. There is scope for research to investigate the structural integrity of dual material cladding of Stellite 6 (superior wear resistance) and Inconel 625 (high impact resistance buffer layer) for repair and service life extension of crossing nose.

References

[1] A. D. Kerr, *The Mechanics of Solids: History and Evolution: a Festschrift in Honor of Arnold D. Kerr*. Associated University Presse, 2008.

[2] R. Lewis and U. Olofsson, *Wheel-rail interface handbook*. Elsevier, 2009.

[3] D. Cannon, K. O. Edel, S. Grassie, and K. Sawley, "Rail defects: an overview," *Fatigue & Fracture of Engineering Materials & Structures,* vol. 26, no. 10, pp. 865-886, 2003.

[4] G. Girsch, A. Jörg, and W. Schoech, "Managing rail life to match performance and cut costs," *Railway Gazette International,* vol. 166, no. 8, pp. 45-48, 2010.

[5] G. Girsch, J. Keichel, R. Gehrmann, A. Zlatnik, and N. Frank, "Advanced rail steels for Heavy Haul application–track performance and weldability," in *IHHA conference, Shanghai*, 2009.

[6] S. Lewis, R. Lewis, and D. Fletcher, "Assessment of laser cladding as an option for repairing/enhancing rails," *Wear,* vol. 330, pp. 581-591, 2015.

[7] A. Clare, O. Oyelola, T. Abioye, and P. Farayibi, "Laser cladding of rail steel with Co–Cr," *Surface Engineering,* vol. 29, no. 10, pp. 731-736, 2013.

[8] A. Clare, O. Oyelola, J. Folkes, and P. Farayibi, "Laser cladding for railway repair and preventative maintenance," *Journal of Laser Applications,* vol. 24, no. 3, p. 032004, 2012.

[9] S. Lewis *et al.*, "Improving rail wear and RCF performance using laser cladding," *Wear,* vol. 366, pp. 268-278, 2016.

[10] Q. Lai *et al.*, "Effects of preheating and carbon dilution on material characteristics of laser-cladded hypereutectoid rail steels," *Materials Science and Engineering: A*, vol. 712, pp. 548-563, 2018.

[11] T. Roy *et al.*, "Effect of deposition material and heat treatment on wear and rolling contact fatigue of laser cladded rails," *Wear,* vol. 412, pp. 69-81, 2018.

[12] Q. Lai *et al.*, "Laser cladding for railway repair: influence of depositing materials and heat treatment on microstructural characteristics," 2017.

[13] *TMC 226, Rail Defects Handbook*. RailCorp Engineering Manual, 2012.

[14] E. Toyserkani, A. Khajepour, and S. F. Corbin, *Laser cladding*. CRC press, 2004.

[15] K. Parker, "Cladding with high power diode lasers," *Welding and Cutting*, vol. 11, pp. 288-289, 2012.

[16] A. Birolini, *Reliability engineering: theory and practice*. Springer, 2017.

[17] S. Kumar, "A study of the rail degradation process to predict rail breaks," Luleå tekniska universitet, 2006.

[18] A. Gholipour, M. Shamanian, and F. Ashrafizadeh, "Microstructure and wear behavior of stellite 6 cladding on 17-4 PH stainless steel," *Journal of Alloys and Compounds,* vol. 509, no. 14, pp. 4905-4909, 2011.

[19] M. Zhong, W. Liu, K. Yao, J.-C. Goussain, C. Mayer, and A. Becker, "Microstructural evolution in high power laser cladding of Stellite 6+ WC layers," *Surface and Coatings Technology,* vol. 157, no. 2-3, pp. 128-137, 2002.

[20] R. Shoja-Razavi, "Laser Surface Treatment of Stellite 6 Coating Deposited by HVOF on 316L Alloy," *Journal of Materials Engineering and Performance,* vol. 25, no. 7, pp. 2583-2595, 2016.

[21] R. Ahmed *et al.,* "Single asperity nanoscratch behaviour of HIPed and cast Stellite 6 alloys," *Wear,* vol. 312, no. 1-2, pp. 70-82, 2014.

[22] J. R. Bailey *et al.*, "Coated oil and gas well production devices," ed: Google Patents, 2012.

[23] G. Wang, J. Zhang, R. Shu, and S. Yang, "High temperature wear resistance and thermal fatigue behavior of Stellite-6/WC coatings produced by laser cladding with Co-coated WC powder," *International Journal of Refractory Metals and Hard Materials,* vol. 81, pp. 63-70, 2019.

[24] Y. Ding, R. Liu, J. Yao, Q. Zhang, and L. Wang, "Stellite alloy mixture hardfacing via laser cladding for control valve seat sealing surfaces," *Surface and Coatings Technology,* vol. 329, pp. 97-108, 2017.

[25] W. Chen, B. Liu, L. Chen, J. Xu, and Y. Zhu, "Effect of Laser Cladding Stellite 6-Cr3C2-WS2 Self-Lubricating Composite Coating on Wear Resistance and Microstructure of H13," *Metals,* vol. 10, no. 6, p. 785, 2020.

[26] H. Paydas, A. Mertens, R. Carrus, J. Lecomte-Beckers, and J. T. Tchuindjang, "Laser cladding as repair technology for Ti–6Al–4V alloy: Influence of building strategy on microstructure and hardness," *Materials & Design,* vol. 85, pp. 497-510, 2015.

[27] J. Leunda, C. Soriano, C. Sanz, and V. G. Navas, "Laser cladding of vanadium-carbide tool steels for die repair," *Physics Procedia,* vol. 12, pp. 345-352, 2011.

[28] Q. Liu, M. Janardhana, B. Hinton, M. Brandt, and K. Sharp, "Laser cladding as a potential repair technology for damaged aircraft components," *International Journal of Structural Integrity,* 2011.

[29] M. Brandt, S. Sun, N. Alam, P. Bendeich, and A. Bishop, "Laser cladding repair of turbine blades in power plants: from research to commercialisation," *International Heat Treatment and Surface Engineering,* vol. 3, no. 3, pp. 105-114, 2009.

[30] T. Torims, "The application of laser cladding to mechanical component repair, renovation and regeneration," *DAAAM international scientific book,* vol. 12, pp. 587-608, 2013.

[31] T. J. Richardson, *Shreir's corrosion*. Elsevier, 2009.

[32] L. Zhu *et al.*, "Recent research and development status of laser cladding: A review," *Optics & Laser Technology,* vol. 138, p. 106915, 2021.

[33] A. A. Siddiqui and A. K. Dubey, "Recent trends in laser cladding and surface alloying," *Optics & Laser Technology,* vol. 134, p. 106619, 2021.

[34] L. Sexton, S. Lavin, G. Byrne, and A. Kennedy, "Laser cladding of aerospace materials," *Journal of Materials Processing Technology,* vol. 122, no. 1, pp. 63-68, 2002.

[35] L. Shepeleva, B. Medres, W. Kaplan, M. Bamberger, and A. Weisheit, "Laser cladding of turbine blades," *Surface and coatings technology,* vol. 125, no. 1-3, pp. 45-48, 2000.

[36] R. Martukanitz and S. Babu, "Development of advanced coatings for laser modifications through process and materials simulation," in *AIP Conference Proceedings*, 2004, vol. 712, no. 1: AIP, pp. 1539-1546.

[37] R. Lupoi, A. Cockburn, C. Bryan, M. Sparkes, F. Luo, and W. O'neill, "Hardfacing steel with nanostructured coatings of Stellite-6 by supersonic laser deposition," *Light: Science & Applications,* vol. 1, no. 5, p. e10, 2012.

[38] W. Ya, "Laser materials interactions during cladding: analyses on clad formation, thermal cycles, residual stress and defects," 2015.

[39] M. Schneider and I. J. Meijer, "Laser cladding with powder: effect of some machining parameters on clad properties," 1998.

[40] G. Abbas and D. West, "Laser surface cladding of stellite and stellite-SiC composite deposits for enhanced hardness and wear," *Wear,* vol. 143, no. 2, pp. 353-363, 1991.

[41] J. T. Hofman, "Development of an observation and control system for industrial laser cladding," 2009.

[42] W. M. Steen and J. Mazumder, *Laser material processing*. springer science & business media, 2010.

[43] W. Darmawan, J. Quesada, F. Rossi, R. Marchal, F. Machi, and H. Usuki, "Improvement in wear characteristics of the AISI M2 by laser cladding and melting," *Journal of Laser Applications,* vol. 21, no. 4, pp. 176-182, 2009.

[44] J. T. M. De Hosson, X. Zhou, and M. Van Den Burg, "Structure-property relationship of metal-ceramic interfaces produced by laser processing," *MRS Online Proceedings Library Archive,* vol. 319, 1993.

[45] R. Gassmann, S. Nowotny, A. Luft, W. Reitzenstein, and J. Shen, "Laser cladding of hard particles rich alloys," in *International Congress on Applications of Lasers & Electro-Optics*, 1992, vol. 1992, no. 1: LIA, pp. 288-300.

[46] K. Van Acker, D. Vanhoyweghen, R. Persoons, and J. Vangrunderbeek, "Influence of tungsten carbide particle size and distribution on the wear resistance of laser clad WC/Ni coatings," *Wear,* vol. 258, no. 1-4, pp. 194-202, 2005.

[47] S. Atamert and H. Bhadeshia, "Comparison of the microstructures and abrasive wear properties of stellite hardfacing alloys deposited by arc welding and laser cladding," *Metallurgical Transactions A,* vol. 20, no. 6, pp. 1037-1054, 1989.

[48] V. Kuzucu, M. Ceylan, H. Celik, and I. Aksoy, "Microstructure and phase analyses of Stellite 6 plus 6 wt.% Mo alloy," *Journal of Materials Processing Technology,* vol. 69, no. 1-3, pp. 257-263, 1997.

[49] B. S. Sidhu, D. Puri, and S. Prakash, "Mechanical and metallurgical properties of plasma sprayed and laser remelted Ni–20Cr and Stellite-6 coatings," *Journal of Materials Processing Technology,* vol. 159, no. 3, pp. 347-355, 2005.

[50] T. Sidhu, S. Prakash, and R. Agrawal, "Studies of the metallurgical and mechanical properties of high velocity oxy-fuel sprayed stellite-6 coatings on Ni-and Fe-based superalloys," *Surface and Coatings Technology,* vol. 201, no. 1-2, pp. 273-281, 2006.

[51] Y. Birol, "Thermal fatigue testing of Inconel 617 and Stellite 6 alloys as potential tooling materials for thixoforming of steels," *Materials Science and Engineering: A,* vol. 527, no. 7-8, pp. 1938-1945, 2010.

[52] S. Kapoor, R. Liu, X. Wu, and M. Yao, "Temperature-dependence of hardness and wear resistance of Stellite alloys," *World Academy of Science, Engineering and Technology,* vol. 67, pp. 964-973, 2012.

[53] S. Apay and B. Gulenc, "Wear properties of AISI 1015 steel coated with Stellite 6 by microlaser welding," *Materials & Design,* vol. 55, pp. 1-8, 2014.

[54] S. Sun, Y. Durandet, and M. Brandt, "Parametric investigation of pulsed Nd: YAG laser cladding of stellite 6 on stainless steel," *Surface and Coatings Technology,* vol. 194, no. 2-3, pp. 225-231, 2005.

[55] G. Xu, M. Kutsuna, and M. Rathod, "Cladding of Stellite-6 and vanadium carbide on carbon steel using a yttrium–aluminum–garnet laser robot system," *Journal of Laser Applications,* vol. 18, no. 1, pp. 47-55, 2006.

[56] S.-S. Chang, H.-C. Wu, and C. Chen, "Impact wear resistance of stellite 6 hardfaced valve seats with laser cladding," *Materials and Manufacturing processes,* vol. 23, no. 7, pp. 708-713, 2008.

[57] N. Hutasoit, W. Yan, R. Cottam, M. Brandt, and A. Blicblau, "Evaluation of microstructure and mechanical properties at the interface region of laser-clad Stellite 6 on steel using nanoindentation," *Metallography, Microstructure, and Analysis,* vol. 2, no. 5, pp. 328-336, 2013.

[58] R. Singh, D. Kumar, S. K. Mishra, and S. Tiwari, "Laser cladding of Stellite 6 on stainless steel to enhance solid particle erosion and cavitation resistance," *Surface and Coatings Technology,* vol. 251, pp. 87-97, 2014.

[59] F. C. R. Hernandez, N. G. Demas, D. D. Davis, A. A. Polycarpou, and L. Maal, "Mechanical properties and wear performance of premium rail steels," *Wear,* vol. 263, no. 1-6, pp. 766-772, 2007.

[60] T. EN, "13674-1: Railway Applications–Track–Rail–Part 1: Vignole Railway Rails 46 kg/m and Above," ed: Brussels, 2011.

[61] A. M. TABATABAEI, "FRACTURE AND FATIGUE CRACK GROWTH CHARACTERIZATION OF CONVENTIONAL AND HEAD HARDENED RAILWAY RAIL STEELS," *MIDDLE EAST TECHNICAL UNIVERSITY. Retrieved from http://etd. lib. metu. edu. tr/upload/12616888/index. pdf*, 2014.

[62] K. Z. Mädler, A & Heyder, Rene & Brehmer, M. , "Rail Materials -Alternatives and Limits," *8th World Congress on Railway Research (WCRR2008)*, Seoul, Korea p. 132, 2008.

[63] I. Guideline, "Definitive guidelines on the use of different rail grades," *Deliverable report D*, vol. 4.

[64] P. Lu, S. Lewis, S. Fretwell-Smith, D. Engelberg, D. Fletcher, and R. Lewis, "Laser cladding of rail; the effects of depositing material on lower rail grades," *Wear*, vol. 438, p. 203045, 2019.

[65] S. Lewis *et al.*, "Full-scale testing of laser clad railway track; Case study–Testing for wear, bend fatigue and insulated block joint lipping integrity," *Wear*, vol. 376, pp. 1930-1937, 2017.

[66] T. Roy *et al.*, "Evaluation of the mechanical properties of laser cladded hypereutectoid steel rails," *Wear*, vol. 432, p. 202930, 2019.

[67] M. Xu, J. Li, J. Jiang, and B. Li, "Influence of powders and process parameters on bonding shear strength and micro hardness in laser cladding remanufacturing," *Procedia CIRP*, vol. 29, pp. 804-809, 2015.

[68] A. Standard, "A264," *Standard Specification for Stainless Chromium-Nickel Steel-Clad Plate*, 2012.

[69] Z. Dhib, N. Guermazi, A. Ktari, M. Gasperini, and N. Haddar, "Mechanical bonding properties and interfacial morphologies of austenitic stainless steel clad plates," *Materials Science and Engineering: A*, vol. 696, pp. 374-386, 2017.

[70] S. Alahakoon, Y. Q. Sun, M. Spiryagin, and C. Cole, "Rail Flaw Detection Technologies for Safer, Reliable Transportation: A Review," *Journal of Dynamic Systems, Measurement, and Control*, vol. 140, no. 2, p. 020801, 2018.

[71] A. TUDOR and N. S. E. TOUNTAS, "Wheel/rail friction power in curved track," *UPB Sci. Bull*, 2009.

[72] A. Shebani, "Prediction of wheel and rail wear using artificial neural networks," University of Huddersfield, 2016.

[73] O. Polach, "Characteristic parameters of nonlinear wheel/rail contact geometry," *Vehicle System Dynamics*, vol. 48, no. S1, pp. 19-36, 2010.

[74] H. Soleimani and M. Moavenian, "Tribological Aspects of Wheel–Rail Contact: A Review of Wear Mechanisms and Effective Factors on Rolling Contact Fatigue," *Urban Rail Transit,* vol. 3, no. 4, pp. 227-237, 2017.

[75] H. Ronkainen, S. Varjus, and K. Holmberg, "Tribological performance of different DLC coatings in water-lubricated conditions," *Wear,* vol. 249, no. 3-4, pp. 267-271, 2001.

[76] S. Shariff, T. Pal, G. Padmanabham, and S. Joshi, "Influence of chemical composition and prior microstructure on diode laser hardening of railroad steels," *Surface and Coatings Technology,* vol. 228, pp. 14-26, 2013.

[77] I. Hutchings, "Wear-resistant materials: into the next century," *Materials Science and Engineering: A,* vol. 184, no. 2, pp. 185-195, 1994.

[78] S. Chang, Y.-s. Pyun, and A. Amanov, "Wear and chattering characteristics of rail materials by ultrasonic nanocrystal surface modification," *International Journal of Precision Engineering and Manufacturing,* vol. 16, no. 11, pp. 2403-2410, 2015.

[79] J. Solis Romero, A. Medina Flores, O. Roblero Aguilar, and J. Oseguera Peña, "Tribological evaluation of plasma nitride H13 steel," *Superficies y vacío,* vol. 26, no. 4, pp. 131-138, 2013.

[80] A. Standard, "Standard test method for wear testing with a pin-on-disk apparatus," *Annual Book of ASTM Standards, G99-05,* vol. 3, 2017.

[81] G. M. Ay and O. N. Çelik, "Inspection of friction and wear properties of railway rails," *Engineering Science and Technology, an International Journal,* 2013.

[82] R. Lewis *et al.,* "Towards a standard approach for the wear testing of wheel and rail materials," *Proceedings of the Institution of Mechanical Engineers, Part F: Journal of Rail and Rapid Transit,* vol. 231, no. 7, pp. 760-774, 2017.

[83] F. C. R. Hernández, N. G. Demas, K. Gonzales, and A. A. Polycarpou, "Correlation between laboratory ball-on-disk and full-scale rail performance tests," *Wear,* vol. 270, no. 7-8, pp. 479-491, 2011.

[84] J. Viesca, S. González-Cachón, A. García, R. González, and A. Hernandez Battez, "Tribological behaviour of microalloyed and conventional C–Mn rail steels in a pure sliding condition," *Proceedings of the Institution of Mechanical Engineers, Part F: Journal of Rail and Rapid Transit,* p. 0954409718765063, 2018.

[85] S. o. T. A. T.E.I. of Piraeus, Department of Mechanical Engineering. "Tribology, Heat Treatments and Q.A.S. Laboratory, Facilities." http://triblab.teipir.gr/en/pg000.html (accessed November 15, 2018.

[86] R. Lewisa and R. Dwyer-Joyce, "Wear mechanisms and transitions in railway wheel steels," *Proceedings of the Institution of Mechanical Engineers, Part J: Journal of Engineering Tribology,* vol. 218, no. 6, pp. 467-478, 2004.

[87] S. Lewis, R. Lewis, G. Evans, and L. Buckley-Johnstone, "Assessment of railway curve lubricant performance using a twin-disc tester," *Wear,* vol. 314, no. 1-2, pp. 205-212, 2014.

[88] N. Tassini, X. Quost, R. Lewis, R. Dwyer-Joyce, C. Ariaudo, and N. Kuka, "A numerical model of twin disc test arrangement for the evaluation of railway wheel wear prediction methods," *Wear*, vol. 268, no. 5-6, pp. 660-667, 2010.

[89] R. Lewis and U. Olofsson, "Mapping rail wear regimes and transitions," *Wear*, vol. 257, no. 7-8, pp. 721-729, 2004.

[90] F. Braghin, R. Lewis, R. Dwyer-Joyce, and S. Bruni, "A mathematical model to predict railway wheel profile evolution due to wear," *Wear*, vol. 261, no. 11-12, pp. 1253-1264, 2006.

[91] E. A. Gallardo-Hernandez and R. Lewis, "Twin disc assessment of wheel/rail adhesion," *Wear*, vol. 265, no. 9-10, pp. 1309-1316, 2008.

[92] T. U. o. S. MERail – Mechanical Engineering Railway Research. "Experimental Facilities." http://merail.group.shef.ac.uk/experimental-facilities/ (accessed November 16, 2018.

[93] S. Lewis, S. Riley, D. Fletcher, and R. Lewis, "Optimisation of a Railway Sanding System, Part 2: Adhesion Tests," 2015.

[94] S. Lewis, S. Riley, D. Fletcher, and R. Lewis, "Optimisation of a railway sanding system, Part 1: Optimal grain entrainment into the wheel/rail contact," *Journal of Rail and Rapid Transit, Proceedings of the IMechE, Part F*, 2015.

[95] R. Stock, D. Eadie, and K. Oldknow, "Rail grade selection and friction management: a combined approach for optimising rail–wheel contact," *Ironmaking & Steelmaking*, vol. 40, no. 2, pp. 108-114, 2013.

[96] R. Stock, D. Eadie, D. Elvidge, and K. Oldknow, "The impact of rail grade selection and friction modifier application on rail degradation," in *9th World Congress on Railway Research*, 2011.

[97] J. Zhang, *Detection and monitoring of wear using imaging methods*. University of Twente [Host], 2006.

[98] G. Straffelini, *Friction and wear: methodologies for design and control*. Springer, 2015.

[99] X. Jin and J. Zhang, "A complementary principle of elastic bodies of arbitrary geometry in rolling contact," *Computers & Structures*, vol. 79, no. 29-30, pp. 2635-2644, 2001.

[100] J. Stokes, "The Theory and Application of the HVOF (High Velocity Oxy-Fuel)," ed: ed, 2011.

[101] B. Bhushan, *Modern tribology handbook, two volume set*. CRC press, 2000.

[102] A. Orvnäs, *Simulation of rail wear on the swedish light rail line Tvärbanan*. 2005.

[103] A. Rovira, A. Roda, M. Marshall, H. Brunskill, and R. Lewis, "Experimental and numerical modelling of wheel–rail contact and wear," *Wear*, vol. 271, no. 5-6, pp. 911-924, 2011.

[104] R. Enblom, "Simulation of Wheel and Rail Profile Evolution: Wear Modelling and Validation," KTH, 2004.

[105] K. D. Van and M. Maitournam, "On some recent trends in modelling of contact fatigue and wear in rail," *Wear,* vol. 253, no. 1-2, pp. 219-227, 2002.

[106] D. T. Eadie *et al.*, "The effects of top of rail friction modifier on wear and rolling contact fatigue: Full-scale rail–wheel test rig evaluation, analysis and modelling," *Wear,* vol. 265, no. 9-10, pp. 1222-1230, 2008.

[107] A. Carpinteri and N. Pugno, "Evolutionary fractal theory of erosion and experimental assessment on MIR space station," *Wear,* vol. 257, no. 3-4, pp. 408-413, 2004.

[108] S. Montgomery, D. Kennedy, and N. O'Dowd, "Analysis of wear models for advanced coated materials," 2009.

[109] M. Hadfield and C. A. Brebbia, *Tribology and Design II*. WIT Press, 2012.

[110] C. R. A. da Silva Jr and G. Pintaude, "Uncertainty analysis on the wear coefficient of Archard model," *Tribology International,* vol. 41, no. 6, pp. 473-481, 2008.

[111] B. Majumdar, *Introduction to tribology of bearings*. S. Chand Publishing, 2008.

[112] A. Zmitrowicz, "Wear patterns and laws of wear–a review," *Journal of theoretical and applied mechanics,* vol. 44, no. 2, pp. 219-253, 2006.

[113] T. Jendel and M. Berg, "Prediction of wheel profile wear: methodology and verification," *Vehicle System Dynamics,* vol. 37, no. sup1, pp. 502-513, 2002.

[114] M. Ignesti, M. Malvezzi, L. Marini, E. Meli, and A. Rindi, "Development of a wear model for the prediction of wheel and rail profile evolution in railway systems," *Wear,* vol. 284, pp. 1-17, 2012.

[115] J. Pombo *et al.*, "Development of a wear prediction tool for steel railway wheels using three alternative wear functions," *Wear,* vol. 271, no. 1-2, pp. 238-245, 2011.

[116] J. Pombo *et al.*, "A railway wheel wear prediction tool based on a multibody software," *Journal of theoretical and applied mechanics,* vol. 48, pp. 751-770, 2010.

[117] R. Enblom, "Deterioration mechanisms in the wheel–rail interface with focus on wear prediction: a literature review," *Vehicle System Dynamics,* vol. 47, no. 6, pp. 661-700, 2009.

[118] C. T. Dick, C. P. Barkan, E. Chapman, and M. Stehly, "Analysis of factors affecting the location and frequency of broken rails," *Proc. World Congr. Railw. Res. Col. Ger,* pp. 1-19, 2001.

[119] H. Hoh, J. Wang, A. Nellian, and J. Pang, "Reliability Centred Maintenance (RCM) Assessment of Rail Wear Degradation," in *Advances in Condition Monitoring and Structural Health Monitoring*: Springer, 2021, pp. 325-332.

[120] G. Chattopadhyay and S. Kumar, "Parameter Estimation for Rail Degradation Model," *International Journal of Performability Engineering*, vol. 5, no. 2, 2009.

[121] M. A. Freitas, M. L. G. de Toledo, E. A. Colosimo, and M. C. Pires, "Using degradation data to assess reliability: a case study on train wheel degradation," *Quality and Reliability Engineering International*, vol. 25, no. 5, pp. 607-629, 2009.

[122] Reliasoft. "Using the Power Law Model for Data Analysis in RGA." http://www.weibull.com/hotwire/issue131/relbasics131.htm. (accessed.

[123] W. Wang, H. Guo, X. Du, J. Guo, Q. Liu, and M. Zhu, "Investigation on the damage mechanism and prevention of heavy-haul railway rail," *Engineering failure analysis*, vol. 35, pp. 206-218, 2013.

[124] X. Cui, G. Chen, H. Yang, Q. Zhang, H. Ouyang, and M. Zhu, "Effect of the wheel/rail contact angle and the direction of the saturated creep force on rail corrugation," *Wear*, vol. 330, pp. 554-562, 2015.

[125] H. Rinne, *The Weibull distribution: a handbook*. Chapman and Hall/CRC, 2008.

[126] A. Aguinaga, X. Luo, V. Hidalgo, E. Cando, and F. Llulluna, "A Feed-Forward Backpropagation Neural Network Method for Remaining Useful Life Prediction of Francis Turbines."

[127] E. Wyrwas, L. Condra, and A. Hava, "Accurate quantitative physics-of-failure approach to integrated circuit reliability," *IPC APEX Expo, Las Vegas, NV*, vol. 13, 2011.

[128] R. Corporation, *Life Data Analysis*. Tucson: AZ: Reliasoft Publishing, 2005.

[129] A. S. Nellian, K. E. Tan, H. J. Hoh, J. H. L. Pang, I. Christian, and S. Y. Chua, "Microstructure and Wear Performance Assessment of Laser Cladded Rail Steel for Service Life Extension at Sharp-Radius Curves," in *2018 International Conference on Intelligent Rail Transportation (ICIRT)*, 2018: IEEE, pp. 1-5.

[130] S. Kapoor, "High-Temperature Hardness and Wear Resistance of Stellite Alloys," Carleton University, 2012.

[131] D. Klarstrom and J. Wu, "Metallography and microstructures of cobalt and cobalt alloys," *Materials Park, OH: ASM International, 2004.*, pp. 762-774, 2004.

[132] A. Standard, "A370," *Standard Test Methods for Mechanical Testing of Steel Product*, 2000.

[133] W. Hofmeister, M. Wert, J. Smugeresky, J. A. Philliber, M. Griffith, and M. Ensz, "Investigating solidification with the laser-engineered net shaping (LENSTM) process," *Jom*, vol. 51, no. 7, pp. 1-6, 1999.

[134] U. De Oliveira, V. Ocelik, and J. T. M. De Hosson, "Residual stress analysis in Co-based laser clad layers by laboratory X-rays and synchrotron diffraction techniques," *Surface and Coatings Technology*, vol. 201, no. 3-4, pp. 533-542, 2006.

[135] G. Xu, M. Kutsuna, Z. Liu, and K. Yamada, "Comparison between diode laser and TIG cladding of Co-based alloys on the SUS403 stainless steel," *Surface and Coatings Technology,* vol. 201, no. 3-4, pp. 1138-1144, 2006.

[136] F. Luo, A. Cockburn, R. Lupoi, M. Sparkes, and W. O'Neill, "Performance comparison of Stellite 6® deposited on steel using supersonic laser deposition and laser cladding," *Surface and coatings technology,* vol. 212, pp. 119-127, 2012.

[137] U. Olofsson and Y. Lyu, "Open System Tribology in the Wheel–Rail Contact—A Literature Review," *Applied Mechanics Reviews,* vol. 69, no. 6, p. 060803, 2017.

[138] G. Tressia, J. I. Pereira, J. J. Penagos, E. Bortoleto, and A. Sinatora, "Effect of in-service work hardening on the sliding wear resistance of a heavy haul rail in the gauge corner," *Wear,* p. 203979, 2021.

[139] R. Lewis, P. Christoforou, W. Wang, A. Beagles, M. Burstow, and S. Lewis, "Investigation of the influence of rail hardness on the wear of rail and wheel materials under dry conditions (ICRI wear mapping project)," *Wear,* vol. 430, pp. 383-392, 2019.

[140] R. Lewis, W. Wang, M. Burstow, and S. Lewis, "Investigation of the influence of rail hardness on the wear of rail and wheel materials under dry conditions," in *Proceedings of the Third International Conference on Railway Technology: Research, Development and Maintenance*, 2016, vol. 110.

[141] N. V. Rao, G. M. Reddy, and S. Nagarjuna, "Weld overlay cladding of high strength low alloy steel with austenitic stainless steel–structure and properties," *Materials & Design,* vol. 32, no. 4, pp. 2496-2506, 2011.

[142] Y. An, H. Vegter, and J. Heijne, "Development of simple shear test for the measurement of work hardening," *Journal of Materials Processing Technology,* vol. 209, no. 9, pp. 4248-4254, 2009.

[143] P. P. Benham, R. J. Crawford, and C. G. Armstrong, *Mechanics of engineering materials*. Pearson, 1996.

[144] Z. Zhu, Y. He, X. Zhang, H. Liu, and X. Li, "Effect of interface oxides on shear properties of hot-rolled stainless steel clad plate," *Materials Science and Engineering: A,* vol. 669, pp. 344-349, 2016.

[145] V. G. Voestalpine, "Operational failure modes of Switches and Crossings," 2015.

[146] A. Mashal, "Analysis and improvement of railway crossing using explicit Finite Element simulations," 2016.

[147] F. R. Hernández, A. Okonkwo, V. Kadekar, T. Metz, and N. Badi, "Laser cladding: The alternative for field thermite welds life extension," *Materials & Design,* vol. 111, pp. 165-173, 2016.

[148] F. C. Robles Hernandez and A. O. Okonkwo, "Laser Cladding of Welds to Improve Railroad Track Safety," 2015.

[149] M. Soodi, "Laser Cladding compared with TIG welding to repair and refurbish railway axles," *CORE 2010: Rail, Rejuvenation and Renaissance*, p. 516, 2010.

[150] M. Soodi, M. Soodi, M. Brandt, and N. Alam, "Fatigue strength properties in rail axles refurbished by laser cladding," in *CORE 2012: Global Perspectives; Conference on railway engineering, 10-12 September 2012, Brisbane, Australia*, 2012: Engineers Australia, p. 25.

[151] N. Thawari, C. Gullipalli, J. K. Katiyar, and T. Gupta, "Influence of buffer layer on surface and tribomechanical properties of laser cladded Stellite 6," *Materials Science and Engineering: B*, vol. 263, p. 114799, 2021.

[152] W. Steen, V. M. Weerasinghe, and P. Monson, "Some aspects of the formation of laser clad tracks," in *High Power Lasers and Their Industrial Applications*, 1986, vol. 650: International Society for Optics and Photonics, pp. 226-234.

[153] V. Ploshikhin, A. Prikhodovsky, M. Makhutin, A. Ilin, and H.-W. Zoch, "Integrated mechanical-metallurgical approach to modeling of solidification cracking in welds," in *Hot cracking phenomena in welds*: Springer, 2005, pp. 223-244.

[154] T. Xie *et al.*, "Investigation on the Rolling Contact Fatigue Behaviors of Different Laser Cladding Materials on the Damaged Rail," *Journal of Tribology*, vol. 143, no. 5, p. 051108, 2021.

[155] J.-W. Seo, J. C. Kim, S.-J. Kwon, and H.-K. Jun, "Effects of laser cladding for repairing and improving wear of rails," *International Journal of Precision Engineering and Manufacturing*, vol. 20, no. 7, pp. 1207-1217, 2019.

Appendix A: Application for Modification (AFM)

Our Reference **MOD 8**

To Chua Si Yun, SE (PWY) Your Reference

From Secretary, SSB (Trains) Date July 17, 2018

NOTICE OF MODIFICATION APPROVAL (CAT D)

This is to inform you that the captioned modification proposal is approved.

Attached are the following document(s) for your necessary action.

Documents

1. Photocopy of RFM
2. Photocopy of AFM

PW2017261/PW0145 – To install Stellite 6 cladded straight rails from CH 25512 to CH 25518 at TIB-RDH (WB). Cladded will be performed in a workshop by Wilhelm Pte Ltd. As there is minimum length requirement between 2 welds, 6m long rails will be provided to Wilhelm. Only 1m length of the rails will be cladded with 1mm thickness of Stellite 6 material.

You are reminded to submit the FORM COM to the SSB (Trains) upon completion of the modification as stipulated in the Modification Procedure.

Thank you

Dennis Tang
M (IMO/SSB)

Attachment 8.7

SMRT	REQUEST FOR MODIFICATION	RFM NO: PW2017261

PART 1 TO BE FILLED BY ORIGINATOR

Name: Wayne Chen Designation: Principal Engineer — Signature/Date: 27/02/18	Department: Permanent Way Engineering

MOD Title:

Phase 1 Trial: Installation of 6m long straight rails, cladded with 1m length of Stellite 6 material of 1mm thickness. 6m long straight rails will be installed from CH 25512 to CH 25518 at TIB-RDH (WB).

Phase 2 Trial: Installation of laser cladded crossing nose on the mainline. This requires deposit of Inconel 625 build-up material prior to Stellite 6 hardfacing.

Funds for MOD Approved: ☑ Yes — Authority: Principal Engineer (PWY Engineering)

Target Starting Date: May 2018 for Phase 1	Target Completion Date: May 2019

PART 2 TO BE FILLED BY CO-ORDINATOR

Name: Chua Si Yun Designation: Senior Engineer — Signature/Date: 26/02/18	Department: Permanent Way Projects

Consideration given to effects on all system	☑ Yes
Acceptance of modification(s) by user and affected parties	☑ Yes
Agreement from affected parties to raise AFM(s) for all changes arising from this MOD	☑ Yes

RFM-Aug 13

Details of Co-ordination:

GENERAL

- This is done jointly by SMRT and NTU under the SMRT-NTU Smart Urban Rail Corporate Laboratory.
- The objective of this mainline trial is to replicate the laser cladding trial performed at BSD test track with similar test set up to be used on the mainline as the train load and frequency at BSD test track is lower than mainline daily operation.
- The mainline trial is planned based on the successful proof of concept of the BSD trial test. 1m length and 1mm thick Stellite 6 cladded straight rail specimen was installed on BSD Test Track on 11 March 2017 and are in service to date with no defects and measureable wear observed.
- Cladding is performed in a workshop by Wilhelm Pte Ltd and welded back onto the test track manually. At Wilhelm Pte Ltd, Non-Destructive Test (NDT) on the cladded rails are performed by qualified and experienced technicians certified to ASNT Level II. To ensure quality of the cladded specimen, material characterisation has been done on the cladded rail by NTU. This includes hardness measurement, microstructure study and porosity check.

PHASE 1 TRIAL

- Phase 1 trial at TIB-RDH (WB) shall follow the same preparation procedures as that of BSD Test Track trial.
- Monthly UT and visual inspection for surface cracks and delamination will be carried out for the first 6 months upon installation to assess its performance. UT results must be satisfactory and delamination/cracks should not be present for trial to be considered satisfactory.
- If above requirements are not met, cladded rail specimen will be removed and reinstated to original condition.
- If cracks/internal flaw are observed, it will be classified accordingly, based on Patrolling Fault Code and Severity Index. Rectification will then be conducted to reinstate the rails to original condition.

PHASE 2 TRIAL

- Phase 2 trial for nose of crossings shall commence when Phase 1 trial is proven to show satisfactory results after 6 months of monitoring as described above.
- Location of Phase 2 trial will be determined upon successful results of Phase 1 trial. As precautionary measure, location selected will be away from the city centre.

Attachment 8.8

SMRT	APPLICATION FOR MODIFICATION	AFM NO: PW0145

PART 3 TO BE FILLED BY APPLICANT

Name: Chua Si Yun Designation: Senior Engineer	24/02/18 Signature/Date	Department Permanent Way Projects

Category B Mod ☐	Category C Mod ☐	Category D Mod ☑ Yes

Modification Proposal:

The mainline trial is to replicate the same trial test carried out on BSD test track in order to study the effect of real time train load and frequency on the cladded track. Through this trial, wear results of cladded rails can be accurately determined under actual train frequency and load, then further extrapolated to predict wear rate of the cladded track for long term operation in future.

The mainline trial is planned based on the successful proof of concept of BSD trial test, which the cladded tracks were installed and used for more than 10 months with no defects and measureable wear observed.

Phase 1 Trial

To install Stellite 6 cladded straight rails from CH 25512 to CH 25518 at TIB-RDH (WB). Cladding will be performed in a workshop by Wilhelm Pte Ltd. As there is minimum length requirement between 2 welds, 6m long rails will be provided to Wilhelm. Only 1m length of the rails will be cladded with 1mm thickness of Stellite 6 material.

Based on trial test at BSD test track, Stellite 6 has proven its capability for laser cladding of rails and excellent tribological properties such as wear resistance and potential for service life extension. Below is the composition of Stellite 6 used:

Elements	Co	Cr	W	Mo	C	Fe	Ni	Si	Mn	P	S	Al	V	N
Stellite 6	Bal	31	4.7	0.1	0.9	1.5	1.8	1.3	0.4	0.002	0.001	-	-	0.08

Remanufacturing process is as follows:

a. 3D scan of rail prior to cladding
b. Removal of 1mm depth of surface material by milling
c. Laser clad with 2mm thick of Stellite 6 material
d. Programmed CNC machining of 1mm depth to grind back to rail profile based on scanned data.

Refer to attached documents for illustration. Cladded rails will be installed permanently, unless proven to be unfit for service.

Phase 2

Cladding will be performed in 3 stages in the sequence from Section A to Section B followed by Section C as shown in attached supporting documents due to the low cooling rate at the nose tip. Inconel 625 will be deposited on the worn nose for material build-up before hardfacing with Stellite 6 on top of Inconel 625 to improve wear performance of the crossing nose. The purpose of adding Inconel 625 build-up serves as a buffer layer between the rail steel and Stellite 6 to prevent formation of crack. Inconel 625 is widely used as a buffer layer between hard parent material and hardfacing materials in order to prevent crack formation during the cladding process. Below is the composition of Inconel 625 used:

Nickel	58.0 min.
Chromium	20.0-23.0
Iron	5.0 max.
Molybdenum	8.0-10.0
Niobium (plus Tantalum)	3.15-4.15
Carbon	0.10 max.
Manganese	0.50 max.
Silicon	0.50 max.
Phosphorus	0.015 max.
Sulfur	0.015 max.
Aluminum	0.40 max.
Titanium	0.40 max.
Cobalt	1.0 max.

Cladding will be performed in a workshop by Wilhelm Pte Ltd. Location to be decided upon satisfactory result of Phase 1 trial. Cladded rails will be installed permanently, unless proven to be unfit for service.

Remanufacturing process is as follows:

a. Removal of 1mm depth of surface material at the crossing nose
b. Laser clad with 2mm thick Inconel 625 material (build-up material)
c. Laser clad with 2mm thick Stellite 6 material
d. Grind off additional clad layer on surface to achieve smooth finish

Reason(s) and Justification(s):

On-site laser cladding point repair and restoration of damaged steel rails is a potential new high impact industry for Mass Transit Railway operator as it helps mitigate very expensive and time consuming Total Rail Replacement procedures used when steel rails exceed prescribed wear or rail head defect of cracking specifications.

Trial of cladded rails on the mainline provides a better gauge to its performance as compared to trial on test track due to increased train frequency, loading and speed.

Is Mod a trial scheme ☐ No ☒ Yes

Is Mod on LTA Asset/Infrastructure ☐ No ☒ Yes

Effects on Documents, specification, etc

☐	Operation Manuals	☐	Specifications (for spares, eqpt)
☐	Maintenance Manuals	☒	Endorsement by relevant Authority, PE,
☐	Training Manuals	☒	Maintenance period
☐	As-Built Drawings	☐	Others : _____

Attachment 8.8

SMRT	APPLICATION FOR MODIFICATION	AFM NO. PW0145

PART 4 TECHNICAL ENDORSEMENT

SMRT	LTA
By Head of Centre / Division	For Mod on LTA Asset/Infrastructure
☑ Approved ☐ Rejected	☑ Approved ☐ Rejected
Name: Jean-Francois Chassin Vice President Permanent Way	Name: Soo Weng Tuck Deputy Director Asset Steward & Inventory
Designation:	Designation: (Deputy Director & Above)
Signature/Date 8/03/18	Signature/Date

PART 5 SVP APPROVAL

☑ Approved ☐ Rejected

Name: Chia Chun Wah
Designation : CMO 1.
Signature/Date 16/3/18

PART 6 (FOR CAT B & C MOD ONLY)

SMRT Safety Board (Trains) Approval - Meeting # & Date :

☐ Approved ☐ Rejected

Name:
Designation (Chairman) Signature/Date

LTA Approval on Acceptance of Safety Analysis

☐ Approved ☐ Rejected

Name:
Designation: Signature/Date

AFM2-8Aug 13

Attachment 8.8

SMRT Co-ordinator (For AFM raised by LTA) : Name : Designation: Signature/Date (Exe Engr & Above)

Appendix B: List of Publications from PhD Research

Patent Filings & Publications:

1. Laser Cladding Repair System for Rail Track and Crossing [Application No - 10201803946X, Filed on 10/05/2018]

2. Modular Laser Cladding System on Railway Trolley Launched from Well-Wagon or Train Gantry Vehicle [Application No - 10201903373T, Filed on 15/04/2019]

3. A Singapore patent was also filed and published for the state-of-the-art "Modular Laser Cladding System" design for portable on-site rail repair applications on railway track: Modular Laser Cladding System [Application No – 10202003426T, Filed on 15/04/2020, Published on 27/11/2020]

AFM (Application for Modification Approved by Land Transport Authority):

1. No. PW 0145 - Phase 1 – Installation of 6 m Long Straight Rails, Cladded with 1 m Length of Stellite 6 Material of 1 mm Thickness. Phase 2 – Installation of Laser Cladded Crossing Nose on the Mainline.

Conference Publications:

1. Nellian Alagu Subramaniam, Kok Ee Tan, Hoh Hsin Jen, John Hock Lye Pang, Ivan Christian, and Si Yun Chua, "Microstructure and Wear Performance Assessment of Laser Cladded Rail Steel for Service Life Extension at Sharp-Radius Curves." 2018 International Conference on Intelligent Rail Transportation (ICIRT). IEEE, 2018.

2. Hoh Hsin Jen, Wang Jinlong, Nellian Alagu Subramaniam, and John Hock Lye Pang, "Reliability Centered Maintenance (RCM) Assessment of Rail Wear Degradation", World Congress on Condition Monitoring (WCCM) 2019, Singapore.

Joint Journal Publications:

1. Liu, Yang, Kin Shun Tsang, Eddie Tan Zhi'En, Nellian Alagu Subramaniam, and John Hock Lye Pang, "Investigation on material characteristics and fatigue crack behavior of thermite welded rail joint." Construction and Building Materials 276 (2021): 122249. (Q1, IF: 4.419)

2. Liu, Yang, Kin Shun Tsang, Nellian Alagu Subramaniam, and John Hock Lye Pang, "Structural Fatigue Investigation of Thermite Welded Rail Joints Considering Weld-induced Residual Stress and Stress Relaxation by Cyclic Load", Engineering Structures 235 (2021): 112033. (Q1, IF: 3.548)

3. Wang, Jinlong, Yi Su, N. Alagu Subramaniam, and John Hock Lye Pang. "Archard Model Guided Feature Engineering Improved Support Vector Regression for Rail Wear Analysis." Engineering Failure Analysis (2022): 106248.